

TURBULENT BUOYANT JETS INTO STRATIFIED  
OR FLOWING AMBIENT FLUIDS

Thesis by

Loh-Nien Fan

In Partial Fulfillment of the Requirements

For the Degree of  
Doctor of Philosophy

California Institute of Technology

Pasadena, California

1967

(Submitted May 26, 1967)

ACKNOWLEDGMENTS

The writer wishes to express his deep gratitude to his advisor, Professor Norman H. Brooks, for suggestion of this project as well as guidance and encouragement offered throughout the investigation. He would also like to thank Dr. Robert C. Y. Koh for discussions and help given in the early stage of this study.

To Professors Vito A. Vanoni and Fredric Raichlen he expresses thanks for their kind advice and assistance.

For design and construction of laboratory equipment, the writer is much indebted to Mr. Elton F. Daly, supervisor of the shop and laboratory. The assistance of Mr. Robert L. Greenway is also much appreciated.

The writer would like to express his gratitude to Messrs. Jiin-jen Lee, Josephat K. Okoye and William W. Owens, Graduate Research Assistants, for their assistance in performing laboratory experiments and reducing data; to Mr. Carl T. Eastvedt for taking motion pictures and laboratory photographs; to Mr. Carl A. Green, Jr., for preparation of graphs and to Mrs. Patricia Rankin for her typing of the manuscript.

This research was supported by research grants WP-00428 and WP-00680 of the U. S. Public Health Service, National Institutes of Health, and research grant WP-01256-01 of the U.S. Federal Water Pollution Control Administration. The experiments were conducted in the W.M. Keck Laboratory of Hydraulics and Water Resources at the California Institute of Technology.

ABSTRACT

Theoretical and experimental studies were made on two classes of buoyant jet problems, namely:

1) an inclined, round buoyant jet in a stagnant environment with linear density-stratification;

2) a round buoyant jet in a uniform cross stream of homogeneous density.

Using the integral technique of analysis, assuming similarity, predictions can be made for jet trajectory, widths, and dilution ratios, in a density-stratified or flowing environment. *Such information is of great importance in the design of disposal systems for sewage effluent into the ocean or waste gases into the atmosphere.*

The present study of a buoyant jet in a stagnant environment has extended the Morton type of analysis to cover the effect of the initial angle of discharge. Numerical solutions have been presented for a range of initial conditions. Laboratory experiments were conducted for photographic observations of the trajectories of dyed jets. In general the observed jet forms agreed well with the calculated trajectories and nominal half widths when the value of the entrainment coefficient was taken to be  $\alpha = 0.082$ , as previously suggested by Morton.

The problem of a buoyant jet in a uniform cross stream was analyzed by assuming an entrainment mechanism based upon the vector difference between the characteristic jet velocity and the ambient velocity. The effect of the unbalanced pressure field on

the sides of the jet flow was approximated by a gross drag term. Laboratory flume experiments with sinking jets which are directly analogous to buoyant jets were performed. Salt solutions were injected into fresh water at the free surface in a flume. The jet trajectories, dilution ratios and jet half widths were determined by conductivity measurements. The entrainment coefficient,  $\alpha$ , and drag coefficient,  $C_d$ , were found from the observed jet trajectories and dilution ratios. In the ten cases studied where jet Froude number ranged from 10 to 80 and velocity ratio (jet: current)  $k$  from 4 to 16,  $\alpha$  varied from 0.4 to 0.5 and  $C_d$  from 1.7 to 0.1. The jet mixing motion for distances within  $250D$  was found to be dominated by the self-generated turbulence, rather than the free-stream turbulence. Similarity of concentration profiles has also been discussed.

CONTENTS

<u>Chapter</u>		<u>Page</u>
I	INTRODUCTION	1
II	PREVIOUS STUDIES	7
	A. Problem of Simple Jets	7
	B. Problem of Simple Plumes	9
	C. Problem of Simple Plumes in Environments with Linear Density Stratification - Integral Analysis by Morton, Taylor and Turner	10
	D. Problem of Vertical Buoyant Jets	15
	E. Problem of Inclined or Horizontal Buoyant Jets	16
	F. On the Coefficient of Entrainment	20
	G. Problem of Jets in Streams	22
	H. Summary and Scope of Present Investigations	25
III	FLOW CONFIGURATIONS AND BASIC ASSUMPTIONS	26
	A. General Assumptions	26
	B. An Inclined Round Buoyant Jet in a Stagnant Environment with Linear Density Stratification	27
	C. A Round Buoyant Jet in a Uniform Cross Stream of Homogeneous Density	31

CONTENTS (continued)

<u>Chapter</u>		<u>Page</u>
IV	THEORETICAL ANALYSIS FOR A ROUND BUOYANT JET IN A STAGNANT ENVIRONMENT WITH LINEAR DENSITY STRATIFICATION	35
	A. Formulation of the Problem	35
	1. Conservation equations	35
	2. Geometric relations	37
	3. Initial conditions	38
	B. Normalized Equations and Dimensionless Parameters	38
	C. Method of Numerical Solution	40
	D. Solutions of Gross Behavior of Jets	41
	E. Application to Practical Problems	45
V	EXPERIMENTAL STUDY FOR A ROUND BUOYANT JET IN A STAGNANT ENVIRONMENT WITH LINEAR DENSITY STRATIFICATION	52
	A. Objectives of the Experimental Investigation	52
	B. Procedure and Apparatus	53
	C. Experimental Results	60
	1. Experiments in linearly density-stratified environments	62
	2. Experiments in uniform environments	72
	3. Experiments on simple jets	72
VI	THEORETICAL ANALYSIS FOR A ROUND BUOYANT JET IN A UNIFORM CROSS STREAM OF HOMOGENEOUS DENSITY	78
	A. Formulation of the Problem	78
	1. Conservation equations	78
	2. Geometric relations	83
	3. Initial conditions	84

CONTENTS (continued)

<u>Chapter</u>		<u>Page</u>
	B. Normalized Equations and Dimensionless Parameters	85
	C. Method of Numerical Solution	87
	D. Solutions of Gross Behavior of Jets	87
	E. Application to Practical Problems	92
VII	EXPERIMENTAL STUDY FOR A ROUND BUOYANT JET IN A UNIFORM CROSS STREAM OF HOMOGENEOUS DENSITY	96
	A. Objectives of the Experimental Investigation	96
	B. Procedure and Apparatus	97
	1. The flume and flume flows	99
	2. Modeling of the gravity effect	105
	3. The nozzles and jet flows	105
	4. Conductivity measurements and apparatus	108
	5. Correction for the change of ambient salt content	113
	6. Photographic techniques	115
	7. Towed jet experiments	115
	C. Experimental Results	116
	1. Photographs of the dyed jets	116
	2. Concentration profiles and the location of the jet axis	124
	3. Trajectories, dilution ratios, $S$ , and half widths, $r_{0.5}$	128
	4. Entrainment coefficients, $\alpha$ , and drag coefficients, $C_d'$ (or $C_d$ )	128
	5. Comparison of results for stationary and towed jet experiments	142

CONTENTS (continued)

<u>Chapter</u>		<u>Page</u>
VIII	DISCUSSION OF THE RESULTS	144
	A. A Round Buoyant Jet in a Stagnant Environment with Linear Density Stratification	144
	1. Limitations of the theoretical solutions	144
	2. Limitations of the experimental investigation	148
	3. Comparison of the theoretical and experimental results	149
	4. Coefficient of entrainment $\alpha$	149
	5. Turbulent Schmidt number $\lambda^2$ or spreading ratio $\lambda$	150
	B. A Round Buoyant Jet in a Uniform Cross Stream of Homogeneous Density	151
	1. Limitations of the theoretical solutions	151
	2. Limitations of the experimental investigation	154
	3. Determination of the entrainment coefficient $\alpha$ and the drag coefficient $C_d'$	155
	4. Comparison of theoretical and experimental results	156
	5. Effect of the ambient turbulence	157
IX	SUMMARY AND CONCLUSIONS	158
	A. Previous Knowledge about a Round Buoyant Jet in a Stagnant Environment	158
	B. Contribution of the Present Study to the Problem of a Round Buoyant Jet in a Stagnant Stratified Environment	166
	1. Theoretical predictions	166
	2. Experimental investigation	167
	C. Previous Knowledge About a Round Jet in a Uniform Cross Stream	168



CONTENTS (continued)

<u>Chapter</u>		<u>Page</u>
D.	Contribution of the Present Study to the Problem of a Round Buoyant Jet in a Uniform Cross Stream of Homogeneous Density	171
	1. Theoretical analysis	171
	2. Experimental investigations	172
	3. Values of the coefficients $\alpha$ and $C_d$	172
	4. Effect of ambient turbulence	173
	5. Concentration profiles	174
	LIST OF REFERENCES	175
APPENDIX A	SUMMARY OF NOTATIONS	180
APPENDIX B	PUBLISHED DISCUSSIONS	184

LIST OF FIGURES

<u>Number</u>	<u>Description</u>	<u>Page</u>
1	Effects of the environmental conditions on the jet behavior	4
2	Buoyant jet problems studied	5
3	A simple jet	8
4	Simple plumes in uniform and stratified environments	12
5	Comparison of results by various investigators on the variation of center-line dilution $S_0$ with vertical distance $y'/D$ for vertical buoyant jets in uniform environments	17
6	Variation of dilution ratios $S_0$ for horizontal buoyant jets in uniform environments. (Original graph by Cederwall (10), with Fan and Brooks's results added)	19
7	Schematic diagram of a round buoyant jet in a stagnant environment with linear density stratification	28
8	Schematic diagram of a round jet in a uniform cross stream	32
9	Variation of volume flux parameter $\mu$ , buoyancy flux parameter $\beta$ and vertical momentum flux parameter $v$ along $\zeta$ -coordinate for a horizontal buoyant jet with $\mu_0 = 0$ and $m_0 = 0.2$	42
10	Trajectories of inclined buoyant jets in stratified environments with $\mu_0 = 0$ , $m_0 = 0.2$	43
11	Variation of terminal height of rise of $\xi_t$ for inclined buoyant jets with $\mu_0 = 0$ to 0.01.	44
12	Variation of terminal volume flux parameter $\mu_t$ for inclined buoyant jets with $\mu_0 = 0$ to 0.01 (Note: the terminal dilution ratio $S = \mu_t/\mu_0$ )	44
13	Variation of terminal height of rise $\xi_t$ for horizontal buoyant jets ( $\theta_0 = 0^\circ$ )	46

LIST OF FIGURES (continued)

<u>Number</u>	<u>Description</u>	<u>Page</u>
14	Variation of terminal volume flux parameter $\mu_t$ for horizontal buoyant jets ( $\theta_o = 0^\circ$ )	47
15	Zone of flow establishment for an inclined buoyant jet	49
16	General experimental setup for jets in stagnant environments (Photo No. 7658.1)	54
17	Two measured density profiles	56
18	Nozzles and orifices used in the experiments	58
19	Schematic flow diagram for jet experiments in stagnant environments	59
20	A horizontal buoyant jet in a stagnant, linearly stratified environment (Jet No. 32, $F = 40$ and $T = 510$ , Photo No. 7645.4)	63
21	An inclined ( $\theta = 45^\circ$ ) buoyant jet in a stagnant, linearly stratified environment (Jet No. 18, $F = 51$ and $T = 210$ , Photo No. 7642.3)	64
22	A vertical buoyant jet in a stagnant, linearly stratified environment (Jet No. 10, $F = 18$ and $T = 100$ , Photo No. 7660)	65
23	Development of a round buoyant jet in a linearly stratified environment (Jet No. 1, $\theta_o = 45^\circ$ , $F = 9.1$ and $T = 48$ , Photo No. 7661) <sup>o</sup>	66
24	Predicted and observed trajectories and nominal boundaries of buoyant jets in linearly stratified environments for cases: a) $F = 9.1$ , $T = 48$ and $\theta_o = 45^\circ$ (Jet No. 1) b) $F = 26$ , $T = 48$ and $\theta_o = 45^\circ$ (Jet No. 2)	67
25	Predicted and observed trajectories and nominal boundaries of buoyant jets in linearly stratified environments for cases: a) $F = 21$ , $T = 107$ and $\theta_o = 43.6^\circ$ (Jet No. 11) b) $F = 13$ , $T = 110$ and $\theta_o = 2.8^\circ$ (Jet No. 12) c) $F = 20$ , $T = 106$ and $\theta_o = 39.1^\circ$ (Jet No. 15)	68

LIST OF FIGURES (continued)

<u>Number</u>	<u>Description</u>	<u>Page</u>
26	Predicted and observed trajectories and nominal boundaries of buoyant jets in linearly stratified environments for cases: a) $F = 26$ , $T = 1200$ and $\theta_o = 0^\circ$ (Jet No. 16) b) $F = 51$ , $T = 210$ and $\theta_o = 45^\circ$ (Jet No. 18) c) $F = 40$ , $T = 5000$ and $\theta_o = 0^\circ$ (Jet No. 30)	69
27	Predicted and observed trajectories and nominal boundaries of buoyant jets in linearly stratified environments for cases: a) $F = 20$ , $T = 510$ and $\theta_o = 0^\circ$ (Jet No. 31) b) $F = 40$ , $T = 510$ and $\theta_o = 0^\circ$ (Jet No. 32) c) $F = 60$ , $T = 510$ and $\theta_o = 0^\circ$ (Jet No. 33)	70
28	A horizontal buoyant jet in a stagnant, uniform environment (Jet No. 27, $F = 40$ , Photo No. 7643.5)	73
29	Predicted and observed trajectories and nominal boundaries for horizontal buoyant jets in uniform environments for cases: a) $F = 33$ (Jet No. 22) b) $F = 10$ (Jet No. 25) c) $F = 13.6$ (Jet No. 26)	74
30	Predicted and observed trajectories and nominal boundaries for horizontal buoyant jets in uniform environments for cases: a) $F = 66$ (Jet No. 23) b) $F = 130$ (Jet No. 24) c) $F = 40$ (Jet No. 27)	75
31	Dilution ratio $S_o$ along the axis of a simple jet ( $R \sim 6,000$ )	77
32	Schematic diagram for the analysis of a round buoyant jet in a cross stream	79
33	Variation of volume flux parameter, $\mu$ , and momentum flux parameter, $m$ , along $\zeta$ -coordinate for a buoyant jet in a uniform cross stream with $k = 4$ and $f = 0.00269$ (for $\alpha = 0.5$ , $F = 20$ )	88

LIST OF FIGURES (continued)

<u>Number</u>	<u>Description</u>	<u>Page</u>
34	Variation of volume flux parameter, $\mu$ , and momentum flux parameter, $m$ , along $\zeta$ -coordinate for a buoyant jet in a uniform cross stream with $k = 8$ and $f = 0.00103$ (for $\alpha = 0.4$ , $F = 40$ )	89
35	Variation of the ratio of the jet center-line velocity, $U_j$ , and jet discharge velocity $U_o$ along $\zeta$ -coordinate for buoyant jets in uniform cross streams	90
36	Trajectory of a buoyant jet in a uniform cross stream with $k = 4$ and $f = 0.00269$ (for $\alpha = 0.5$ , $F = 20$ )	91
37	Definition sketch and measured trajectories for the zone of flow establishment ( $O' \rightarrow O$ ) of round jets in cross streams at $k = 4, 6$ and $8$	93
38	Values of $s_e'/D$ , length of the zone of flow establishment, as a function of $1/k$ for jets in uniform cross streams	94
39	Initial angle $\theta_o$ as a function of $1/k$ for jets in uniform cross streams	94
40	General experimental setup for buoyant jets in cross streams (Photo No. 7651.1)	100
41	The 40-meter precision tilting flume (from Vanoni (34), p. 7)	101
42	A measured velocity distribution in flume (cross section looking downstream)	101
43	The location of the jet discharge point $O'$ relative to the flume center line and the region assumed to affect the jet flow (shaded zone). The values shown are percentage deviations from the average velocity $U_a$ when at $19.2$ cm/sec	103
44	Schematic flow diagram of buoyant jet experiments in flowing environments	106
45	The constant head tank and the jetting box (Photo No. 7651.4)	107
46	The instrument carriage, the tilting point gage and the probe (Photo No. 7651.3)	107

LIST OF FIGURES (continued)

<u>Number</u>	<u>Description</u>	<u>Page</u>
47	The conductivity probe (From Koh (19), p. 57)	109
48	The bridge circuit used in conjunction with the Sanborn recorder for the measurement of the conductivity (From Koh (19), p. 59)	110
49	Typical calibration curves of the conductivity probe	112
50	A sample of the record of the concentration measurements (Run 20-4, $s_e'/D = 9.5$ and $\frac{s_e'}{D} = 123$ )	114
51	Buoyant jets in cross streams with $F = 20$ at various velocity ratios $k = 4, 6$ and $8$ (Photo No. 7662)	119
51	Buoyant jets in cross streams with $F = 20$ at various velocity ratios $k = 12$ and $16$ (Photo No. 7663)	120
52	Buoyant jets in cross streams with $k = 8$ at various Froude numbers $F = 10, 20$ and infinity (Photo No. 7664)	121
53	Buoyant jets in cross streams with $k = 16$ at various Froude numbers $F = 20, 40$ and infinity (Photo No. 7665)	122
54	Buoyant jets in cross streams with $F = 40$ at velocity ratio $k = 8$ and $12$ (Photo No. 7666)	123
55	Stationary and towed buoyant jets for the case $F = 80$ and $k = 16$ (Photo No. 7667)	125
56	Two measured concentration profiles for the case $F = 20$ and $k = 4$ (0.76 cm orifice)	126
57	A complete concentration profile for the case $F = 20$ and $k = 8$ (0.76 cm orifice)	127
58	A complete concentration profile for the case $F = 40$ and $k = 8$ (0.76 cm orifice)	127
59	Normalized concentration distribution on the plane of symmetry	129

LIST OF FIGURES (continued)

<u>Number</u>	<u>Description</u>	<u>Page</u>
60	Comparison of observed and theoretical trajectory, half widths, $r_{0.5}/D$ , and center-line dilution ratios, $S$ , of a buoyant jet in a uniform cross stream.	
	a) $F = 10$ and $k = 4$	130
	b) $F = 10$ and $k = 8$	131
	c) $F = 20$ and $k = 4$	132
	d) $F = 20$ and $k = 8$	133
	e) $F = 20$ and $k = 12$	134
	f) $F = 40$ and $k = 4$	135
	g) $F = 40$ and $k = 8$	136
	h) $F = 40$ and $k = 12$	137
	i) $F = 40$ and $k = 16$	138
	j) $F = 80$ and $k = 16$	139
61	Variations of the entrainment coefficient $\alpha$ and the reduced drag coefficient $C_d'$ for a buoyant jet in a uniform cross stream	141
62	Types of buoyant jet flows in stagnant, density-stratified environments	146

LIST OF TABLES

<u>Number</u>	<u>Description</u>	<u>Page</u>
1	Summary of Experiments on Round Jets in Stagnant Environments	61
2	Terminal Heights of Rise $y_t'/D$ of Vertical Buoyant Jets in Linearly Stratified Environments	71
3	Deviation from Ambient Mean Velocity $U_a$ in the Shaded Zone Shown in Fig. 43	104
4	Summary of Buoyant Jet Experiments in Flowing Environments	117
5	Values of the Entrainment Coefficients, $\alpha$ , and Drag Coefficients, $C_{d1}'$ and $C_{d1}$ , Determined from the Experimental Results	140
6	A Brief Summary of Studies on Jets in Stagnant Environments	159
7	A Brief Summary of Studies on Jets in Cross Streams	169



## CHAPTER I

### INTRODUCTION

Disposal of sewage into the ocean and lakes has been practiced by many coastal cities around the world. Inadequate dispersal of the pollutants has often resulted in serious contamination of the coastal areas. Controlling of such pollution problems relies on a clear understanding of the basic flow phenomena involved.

The recent practice of marine disposal is to discharge the sewage effluent in jets through numerous ports widely spaced along the ocean outfall diffusers deep under the surface into the environment as indicated by Rawn, Bowerman and Brooks (27) and Brooks (7). The initial mixing of the sewage effluent with the sea water is induced by the turbulent jet motion. The basic flow phenomenon can be regarded as a submerged turbulent jet.

The simplest case of such turbulent jet flows is an ordinary momentum jet (or a simple jet) where the fluids involved are of identical density. But in marine disposal problems, the following environmental conditions must be taken into consideration:

1. Buoyancy effect

The density of the sewage effluent is different from the density of the sea water or brackish estuary water. Since sewage effluent has nearly the same density as fresh water, it is about 2.5% lighter than sea water. Although the difference is small, the buoyancy effect on the jet behavior is drastic. For example, a jet discharging horizontally (or obliquely) into a heavier fluid will be

deflected upwards. Such a jet, which has initial buoyancy flux as well as the momentum flux, is called a buoyant jet (or forced plume). The limiting case where the flow is generated solely by buoyancy flux is called a simple plume.

Buoyant jets are also produced in fresh water lakes by discharge of warm water used for cooling in industrial processes and steam generation of electric power.

## 2. Density stratification

Oceans and lakes are frequently stratified in density due to non-uniform temperature and/or salinity. In a stably stratified ocean, it is possible to prevent rising sewage jets from reaching the surface by inducing rapid mixing of the buoyant jets with heavy bottom water, thus producing a neutrally buoyant cloud (Brooks (7)). The submergence of the sewage field is often the most favorable situation for pollution control. To be able to predict the conditions for the submergence of the jet flow field and the dilution in the cloud produced is of great importance in problems of disposal of waste water.

## 3. Current effect

The ocean, like the atmosphere, is seldom stagnant. The ocean currents and regular tidal motions affect not only the movement of the sewage field established at or near the surface, but also the initial jet mixing characteristics. The waste gas disposal through smoke stacks is a similar problem. The effect can not be overlooked even if the current velocity is only a fraction of the jet discharge velocity.

Schematic diagrams demonstrating these environmental effects are shown in Fig. 1. These three effects are considered to be the most important in considering the jet behavior. Two other factors are described below.

4. Ambient turbulence

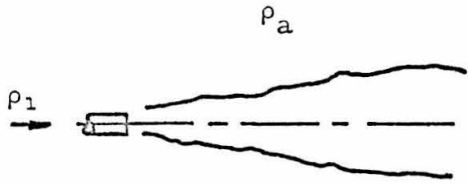
Turbulence in the environment also affects the jet behavior. However, the effects on initial jet mixing are believed to be of secondary importance unless the jet motion is relatively weak. There is little information on this subject.

5. Jet interference

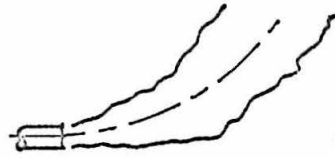
When jets are closely spaced in a row they will gradually merge as they spread. For example, a row of round jets behaves like a jet from a two-dimensional slot far away from the source. Interference effects may be anticipated by prediction of the rate of growth of the diameter of a jet.

It is difficult to solve a general problem including all these factors. Buoyant jet (or plume) problems have been under extensive studies by investigators from various fields (see Chapter II). The present investigation seeks solutions for two specific classes of buoyant jet problems:

- 1) an inclined round buoyant jet (or forced plume) in a stagnant environment with linear density stratification as shown in Fig. 2a,
- 2) a round buoyant jet discharging vertically into a uniform horizontal wind (or cross stream) of homogeneous density, as shown in Fig. 2b.

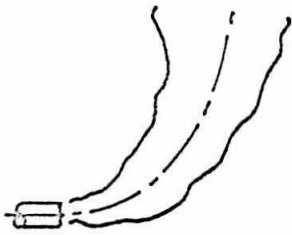


No density difference  
( $\rho_1 = \rho_a$ )

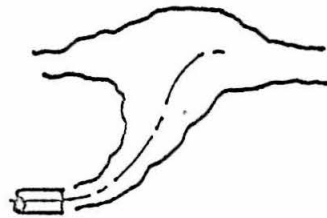


With density difference  
( $\rho_1 < \rho_a$ )

Buoyancy Effect

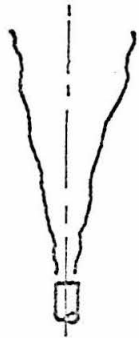


Homogeneous  
( $\rho_a = \text{constant}$ )



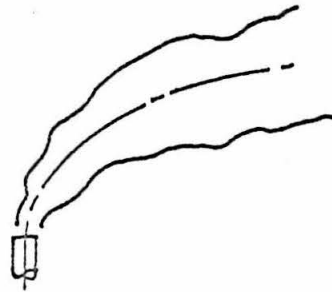
Stratified  
( $\rho_a \neq \text{constant}$ )

Stratification Effect



Stagnant  
( $U_a = 0$ )

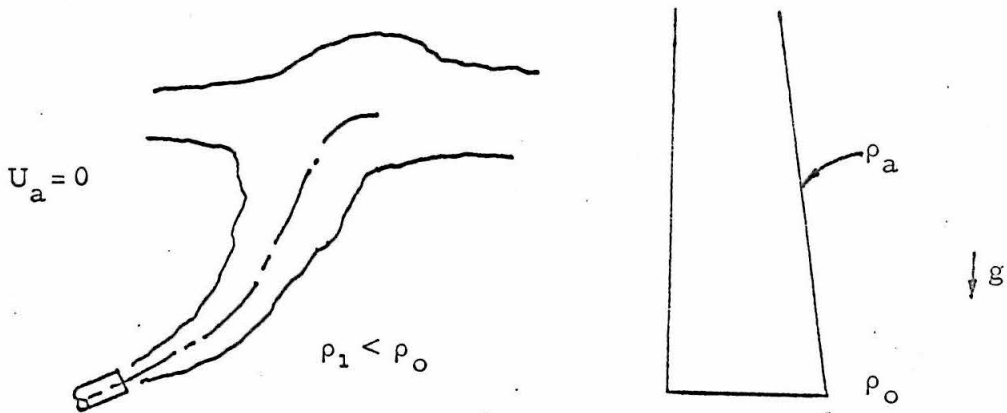
$U_a$



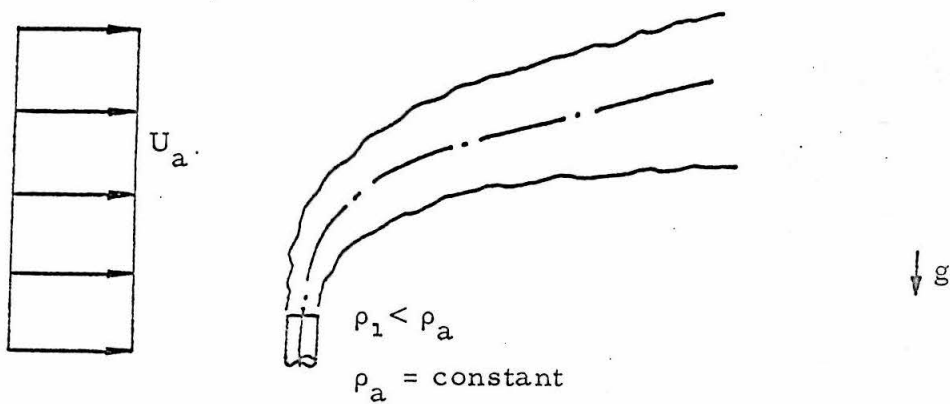
With current  
( $U_a \neq 0$ )

Current Effect

Fig. 1. Effects of the environmental conditions on the jet behavior



- a) An inclined round buoyant jet (forced plume) in a stagnant environment with linear density-stratification



- b) A vertical round buoyant jet in a uniform horizontal wind (cross stream)

Fig. 2. Buoyant jet problems studied

The solutions on jet behavior will be useful not only to the marine disposal problems but also to the problems of a similar nature such as the disposal of hot waste gases into the atmosphere or hot water from a thermal power plant into a lake.

Previous studies related to the buoyant jet problems are described in Chapter II.

Chapter III gives a summary of the basic assumptions and flow configurations for both classes of problems.

Chapters IV and V are respectively theoretical and experimental investigations of the problem of an inclined buoyant jet in a stagnant, stratified environment.

Chapters VI and VII are the corresponding studies on the problem of a buoyant jet in a uniform cross stream.

The results are discussed in Chapter VIII. Chapter IX gives a summary of the present work and conclusions.

## CHAPTER II

### PREVIOUS STUDIES

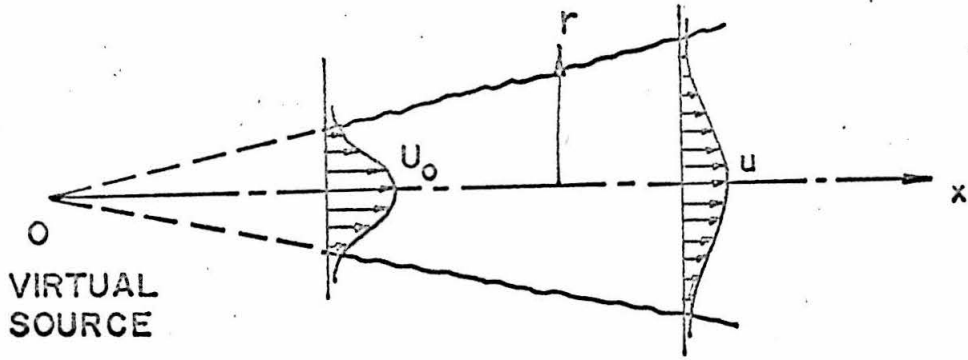
In this chapter, a survey of previous studies on jet and plume problems is presented. The integral technique used by Morton, Taylor and Turner (23) in solving the problem of a simple plume in a linearly density-stratified environment is briefly illustrated in Section II-C. The nature of the entrainment coefficient  $\alpha$  is discussed in Section II-F. The scope of the present investigation is summarized in Section II-H.

#### II-A. Problem of Simple Jets

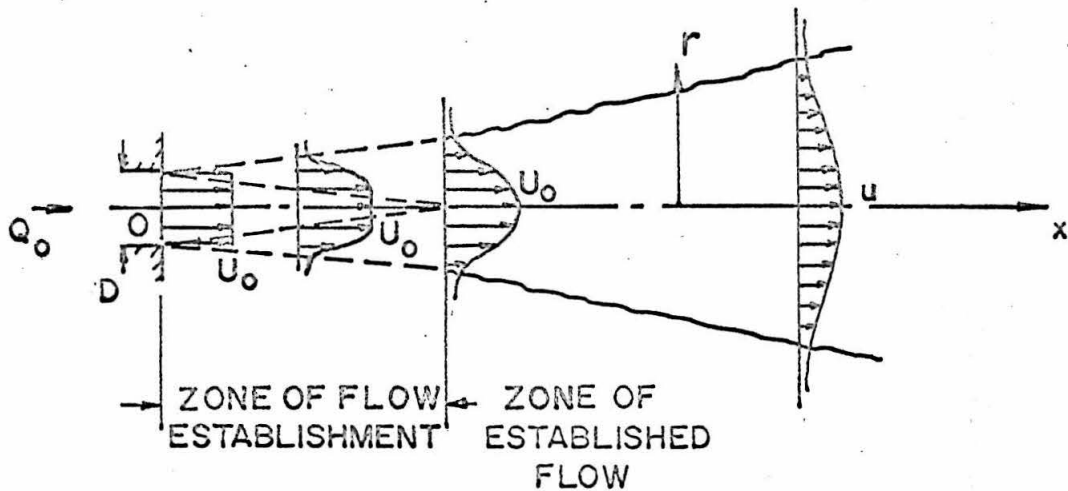
A simple jet (or an ordinary momentum jet) is the turbulent flow pattern generated by a continuous source of momentum as shown in Fig. 3a. This is one of the most fundamental cases of free turbulent flows. The details of the flow have been determined by numerous investigators.

Experimental results by Albertson, Dai, Jensen and Rouse (5) demonstrated the similarity of velocity profiles and linear expansion of nominal jet boundary ( $b \sim x$ ). The velocity profile was shown to follow a Gaussian distribution closely. The center-line longitudinal velocity  $u$  was found to be inversely proportional to the distance of travel  $x$  ( $u \sim x^{-1}$ ), and gross volume flux  $Q$  over a cross section increased linearly with  $x$ , i. e.,

$$u \sim \bar{x}^{-1}$$
$$b \sim x$$
$$ub^2 \sim x$$
$$u^2 b^2 = \text{CONSTANT}$$



A) CONCEPT OF A VIRTUAL SOURCE



B) ZONE OF FLOW ESTABLISHMENT AND ZONE OF ESTABLISHED FLOW (AFTER ALBERTSON ET AL.(4))

Fig. 3. A simple jet (axisymmetric case)



$$\frac{Q}{Q_0} = 0.32 \frac{x}{D} \quad (1)$$

where  $Q_0$  is the initial volume flux at the nozzle, and

$D$  is the diameter of the nozzle as shown in Fig. 3b.

Other studies concerning the problem gave the same relations.

Ricou and Spalding's (29) measurement of entrainment into the jet confirmed eq. (1).

In a practical problem, the jet flow originates from a finite size nozzle with a column flow of uniform velocity. A short region, the so-called zone of flow establishment, exists before the velocity profiles develop fully into Gaussian distributions. The fully developed region is called the zone of established flow as shown in Fig. 3b. The length of the zone of flow establishment is approximately 6.2 diameters of the nozzle based upon Albertson et al's result. A recent work by Sami, Carmody and Rouse (31) gives detailed flow characteristics in the zone of flow establishment.

## II-B. Problem of Simple Plumes

A simple plume is the turbulent flow pattern generated by a continuous source of buoyancy such as caused by a steady release of heat. The main direction of flow is in the direction of buoyancy force. The plume has no initial momentum flux. Due to continuous action of the buoyancy force, the momentum flux of the plume increases with increasing height.

In separate studies by Schmidt (32) and Rouse, Yih and Humphreys (30), the velocity profiles as well as the buoyancy profiles were found to be similar at all cross sections. Both studies showed that the center-line velocity followed negative one-third power of the distance of travel ( $u \sim y^{-1/3}$ ) and the expansion of the nominal boundary was linear with distance ( $b \sim y$ ). The velocity and buoyancy profiles can be represented well by Gaussian distributions as pointed out by Rouse et al.

The experimental values of Schmidt were obtained by measurements over heated grids with an overall diameter of 5.5 cm at levels up to 80 cm above. Rouse et al. covered longer distances by measuring over a gas flame and their results were later confirmed by Ricou and Spalding (29). Therefore the numerical values determined by Rouse et al. are considered to be more reliable and adopted by most investigators such as Morton (22), Abraham (1,3) and Fan and Brooks (12) in their studies.

### II-C. Problem of Simple Plumes in Environments with Linear Density Stratification - Integral Analysis by Morton, Taylor and Turner

If a plume is in a stably stratified environment it will not rise indefinitely as a plume in a uniform environment as shown in Fig. 4. The mixing near the source makes the plume denser while density of the ambient fluid decreases steadily upwards. Eventually the buoyancy force acting on the plume will change sign and become negative. The plume will stop rising when the upward momentum vanishes

by the action of the negative buoyancy force. Thus the plume has a finite height of rise and will then spread out horizontally in a thin layer.

Morton, Taylor and Turner (23) analyzed the problem by applying an integral technique as follows based upon the following three assumptions:

1) The profiles of mean vertical velocity  $u^*(y, r)$  and mean buoyancy force  $g \frac{\rho_a - \rho^*}{\rho_o}$  in horizontal sections are of similar form:

$$u^*(y, r) = u(y) e^{-r^2/b^2} \quad (2)$$

and

$$g \frac{\rho_a - \rho^*}{\rho_o} (y, r) = g \frac{\rho_a - \rho}{\rho_o} (y) e^{-r^2/b^2} \quad (3)$$

where  $u$  is a local characteristic velocity,

$b$  is a local characteristic length,

$\rho$  is the local characteristic density,

$\rho_o$  is the reference density.

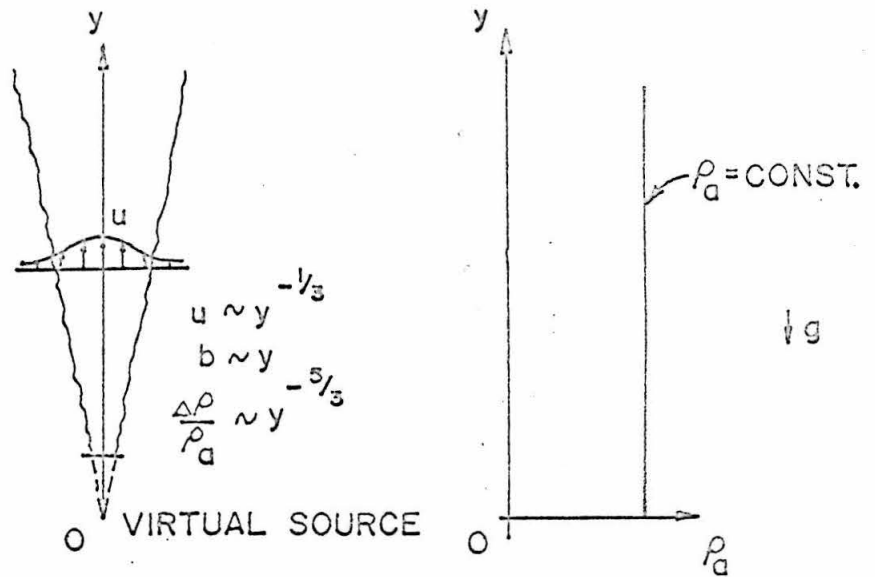
2) The rate of entrainment at the edge of the plume is proportional to some characteristic velocity at that height:

$$\frac{dQ}{dy} = 2\pi \alpha u b \quad (4)$$

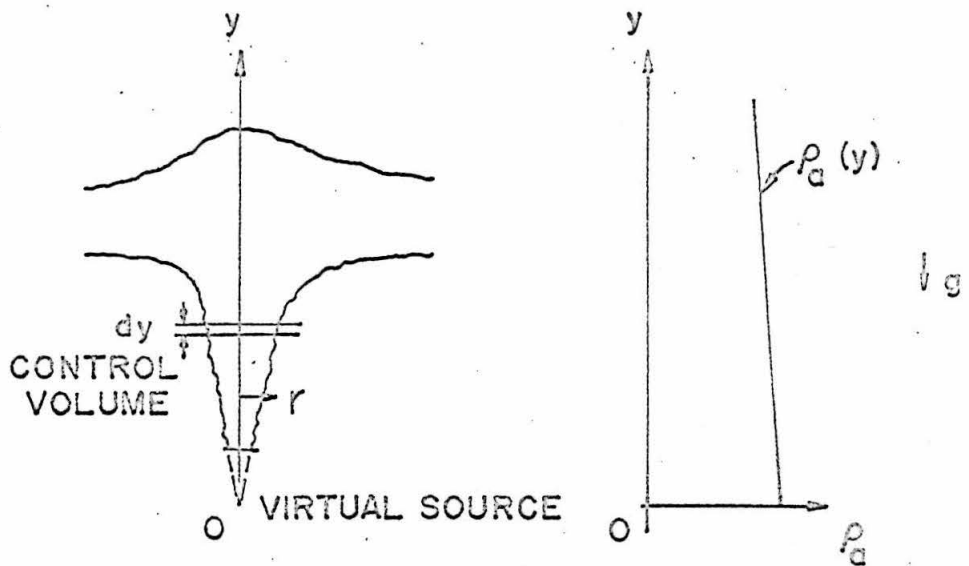
where  $\frac{dQ}{dy}$  is the rate of change of volume flux, and

$\alpha$  is defined to be an entrainment coefficient assumed to be constant in the analysis.

3) The variation of density is small in comparison with the reference density  $\rho_o$ .



A) A SIMPLE PLUME IN A UNIFORM ENVIRONMENT



B) A SIMPLE PLUME IN A LINEARLY STRATIFIED ENVIRONMENT

Fig. 4. Simple plumes in uniform and stratified environments

The problem was then formulated by taking a control volume as shown in Fig. 4b and applying conservation laws:

1. Conservation of volume flux:

$$\frac{d}{dy} \int_A u^* dA = \frac{dQ}{dy} \quad (5)$$

By substituting eqs. (2) and (4), eq. (5) becomes:

$$\frac{d}{dy} \int_0^{\infty} 2\pi r u e^{-r^2/b^2} dr = \frac{d}{dy} \pi u b^2 = 2\pi \alpha u b \quad (6)$$

2. Conservation of momentum:

$$\frac{d}{dy} \int_A \rho^* u^{*2} dA = \int_A (\rho_a - \rho^*) g dA \quad (7)$$

Since the variation of density with respect to the reference density  $\rho_o$  is assumed to be small,  $\rho^*$  in the left-hand side of eq. (7) is taken to be approximately  $\rho_o$ . Thus, by applying eqs. (2) and (3), eq. (7) becomes:

$$\frac{d}{dy} \frac{\pi u^2 b^2}{2} = \pi g b^2 \frac{\rho_a - \rho}{\rho_o} \quad (8)$$

3. Conservation of density deficiency:

The rate of change of heat (or salt deficiency) flux through a cross section of the plume is equal to the amount entrained from the ambient fluid. Since the variation of density was assumed to be small, in this range the density could be regarded as a linear function of the heat or salt content. Therefore the relation was indirectly expressed

as conservation of the density deficiency:

$$\frac{d}{dy} \int_A (\rho_o - \rho^*) u^* dA = 2\pi\alpha bu(\rho_o - \rho_a) \quad (9)$$

The left-hand side was integrated as

$$\begin{aligned} & \frac{d}{dy} \int_A \left[ (\rho_o - \rho_a) u^* + (\rho_a - \rho^*) u^* \right] dA \\ &= \frac{d}{dy} \left[ (\rho_o - \rho_a) \pi u b^2 + \frac{\pi}{2} u b^2 (\rho_a - \rho) \right] \\ &= (\rho_o - \rho_a) \frac{d}{dy} (\pi u b^2) - \pi u b^2 \frac{d\rho_a}{dy} + \frac{d}{dy} \left[ \frac{\pi}{2} u b^2 (\rho_a - \rho) \right] \\ &= 2\pi\alpha bu (\rho_o - \rho_a) - \pi u b^2 \frac{d\rho_a}{dy} + \frac{d}{dy} \left[ \frac{\pi}{2} u b^2 (\rho_a - \rho) \right] \end{aligned}$$

Therefore eq. (9) becomes:

$$\frac{d}{dy} \left[ \frac{\pi}{2} u b^2 (\rho_a - \rho) \right] = \pi u b^2 \frac{d\rho_a}{dy} \quad (10)$$

Eqs. (6), (8) and (10) are three equations with three unknowns  $u$ ,  $b$  and  $\rho$ . The equations were normalized by introducing dimensionless volume, momentum and buoyancy flux parameters and then solved numerically.

The coefficient of entrainment  $\alpha$  was assumed to be constant. Gross behavior of the plume was determined by such integral technique. The technique has been adopted by many later investigators in solving jet and plume problems. The present investigation is also based upon

such technique in solving more general buoyant jet problems (see Chapters IV and V). The basic assumptions are summarized in Chapter III.

#### II-D. Problem of Vertical Buoyant Jets

If the flow is generated from a continuous source not only of buoyancy but also of initial momentum, then it is called a "buoyant jet" (or forced plume). The simple jet and simple plume are thus the two limiting cases of buoyant jets. In a homogeneous environment the vertical momentum flux will increase with the distance of travel because of the action of buoyancy forces.

Morton (22) analyzed the problem using the same technique mentioned in Section II-C by assuming a constant coefficient of entrainment. Abraham (1) obtained the jet gross behavior by setting up a scheme successively approximating the growth rate of the jet width as to match the limiting conditions of a simple jet and a simple plume. Frankel and Cumming (14) made concentration measurements in the buoyant jets and thus determined the center-line dilution ratios  $S_0$  along the jet axis.

Morton constructed the solutions from a virtual source, while in practical cases a jet is discharged through a finite size opening. A convenient parameter of the problem is the jet Froude number  $F$  defined as:

$$F = \frac{U_0}{\sqrt{\frac{\rho_a - \rho_1}{\rho_a} g D}} \quad (11)$$

where  $U_0$  is the initial jet discharge velocity,

$\rho_1$  is the initial jet discharge density,

$\rho_a$  is the ambient density,

$D$  is the initial diameter of the jet.

In order to compare Morton's type of analysis with Abraham's, integral solutions were carried out by the writer for vertical buoyant jets, following exactly the same approach of Fan and Brooks (12, see Appendix B-2). Fig. 5 shows the volumetric dilution ratio  $S_0$  (i. e. the inverse of the concentration of original jet fluid in the mixture) as a function of the ratio of the height of rise  $y'$  to the initial diameter  $D$  for several values of  $F$ . Also shown are theoretical curves by Abraham, and experimental curves by Frankel and Cumming, as previously presented by Fan and Brooks (11).

In a stably stratified environment a buoyant jet, like a plume, will not rise indefinitely. Morton (22) analyzed the problem of a vertical axisymmetrical jet in a linearly density-stratified ambient fluid. The corresponding two-dimensional case was solved by Brooks and Koh (8), and the results were applied to predict behavior of jets of sewage effluent from a diffuser into a density-stratified ocean.

#### II-E. Problem of Inclined or Horizontal Buoyant Jets

In many practical problems a buoyant jet is not discharged vertically. For example, in ocean disposal the common practice is to discharge sewage out horizontally, or sometimes in an inclined direction. Such inclined buoyant jets will take a curved path due to combined effects of gravity and initial horizontal momentum. Thus the trajectory of the jet becomes part of the solution to be determined.



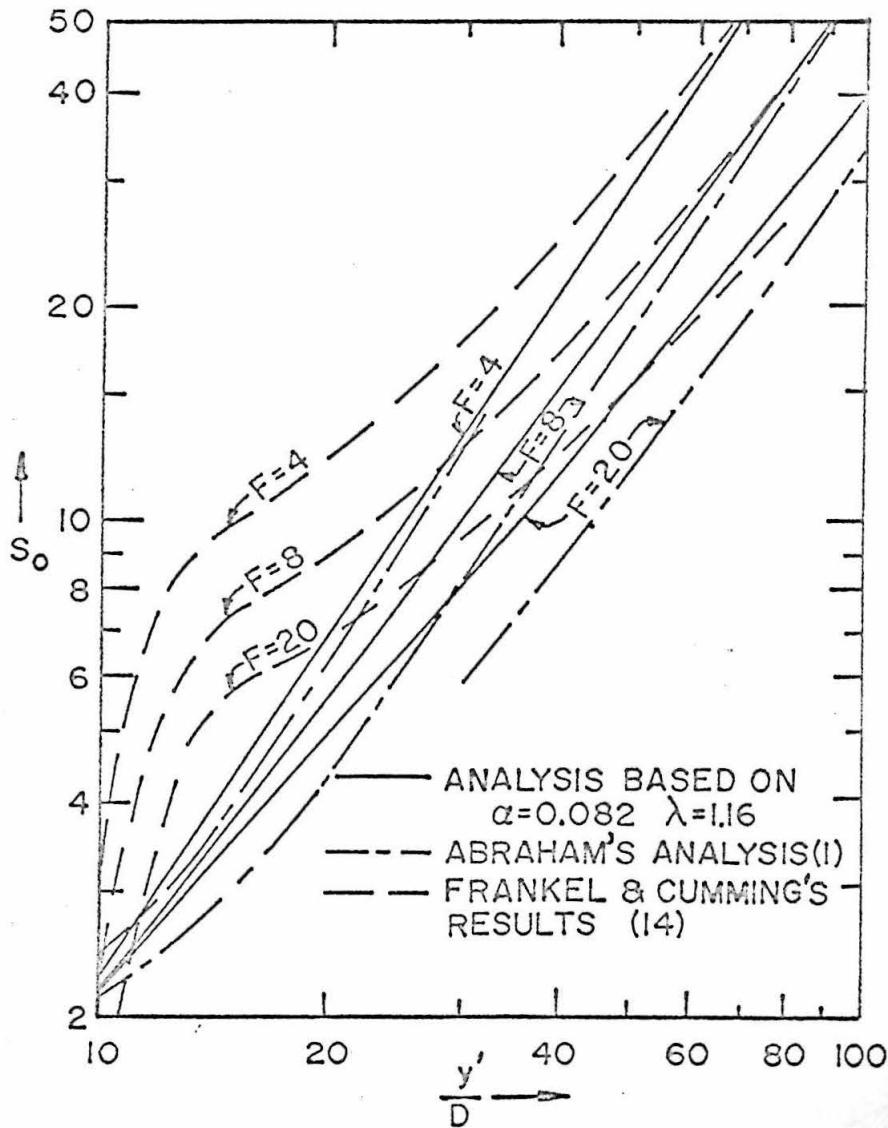


Fig. 5. Comparison of results by various investigators on the variation of center-line dilution  $S_0$  with vertical distance  $y'/D$  for vertical buoyant jets in uniform environments

Rawn, Bowerman and Brooks (27) obtained the variation of center-line dilution after the jet has reached the free surface as a function of initial Froude number  $F$  and vertical distance ratio  $y'/D$ . Bosanquet, Horn and Thring (6) determined the trajectories by explicitly using the entrainment relation of an ordinary momentum jet. Abraham (1, 2) obtained solutions covering jet gross behavior by specifying the rate of growth of jets as functions of local angle of inclination. However, his study did not include inclined jets of arbitrary initial angle of discharge. Frankel and Cumming (14) made measurements of center-line concentration for jets of various degrees of inclination. Both results of Abraham, and Frankel and Cumming were discussed by Fan and Brooks (12, 13, see Appendix B). Fan and Brooks (12) also carried out a Morton type of analysis by assuming a constant coefficient of entrainment. All these results for a horizontal buoyant jet are compared as shown in Fig. 6 along with analytical and experimental results by Cederwall (10). The experimental results of Danish Isotope Center were based on those cited by Cederwall. Both Abraham's and Cederwall's analytical results collapsed into single curves by choosing dimensionless parameters as shown in the same figure. Fan and Brooks's results seemed to agree with the experimental data better, but their curves do not collapse as in the other analyses.

All these investigations were limited to buoyant jets in uniform environments.

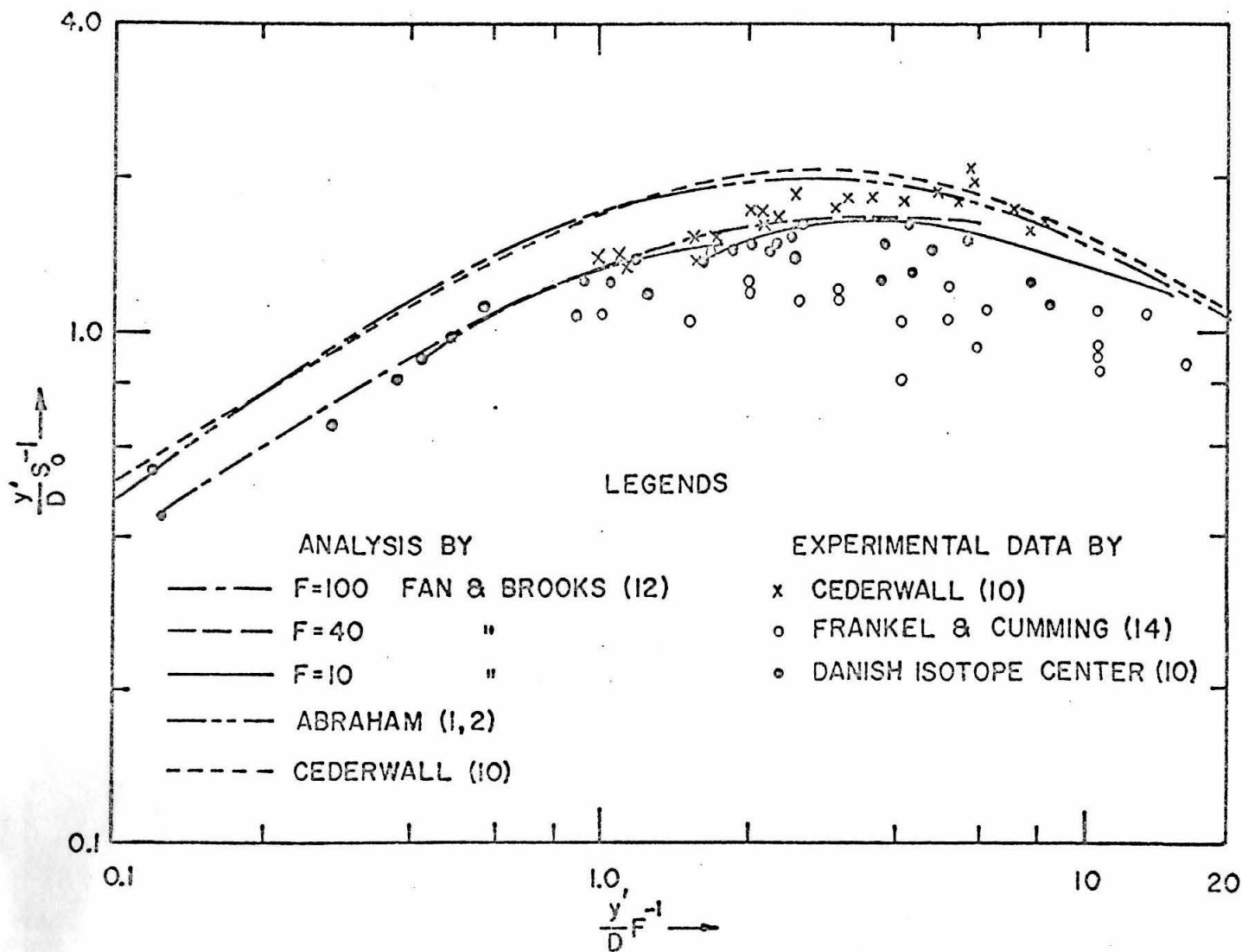


Fig. 6. Variation of dilution ratios  $S_0$  for horizontal buoyant jets in uniform environments. (Original graph by Cederwall (10), with Fan and Brooks's results added.)

## II-F. On the Coefficient of Entrainment

A crucial problem in determining buoyant jet behavior by the integral technique is to specify the rate of entrainment. Morton et al. (23) first proposed an entrainment mechanism represented by eq. (4). They assumed a constant coefficient of entrainment  $\alpha$  in their analysis.

For a simple jet, the coefficient  $\alpha$  is constant and equal to 0.057 according to Albertson et al.'s (5) results. For a simple plume, the coefficient is also a constant but equal to a different value of 0.082 based upon Rouse et al.'s (30) results. Therefore, the coefficient of entrainment cannot be a universal constant. The difference in these two values leads to an important question whether the coefficient can be assumed constant in analyzing buoyant jet problems.

Abraham (1, 2, 3) argued that such an assumption cannot hold since a buoyant jet should behave more like a momentum jet near the source and like a plume at large distances. He bypassed the continuity relation and solved the problems by explicitly assuming the rate of growth relations so as to match both limiting cases of a simple jet and a simple plume. Such relations were arbitrary in the intermediate range and complicated in application to more general problems. The results obtained showed little difference from those by assuming a constant  $\alpha$  value of 0.082 as shown in Figs. 5 and 6. In fact, as shown in Fig. 6, the experimental data seem to agree with Fan and Brooks's (12) analysis better than Abraham's.

At present there is no direct determination on the rate of entrainment into a buoyant jet. The existing experimental results seem to justify the assumption of a constant entrainment coefficient. It is probably a reasonable approximation and consistent with numerous other assumptions made throughout the analysis (see Chapter III). However, the choice of the value of  $\alpha$  is important. For a simple jet an  $\alpha$  value of 0.057 must be used; but for a simple plume or a buoyant jet a value of 0.082 is adequate. The numerical value of  $\alpha$  depends also on the shape of velocity and buoyancy profiles assumed. For example, if a top-hat profile is assumed, a factor of  $\sqrt{2}$  must be multiplied to the above values of  $\alpha$  as pointed out by Morton et al.

A similar assumption was found to hold in Lee and Emmons's (20) study of two-dimensional buoyant jets. Their analysis using a constant coefficient of entrainment based upon Rouse et al.'s results agreed well with their experimental data.

In a stratified environment, the assumption of a constant coefficient of entrainment is a further approximation. Grigg and Stewart (16), by observing the mixing and depth of penetration of cylinders of fluid injected into both uniform and weakly density-stratified environments, found that the smaller scale motions such as lateral spread of the puff were little affected by the ambient stratification. The effect of density stratification was almost entirely upon the large scale motion such as the depth of penetration. Thus the use of an

entrainment coefficient for a buoyant jet in a density-stratified environment is reasonable. But the analysis based on such an assumption should be verified experimentally.

## II-G. Problem of Jets in Streams

The solution of the problem of an ordinary momentum jet in a coflowing uniform stream is a simple extension of the solution of a simple jet in a stagnant ambient fluid. Morton (21) analyzed the problem of buoyant jets in uniform coflowing streams using the integral technique assuming a constant coefficient of entrainment.

The most general problem of a buoyant jet in a uniform stream will involve three vector quantities; namely, initial momentum flux, gravity, and the ambient current. It is thus very complicated. Therefore, as a first step, a special case where the jet discharging at a right angle into a uniform stream is investigated.

The trajectory of a jet into a cross stream will bend over toward the downstream direction due to the combined effects of the entrainment of horizontal momentum and the presence of pressure field induced by the interaction of the jet and the oncoming stream.

Jordinson (17) measured total head distributions within jets into cross streams of different velocity ratios 4, 6 and 8. Here the velocity ratio  $k$  is defined as the ratio between the initial jet discharge velocity  $U_o$  and the oncoming stream velocity  $U_a$ . Grdier (15), conducting experiments in a water tunnel, measured total and static head distributions for velocity ratios 4, 6 and 8. Trajectories and

decay of maximum velocity were determined for these velocity ratios. The decay of velocity was found to be much faster than in the jet in a stagnant fluid. Keffer and Baines (18) carried out experiments in a wind tunnel using hot wire technique to measure the velocity distribution as well as some turbulence characteristics for the cases of velocity ratios of 2, 4, 6, 8 and 10. The mean velocity distribution in the lateral direction was found to be similar if the proper length scale was chosen. The jet flows were found to display similarity along the natural system of axes. Trajectories of these cases were obtained as well as the decay of maximum velocity.

All these measurements were conducted quite close to the orifice because of the rapid decay of the velocity excess. Methods had been devised to eliminate the effect of the boundary layer. One important characteristic of such flows that was observed in all these studies was the horse-shoe shaped distribution of velocity at a cross section. Keffer and Baines analyzed the problem by the integral type approach assuming an entrainment mechanism based upon the scalar difference of local maximum velocity and the free stream velocity. The coefficient of entrainment thus defined was found to be variable and grew with distance of travel from their experimental results.

Some other investigations with specific interest in trajectories of the jet were made by Callaghan and Ruggeri (9) and some Russian studies cited by Abramovich (4). Some empirical relations were derived either for the depth of penetration or trajectory including the

effect of initial density difference. Callaghan and Ruggeri performed their experiments in a rather narrow wind tunnel with a width of eight diameters or less. Viesel and Mostinskii (35) obtained analytical expressions for the jet trajectories by assuming that the jet was bent over entirely due to the effect of forces acting on the jet as if it were an airfoil. But their values for the drag coefficients had to be larger than those for a solid body for the trajectories to fit the experimental results.

Priestley (26) presented some methods in predicting the trajectories of smoke plumes in winds. He assumed that the plume rose vertically and was then sheared over by the horizontal wind. The height of rise was found to follow the  $3/4$ th power of horizontal distance far from the source. Csanady (11) studied the behavior of a smoke plume at large distance where the plume, as he suggested, should be similar to a line thermal. Perturbation technique was used to analyze the laminar case which he suggested to be analogous to the turbulent case if the correct rate of growth of the cloud was assessed. A vortex pair structure was found from the analysis with a temperature excess of 28% at the centers of the vortices in comparison with the temperature at the center of the plume. Turner (33) analyzed the behavior of a buoyant vortex pair and found that the rate of spreading of the pair was exponential with the height or linearly with the distance downwind. He also studied the case in a linearly stratified environment.



## II-H. Summary and Scope of Present Investigation

The first part of the present study is intended to analyze the gross behavior of an inclined buoyant jet in a stagnant, stratified environment with linear density gradient. Such study will be an extension of the existing knowledge on buoyant jets and should be useful in many practical problems. Experimental studies were carried out in a tank to confirm the analysis.

The second part of this study is concerned with a vertical buoyant jet in a horizontal current, analyzed by the integral approach to predict gross behavior. Experimental studies were carried out to verify the analysis and provide numerical constants involved in the analysis. Effects of ambient turbulence and different angles of discharge are not included in the investigation.

## CHAPTER III

### FLOW CONFIGURATIONS AND BASIC ASSUMPTIONS

In this chapter, the assumptions involved in the analyses are summarized. The general assumptions common to both classes of problems are presented first. The next two sections give the flow configurations and specific assumptions for each of the two types of problems, namely (1) an inclined buoyant jet in a stagnant, stratified environment with linear density gradients, and (2) a vertical buoyant jet in a uniform cross stream.

#### III-A. General Assumptions

The general assumptions underlying the analyses made in this investigation are listed as follows:

1. The fluids are incompressible.
2. Variations of fluid density throughout the flow field are small compared with the reference density chosen. The variation of density can be neglected in considering inertial terms but it must be included in gravity terms. Since the variation in density is assumed small, this leads to the approximation that the conservation of mass flux can be replaced by the conservation of volume flux. This is commonly called the Boussinesq assumption.
3. Within the range of variation the density of the fluid is assumed to be a linear function of either salt concentration or heat content above the reference level.

4. Flow is fully turbulent. Molecular transports can be neglected in comparison with turbulent transports. There is no Reynolds number dependence.

5. Longitudinal turbulent transports are small compared with longitudinal convective transports.

6. Curvature of the trajectory of the jet is small. In other words, the ratio of local characteristic length and the radius of curvature is small. The effect of curvature will be neglected.

7. The velocity profiles are similar at all cross sections normal to the jet trajectory. Similarity is also presumed for profiles of buoyancy and concentration of any tracer. The specific forms of the profiles are given in the next two sections. Thus, the analyses apply only to the zone of established flow where all the profiles are fully developed. However, for practical applications, the initial conditions must be adjusted to take account of the zone of flow establishment, as discussed later in Chapters IV and VI.

### III-B. An Inclined Round Buoyant Jet in a Stagnant Environment with Linear Density Stratification

Fig. 7 shows a round buoyant jet issuing from the origin at an angle of inclination  $\theta_0$  with the horizontal. The axis of the jet is taken as a parametric coordinate axis  $s$ . The angle between the  $s$ -axis and the horizontal is denoted as  $\theta$ . The radial distance to the  $s$ -axis at a normal cross section is chosen to be the  $r$ -coordinate. The angular coordinate  $\varphi$  is denoted as shown in Fig. 7.

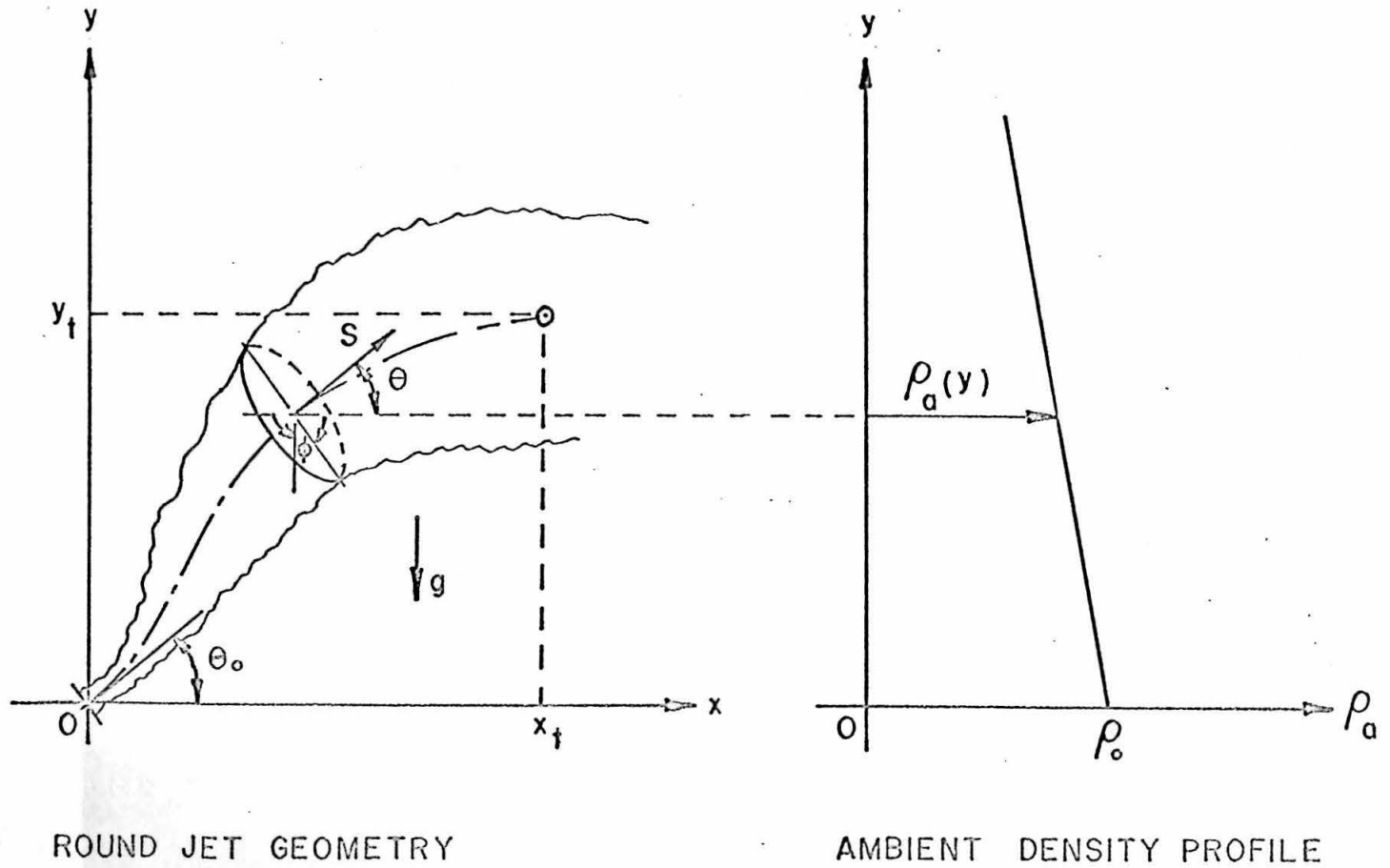


Fig. 7. Schematic diagram of a round buoyant jet in a stagnant environment with linear density stratification

$u^*$  and  $\rho^*$  are respectively local mean velocity and density which are in general functions of  $r$ ,  $s$  and  $\varphi$ , while  $u$  and  $\rho$  are characteristic velocity and density at the  $s$ -axis and are functions only of  $s$ . The corresponding ambient density values are similarly denoted as  $\rho_a^*$  and  $\rho_a$ .

The jet axis is first deflected upwards because of the increase of vertical momentum flux due to the action of buoyancy force. Because of the turbulent mixing the jet entrains the denser ambient fluid and grows heavier with reduction of the driving buoyancy force. Since the density of the ambient fluid is decreasing with height, the jet will eventually become as heavy as, and then heavier than, the ambient fluid at the same height. The buoyancy force thus reverses its direction and in the end will stop the rising of the jet at a terminal point  $(x_t, y_t)$  where the vertical momentum flux vanishes. The trajectory of the jet is therefore in general an S-shaped curve. After reaching the terminal point the horizontal momentum flux will keep the jet moving in the  $x$ -direction. But the flow cannot maintain the characteristics of a turbulent jet soon after reaching the terminal level and collapses in the vertical direction because of the suppression of vertical motion imposed by the density stratification. The analysis will not cover that part.

Specific assumptions related to the analysis are listed as follows:

1. The entrainment relation is given by the equation:

$$dQ/ds = 2\pi\alpha u b \quad (12)$$

where  $\alpha$  is a constant coefficient of entrainment,  $b$  is the characteristic length defined in eq. (13).

2. Velocity profiles are assumed to be Gaussian, with no dependence on  $\varphi$ -coordinate:

$$u^*(s, r, \varphi) = u(s) e^{-r^2/b^2} \quad (13)$$

where  $b = b(s)$  is a characteristic length defined by the velocity profile.  $\sqrt{2} b (=2\sigma)$  is commonly defined to be the nominal half width of the jet.

3. Profiles of density deficiency with respect to the ambient density are assumed to be Gaussian, with no dependence on  $\varphi$ :

$$\frac{\rho_a^*(s, r, \varphi) - \rho^*(s, r, \varphi)}{\rho_o} = \frac{\rho_a(s) - \rho(s)}{\rho_o} e^{-r^2/(\lambda b)^2} \quad (14)$$

where  $\lambda b$  is the characteristic length of the profiles.  $\lambda^2$  is the turbulent Schmidt number and is assumed to be a constant. Such profiles can also be regarded as buoyancy profiles.

4. Profiles of a certain tracer concentration are also similar and assumed to be Gaussian:

$$c^*(r, s, \varphi) = c(s) e^{-r^2/(\lambda b)^2} \quad (15)$$

5. Pressure is hydrostatic throughout the flow field.

The analysis will not cover the zone of the flow establishment. The results by Albertson et al. (5) for this region will be adopted in application to practical problems as indicated in Section IV-E.

III-C. A Round Buoyant Jet in a Uniform Cross Stream of Homogeneous Density

Fig. 8 shows a round buoyant jet discharging at a velocity  $U_o$  into a uniform cross stream of velocity  $U_a$ . The densities of the discharged fluid and the ambient fluid are respectively  $\rho_1$  and  $\rho_a$ . The flow becomes fully developed into horse-shoe shaped profiles at a short distance  $s'_e$  from the nozzle. The origin O is taken at the beginning of the zone of established flow. Again the locus of maximum velocity points on the plane of symmetry is taken to be the jet trajectory and denoted as s-axis.  $\theta$  is the angle of inclination of the trajectory with respect to the horizontal x-axis.

The trajectory of the jet bends over toward the downstream direction due to two effects. First is the low pressure or wake like region established behind the jet. This effect is especially important when the jet trajectory is nearly normal to the oncoming stream. The second factor is the entrainment of ambient horizontal momentum as the jet entrains the fluid of the cross stream. These two factors also cause the profiles of the velocity to deform into horse-shoe shapes. But the jet will continue to rise due to both initial vertical momentum flux and buoyancy flux possessed by the jet.

By dimensional analysis, the flow is not only characterized by the densimetric jet Froude number  $F$  defined by eq. (11), but also by a velocity ratio which represents the relative strength of the jet to the cross stream and is defined as:

$$k = U_o / U_a \quad (16)$$

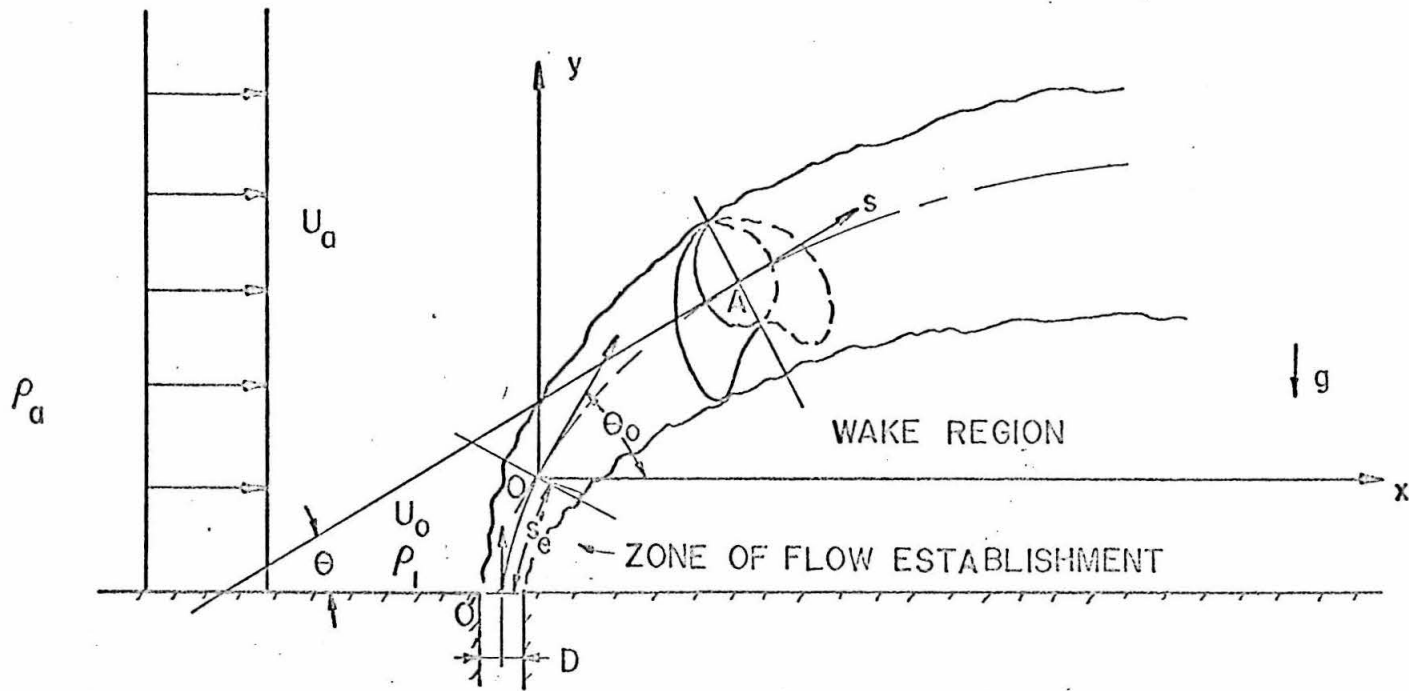


Fig. 8. Schematic diagram of a round jet in a uniform cross stream



The ordinary momentum jet is then a limiting case when  $k$  is infinity. For  $k$  less than 4 the jet was found to have its lower edge attached to the boundary. This case will not be covered in the present study.

Specific assumptions adopted in the later analysis are listed as follows.

1. The entrainment relation for a jet in a cross stream is assumed to be represented by the equation:

$$dQ/ds = 2\pi \alpha b |\bar{U}_j - \bar{U}_a| \quad (17)$$

where  $b$  is again a characteristic length defined by the assumed velocity profile by eq. (18).  $|\bar{U}_j - \bar{U}_a|$  is the magnitude of the vector difference of the two velocities.  $\alpha$  is the coefficient of entrainment for the jet in a cross stream. It is assumed to be constant in the analysis.

2. Velocity profiles are assumed to be similar and Gaussian above the component of the ambient velocity  $U_a \cos \theta$  :

$$u^*(s, r, \varphi) = U_a \cos \theta + u(s) e^{-r^2/b^2} \quad (18)$$

where  $b$  is the local characteristic length. This assumption is a gross simplification of the actual velocity profiles. A more realistic shape of the profiles can be used based upon experimental measurements, but in view of the nature of other assumptions involved in the analysis it seems to be unnecessary and will make the calculation much more complicated.

3. Buoyancy profiles are also Gaussian:

$$\rho_a - \rho^*(s, r, \varphi) = [\rho_a - \rho(s)] e^{-r^2/b^2} \quad (19)$$

Here the turbulent Schmidt number  $\lambda^2$  is taken to be unity.

4. Concentration profiles of a certain tracer are Gaussian:

$$c^*(s, r, \varphi) = c(s) e^{-r^2/b^2} \quad (20)$$

5. The effect of the presence of the pressure field can be lumped into a gross drag term proportional to the square of the velocity component of the oncoming stream normal to the jet axis. The drag coefficient is assumed to be a constant.

The analysis based upon these assumptions will not be as reliable as the analysis for the problem of a buoyant jet in a stagnant, stratified environment. But nevertheless these assumptions provide a quite reasonable description of the flow while on the other hand they pave the way for a simple formulation of the problem. The analysis and experimental studies are presented in Chapters VI and VII.

## CHAPTER IV

### THEORETICAL ANALYSIS FOR A ROUND BUOYANT JET IN A STAGNANT ENVIRONMENT WITH LINEAR DENSITY STRATIFICATION

In this chapter theoretical solutions are obtained for an inclined round buoyant jet in a stagnant, density-stratified environment. The present study extends the Morton type analysis to cover the effect of the initial angle of discharge.

Formulation of the problem is presented first based upon the assumptions listed in the previous chapter. Equations are normalized and expressed in dimensionless parameters. Numerical solutions are presented for certain specific cases to illustrate the effects of various parameters. Section IV-E gives relations important for practical applications. Limitations of the analysis are discussed in Section VIII-A.

#### IV-A. Formulation of the Problem

##### 1. Conservation equations

The equation of continuity, based upon the assumed entrainment mechanism and a small variation of density, can be expressed as:

$$\frac{d}{ds} \int_0^{\infty} \int_0^{2\pi} u^* r \, dr \, d\varphi = 2\pi \alpha b u \quad (21)$$

The left-hand side can be integrated after substituting  $u^*$  from eq. (13).

Then,

$$\frac{d}{ds}(u b^2) = 2\alpha u b \quad (\text{continuity}) \quad (22)$$

Since the pressure is assumed to be hydrostatic and there is no other force acting in the horizontal direction, the x-momentum flux should be conserved:

$$\frac{d}{ds} \int_0^\infty \int_0^{2\pi} \rho^* u^* (u^* \cos \theta) r \, dr \, d\varphi = 0 \quad (23)$$

After substituting  $u^*$  from eq. (13):

$$\frac{d}{ds} \left( \frac{u^2 b^2}{2} \cos \theta \right) = 0 \quad (\text{x-momentum}) \quad (24)$$

In the vertical direction there is a buoyancy force acting on the jet; therefore it is equal to the rate of change of y-momentum flux:

$$\frac{d}{ds} \int_0^\infty \int_0^{2\pi} \rho^* u^* (u^* \sin \theta) r \, dr \, d\varphi = g \int_0^\infty \int_0^{2\pi} (\rho_a^* - \rho^*) r \, dr \, d\varphi \quad (25)$$

Simplifying by using both eqs. (13) and (14), eq. (25) becomes:

$$\frac{d}{ds} \left( \frac{u^2 b^2}{2} \sin \theta \right) = g \lambda^2 b^2 \frac{\rho_a - \rho}{\rho_0} \quad (\text{y-momentum}) \quad (26)$$

The heat content or the amount of shortage of salt released from the origin must be conserved with respect to a chosen reference level. By the assumption of small variation of density, this is directly equivalent to the conservation of density deficiency about the

reference density  $\rho_o$ . The relation can be expressed as:

$$\frac{d}{ds} \int_0^\infty \int_0^{2\pi} u^*(\rho_o - \rho^*) r dr d\varphi = \alpha u b \int_0^{2\pi} (\rho_o - \rho_a^*(s, b, \varphi)) d\varphi \quad (27)$$

For linear ambient density gradient the relation can be simplified to:

$$\frac{d}{ds} [u b^2 (\rho_a - \rho)] = \frac{1 + \lambda^2}{\lambda^2} b^2 u \frac{d\rho_a}{ds} \quad (\text{density deficiency}) \quad (28)$$

The relation of continuity for a certain tracer substance present in source flow only is:

$$\frac{d}{ds} \int_0^\infty \int_0^{2\pi} c^* u^* r dr d\varphi = 0 \quad (29)$$

by introducing eq. (15) it can be written as:

$$\frac{d}{ds} (c u b^2) = 0 \quad (30)$$

(continuity of tracer)

## 2. Geometric relations

To determine the jet trajectory the following geometric equations must be solved simultaneously with the previous set of equations:

$$\frac{dx}{ds} = \cos \theta \quad (\text{geometry}) \quad (31)$$

and,

$$\frac{dy}{ds} = \sin \theta \quad (\text{geometry}) \quad (32)$$

Therefore, the problem has seven unknowns, namely,  $u$ ,  $b$ ,  $\rho_a - \rho$ ,  $\theta$ ,  $c$ ,  $x$  and  $y$  to be solved from seven equations, i. e., eqs. (22), (24), (26), (28), (30), (31) and (32).

### 3. Initial conditions

The initial conditions given at the origin for this system of ordinary differential equations are:

$$\begin{aligned} u(0) = U_0, \quad b(0) = b_0, \quad \rho(0) = \rho_1, \quad \theta(0) = \theta_0, \\ c(0) = c_0, \quad x = 0 \text{ and } y = 0 \text{ at } s = 0 \end{aligned} \tag{33}$$

Eqs. (24) and (30) can be integrated immediately. The equation of x-momentum is:

$$\frac{u^2 b^2}{2} \cos \theta = \text{const.} \quad (\text{x-momentum}) \tag{34}$$

The equation of tracer concentration is simply:

$$c u b^2 = \text{const.} = c_0 U_0 b_0^2 \tag{35}$$

which is directly related to the solutions of  $u$  and  $b$ . Thus this equation will not be carried through the following calculation.

#### IV-B. Normalized Equations and Dimensionless Parameters

In order to transform the system of equations into a simple normalized form, dimensionless parameters are defined as follows:

Volume flux parameter: 
$$\mu = \left\{ \frac{G^5}{F_o^6 64 \alpha^4 (1+\lambda^2)} \right\}^{1/8} u b^3 \quad (36)$$

Momentum flux parameters:

$$m = \left\{ \frac{G}{(1+\lambda^2) F_o^2} \right\} b^4 u^4 / 4 \quad (\text{in } s\text{-direction})$$

$$h = m \cos^2 \theta \quad (\text{in } x\text{-direction}) \quad (37)$$

$$v = m \sin^2 \theta \quad (\text{in } y\text{-direction})$$

Buoyancy flux parameter: 
$$\beta = \left\{ \frac{\lambda^2}{1+\lambda^2} b^2 u g \frac{\rho_a - \rho}{\rho_o} \right\} / F_o \quad (38)$$

Coordinates:

$$\begin{aligned} s; \quad \zeta &= \left\{ \frac{G^3 64 \alpha^4 (1+\lambda^2)}{F_o^2} \right\}^{1/8} s \\ x; \quad \eta &= \left\{ \frac{G^3 64 \alpha^4 (1+\lambda^2)}{F_o^2} \right\}^{1/8} x \\ y; \quad \xi &= \left\{ \frac{G^3 64 \alpha^4 (1+\lambda^2)}{F_o^2} \right\}^{1/8} y \end{aligned} \quad (39)$$

where  $G = -\frac{g}{\rho_o} \frac{d\rho_a}{dy}$  and  $F_o = \frac{\lambda^2}{1+\lambda^2} b_o^2 U_o g \frac{\rho_o - \rho_1}{\rho_o}$  are not dimensionless.

Equations (22), (24), (26), (28), (31) and (32) then become:

$$d\mu/d\zeta = m^{1/4} \quad (40)$$

$$h = h_o = \text{const.} \quad (41)$$

$$dv/d\zeta = \beta \mu (v/m)^{1/2} \quad (42)$$

$$d\beta/d\zeta = -\mu (v/m)^{1/2} \quad (43)$$

$$dy/d\zeta = (h/m)^{1/2} \quad (44)$$

$$d\xi/d\zeta = (v/m)^{1/2} \quad (45)$$

The corresponding initial conditions (33) are:

$$\begin{aligned} \mu(0) = \mu_0, \quad m(0) = m_0, \quad \theta = \theta_0, \quad \beta = 1 \\ \eta = 0 \text{ and } \xi = 0 \text{ at } \zeta = 0 \end{aligned} \tag{46}$$

The solutions to the system of differential equations cannot be obtained in closed analytical form. Thus numerical integrations were carried out.

#### IV-C. Method of Numerical Solution

The numerical solutions were obtained by direct step-by-step integration on an IBM 7094 digital computer using a subroutine "DEQ/DIFFERENTIAL EQUATION SOLVER" at Booth Computing Center of California Institute of Technology. The subroutine was based upon Runge-Kutta-Gill method with automatic control of truncation error (CIT programmer's manual pp. 128-34). Integration step size was chosen so that four significant figures could be obtained.

There are three relevant parameters for the problem, namely  $\mu_0$ ,  $m_0$  and  $\theta_0$ . For each combination of these parameters a computer run was made. The integration stopped at the terminal point of the jet. A substantial range of initial conditions was covered by the numerical computation. Only a portion will be shown in this report. More complete information useful for practical design purposes will be provided in a future report.



#### IV-D. Solutions of Gross Behavior of Jets

Fig. 9 shows the variations of gross jet characteristics  $v$ ,  $\beta$  and  $\mu$  along the  $\zeta$ -coordinate for the case  $m_o = 0.2$ ,  $\mu_o = 0$  and  $\theta_o = 0$ . The vertical momentum flux parameter  $v$  first increases with  $\zeta$  and reaches its maximum at the point where  $\beta$  changes sign and then decreases under negative buoyancy and finally vanishes at the terminal point  $\zeta_t$ . The buoyancy flux parameter  $\beta$  decreases monotonically from unity to a minimum at  $\zeta_t$ . The volume flux parameter  $\mu$  increases with  $\zeta$  and reaches  $\mu_t$  at  $\zeta_t$ .

The effect of initial angle of discharge  $\theta_o$  on the jet trajectory is demonstrated in Fig. 10. For  $m_o = 0.2$  and  $\mu_o = 0$ , trajectories are obtained for different  $\theta_o$  values. The terminal height of rise  $\xi_t$  increases with increasing  $\theta_o$ .

The variation of the terminal height of rise  $\xi_t$  for the range  $\mu_o = 0$  to 0.01 is shown in Fig. 11. The curve for  $m_o = 2.0$  shows a faster rate of decrease in  $\xi_t$  as the angle  $\theta_o$  decreases than the cases for smaller  $m_o$  values. For a simple plume where  $m_o$  vanishes the height is independent of the initial angle of discharge. Fig. 12 shows the variation of the terminal volume flux parameter  $\mu_t$  over the same range of initial conditions. A substantial increase in  $\mu_t$  can be achieved by decreasing the  $\theta_o$  at large  $m_o$  values. Both Figs. 11 and 12 demonstrate that the variation of the terminal quantities  $\xi_t$  and  $\mu_t$  are almost independent of the initial volume flux parameter  $\mu_o$  in the range to 0.01. Since the dilution ratio  $S$  is

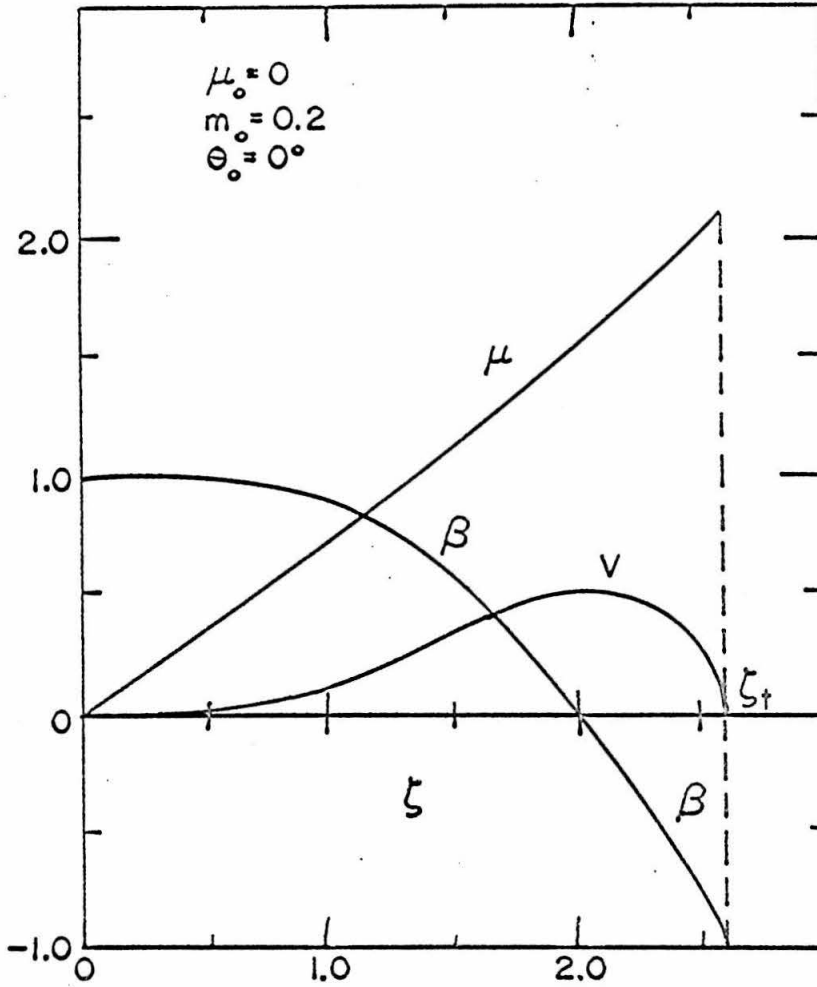


Fig. 9. Variation of volume flux parameter  $\mu$ , buoyancy flux parameter  $\beta$  and vertical momentum flux parameter  $v$  along  $\zeta$ -coordinate for a horizontal buoyant jet with  $\mu_0 = 0$  and  $m_0 = 0.2$ .

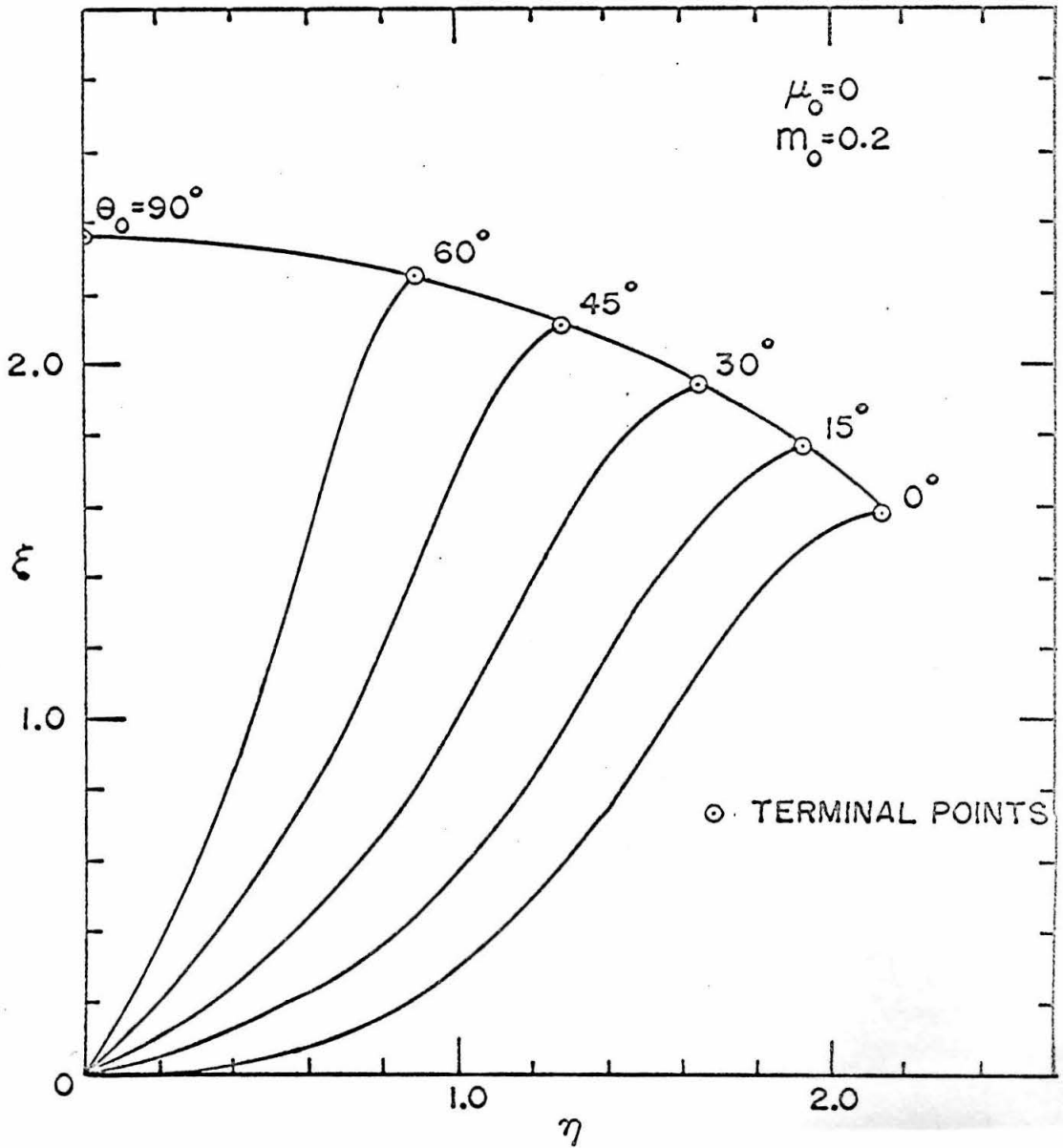


Fig. 10. Trajectories of inclined buoyant jets in stratified environments with  $\mu_0 = 0$ ,  $m_0 = 0.2$ .

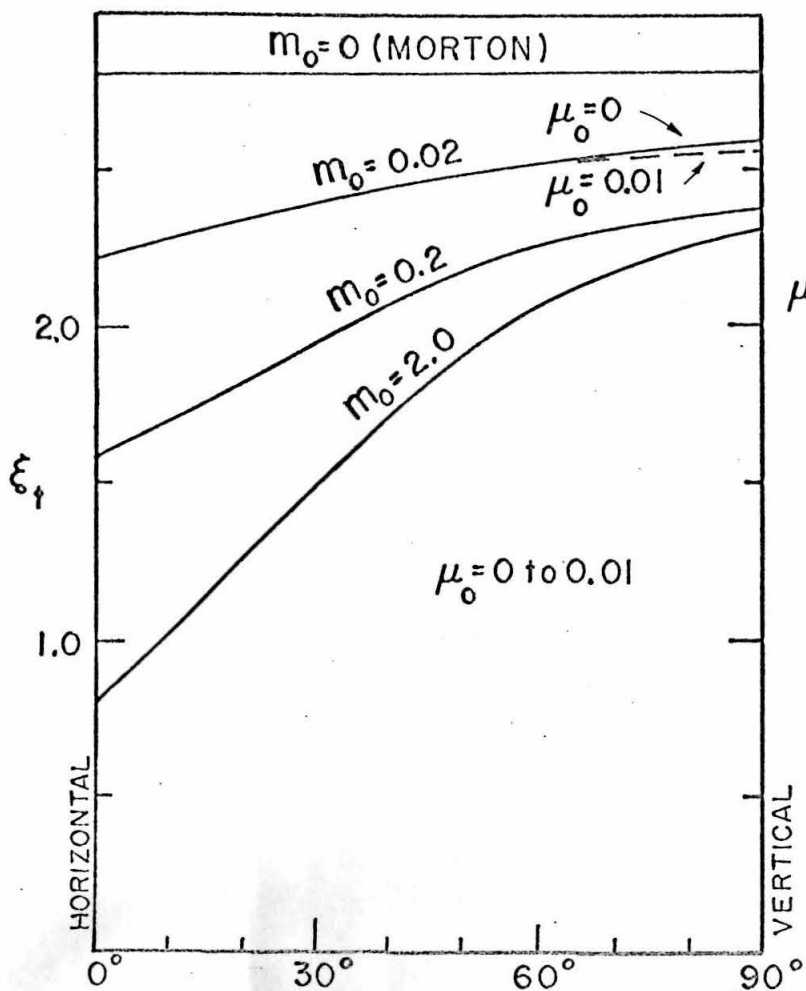


Fig. 11. Variation of terminal height of rise  $\xi_t$  for inclined buoyant jets with  $\mu_o = 0$  to 0.01.

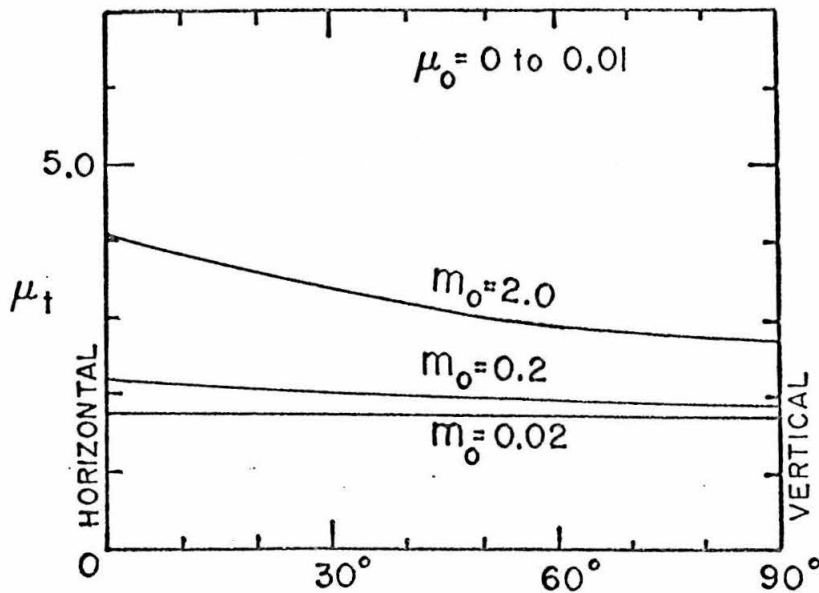


Fig. 12. Variation of terminal volume flux parameter  $\mu_t$  for inclined buoyant jets with  $\mu_o = 0$  to 0.01.

(Note: the terminal dilution ratio  $S = \mu_t / \mu_o$ .)

simply the ratio of the terminal and initial volume flux parameters, an increase in the terminal dilution ratio can be obtained by decreasing  $\mu_0$ .

Numerical solutions for horizontal buoyant jets were carried out covering a wide range of initial conditions. The variations of the  $\xi_t$  and  $\mu_t$  values are shown in Figs. 13 and 14. For large  $m_0$ , the terminal quantities seem to be independent of the  $\mu_0$  when  $\mu_0$  is small. On the other hand, for large  $\mu_0$ , the quantities  $\xi_t$  and  $\mu_t$  tend to be independent of the  $m_0$  when  $m_0$  is small.

#### IV-E. Application to Practical Problems

For application to practical problems where the jet is issued from a nozzle or orifice, it is necessary to consider the zone of flow establishment. Assuming that Albertson et al.'s (5) result applies also for the zone of flow establishment of an inclined buoyant jet, the length of the zone is taken to be  $6.2D$  where  $D$  is the initial jet diameter as shown in Fig. 15. The initial top-hat profiles at  $O'$  develop into Gaussian distributions given by eqs. (13), (14) and (15) at the end of the zone.

The initial value  $b_0$  can be obtained by applying the momentum relation between cross sections at  $O$  and  $O'$  assuming that the buoyancy force is negligible in such a short region:

$$\begin{aligned} \frac{\pi}{4} D^3 U_0^3 &= \int_{A \text{ at } O} u^{*3} dA \\ &= \frac{\pi b_0^3 U_0^3}{2} \end{aligned} \quad (47)$$

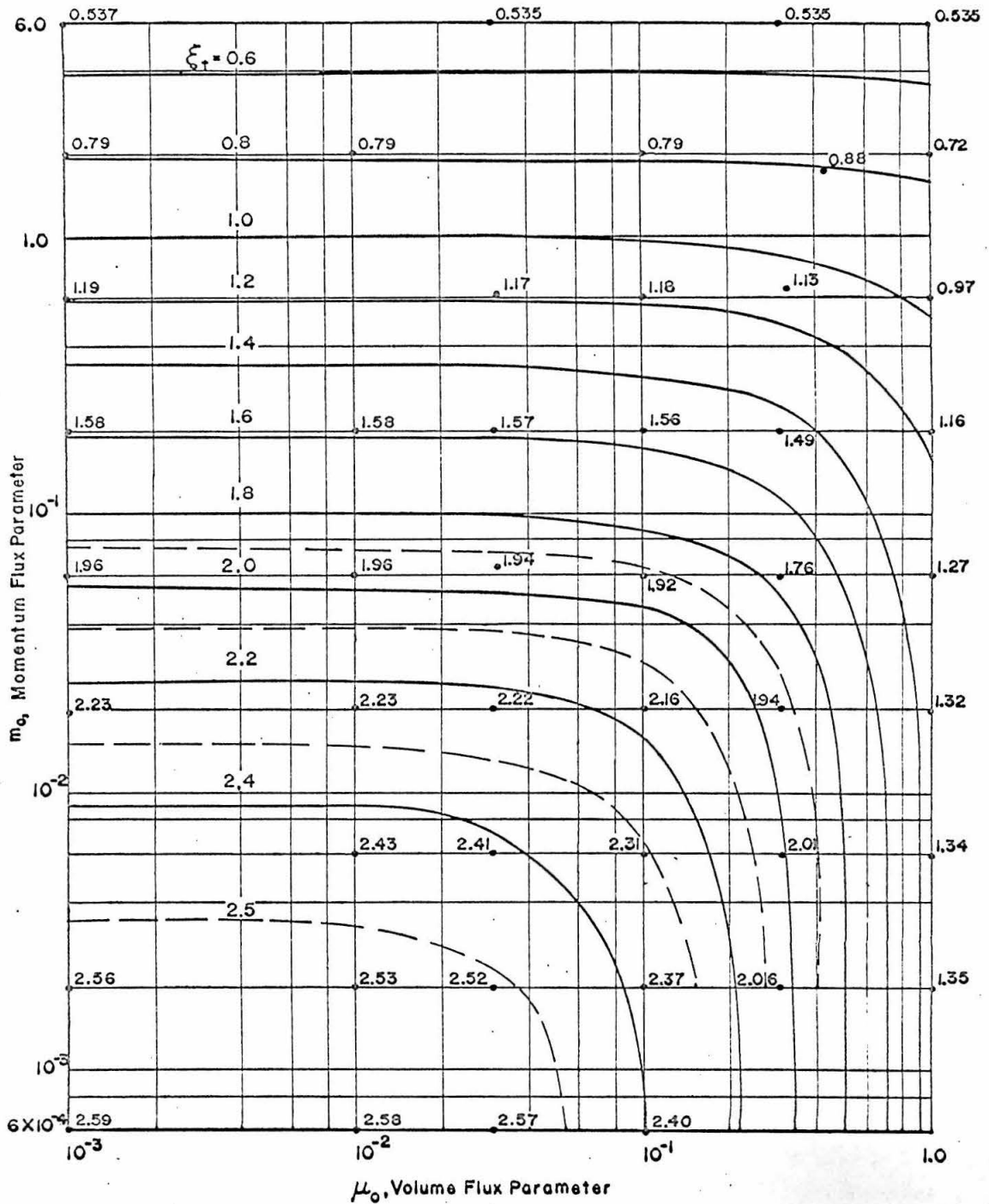


Fig. 13. Variation of terminal height of rise  $\xi_t$  for horizontal buoyant jets ( $\theta_0 = 0^\circ$ ).

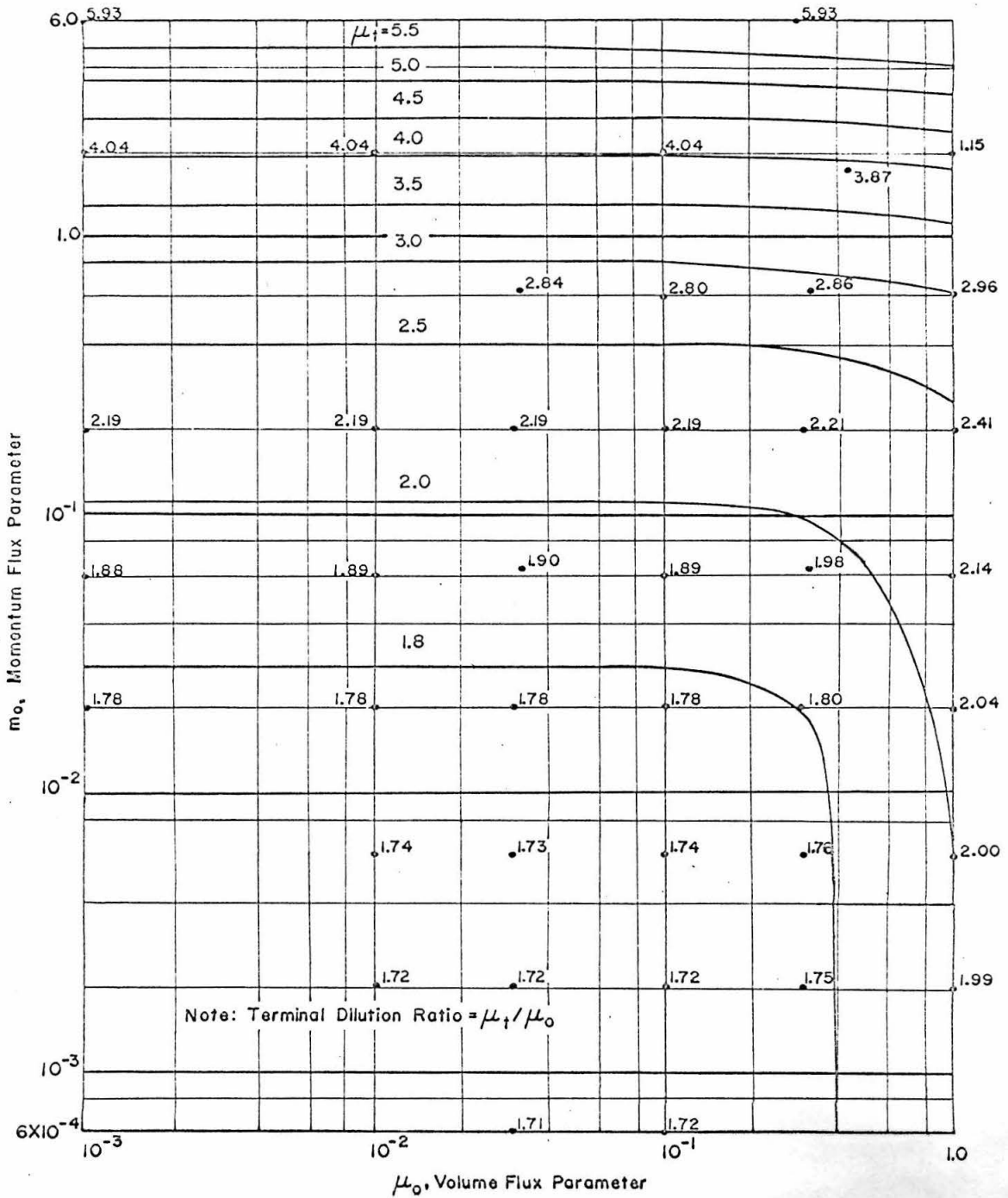


Fig. 14. Variation of terminal volume flux parameter  $\mu_t$  for horizontal buoyant jets ( $\theta_0 = 0^\circ$ ).

thus,

$$b_o = \frac{D}{\sqrt{2}} \quad (48)$$

The trace concentration  $c_o$  at O, assuming that the concentration at O' is unity, can be obtained by considering the continuity relation for the tracer:

$$\begin{aligned} \frac{\pi}{4} D^2 U_o &= \int_{A \text{ at } O} u * c * dA \\ &= \frac{\lambda^2}{1+\lambda^2} \pi b_o^2 U_o c_o \end{aligned} \quad (49)$$

thus,

$$c_o = \frac{1+\lambda^2}{2\lambda^2} \quad (50)$$

If a densimetric jet Froude number F is defined as:

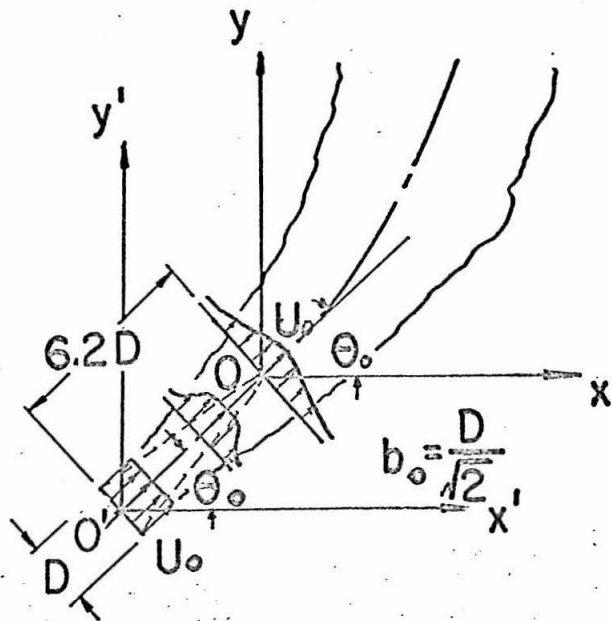
$$F = \frac{D}{\sqrt{\frac{\rho_o - \rho_1}{\rho_o} g D}} \quad (51)$$

and a stratification parameter T as:

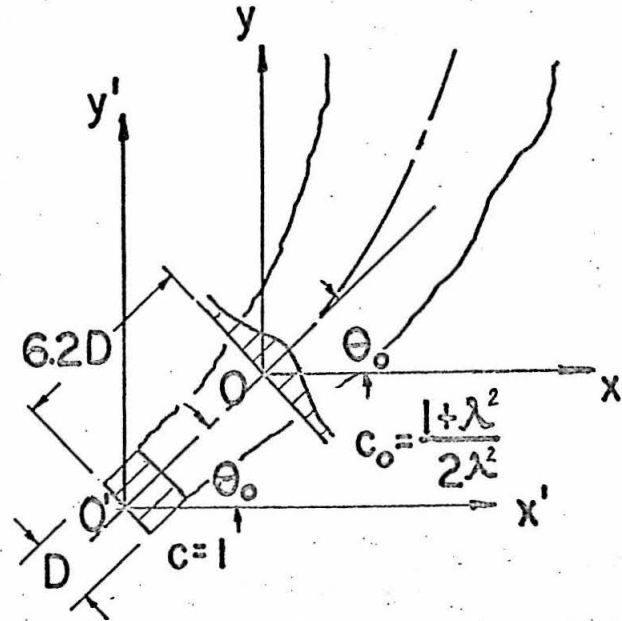
$$T = \frac{\rho_o - \rho_1}{D \left( -\frac{d\rho_a}{dy} \right)} \quad (52)$$

it can be shown that the problem of an inclined buoyant jet in a linearly stratified environment is characterized by three parameters, namely F, T and  $\theta_o$ . The relationships between the set of parameters F, T and the set  $m_o, \mu_o$  are:





VELOCITY



CONCENTRATION  
& BUOYANCY

Fig. 15. Zone of flow establishment for an inclined buoyant jet

$$m_o = \frac{(1+\lambda^2) F^2}{4\lambda^4 T} \quad (53)$$

$$\mu_o = \frac{F^{1/4} (1+\lambda^2)^{5/8}}{2\alpha^{1/2} \lambda^{3/2} T^{5/8}} \quad (54)$$

or:

$$F = \frac{2^{1/4} \lambda m_o^{5/8}}{\alpha^{1/2} \mu_o} \quad (55)$$

$$T = \frac{(1+\lambda^2) m_o^{1/4}}{2^{3/2} \alpha \lambda^2 \mu_o^2} \quad (56)$$

The set of parameters  $m_o$  and  $\mu_o$  is adopted in the analysis for mathematical simplicity, and because the solutions found are independent of  $\alpha$  and  $\lambda$  values chosen. But in practical application it is more convenient to use  $F$  and  $T$  as parameters.

The dilution ratio  $S$  is defined to be corresponding to the concentration  $c_o$  at  $O$ :

$$S = \frac{c_o}{c} = \frac{\mu}{\mu_o} \quad (57)$$

The dilution ratio  $S_o$  corresponding to the concentration at  $O'$  is:

$$S_o = \frac{2\lambda^2}{1+\lambda^2} \frac{c_o}{c} = \frac{2\lambda^2}{1+\lambda^2} \frac{\mu}{\mu_o} \quad (58)$$

Both  $S$  and  $S_o$  refer to dilution ratios along the jet axis.

The suggested values for the coefficient of entrainment  $\alpha$  and the turbulent spreading ratio  $\lambda$  are respectively 0.082 and 1.16 based upon Rouse et al's (30) data for a simple plume. The problem on the coefficient of entrainment has been discussed in detail in Section II-F. For application to jets in stratified environments it is a further generalization. However, experimental investigations on jet trajectories and nominal half widths presented in the next chapter have confirmed such a choice.

## CHAPTER V

### EXPERIMENTAL STUDY FOR A ROUND BUOYANT JET IN A STAGNANT ENVIRONMENT WITH LINEAR DENSITY STRATIFICATION

Experiments were conducted in a laboratory tank to observe trajectories of inclined buoyant jets in stagnant environments. In this chapter objectives of the experiments are defined first, a detailed description of the experimental procedure and apparatus is given next in Section V-B, and the experimental results are summarized and compared with calculated values in Section V-C. The results are discussed in Chapter VIII.

#### V-A. Objectives of the Experimental Investigation

The main objective of this experimental study is to test the applicability of the theoretical solutions of inclined round buoyant jets in stagnant environments with linear density stratification (see Chapter IV). Experiments were conducted to observe photographically the jet trajectories and nominal half widths ( $\sqrt{2}b$ ) over a range of initial conditions. The results were then compared with the values obtained by theoretical calculations.

For a complete experimental check on the theory, it is necessary to determine values of the jet velocity and the density. Practically however, laboratory experiments on density-stratified flows are usually limited in scale and do not allow the time required in

measuring time-fluctuating quantities. On the other hand, the jet trajectories and nominal half widths can be determined conveniently by photographic methods. These two quantities are inter-related with other jet characteristics. Thus the comparison of the observed and the calculated values of these two quantities is believed to be indicative of the applicability of the theoretical solutions. The experiments carried out were limited to the determination of these values.

#### V-B. Procedure and Apparatus

The experiments were performed in a laboratory tank filled with a density-stratified fluid. The tank was 226 cm long, 107 cm wide and 61 cm deep. It was lined with 1.8 cm thick plane glass plates. The general experimental setup is shown in Fig. 16.

The variation of density was modeled by using aqueous solutions of sodium chloride based upon tables prepared by Owens (25). Tap water was used as the base fluid. For the runs where concentration measurements were made the tap water was filtered before use. The temperatures of the fluids were between 20 and 22°C for all experiments. The density variation induced by the temperature difference was neglected for any one experiment. Food grade "999" salt produced by Morton Salt Company was used in all experiments.

The density stratification of the tank fluid was achieved by filling layer by layer with solutions of different densities. The filling procedure followed the method described by Koh (19). First, a solution of predetermined density was well mixed in an 180 liter tank.

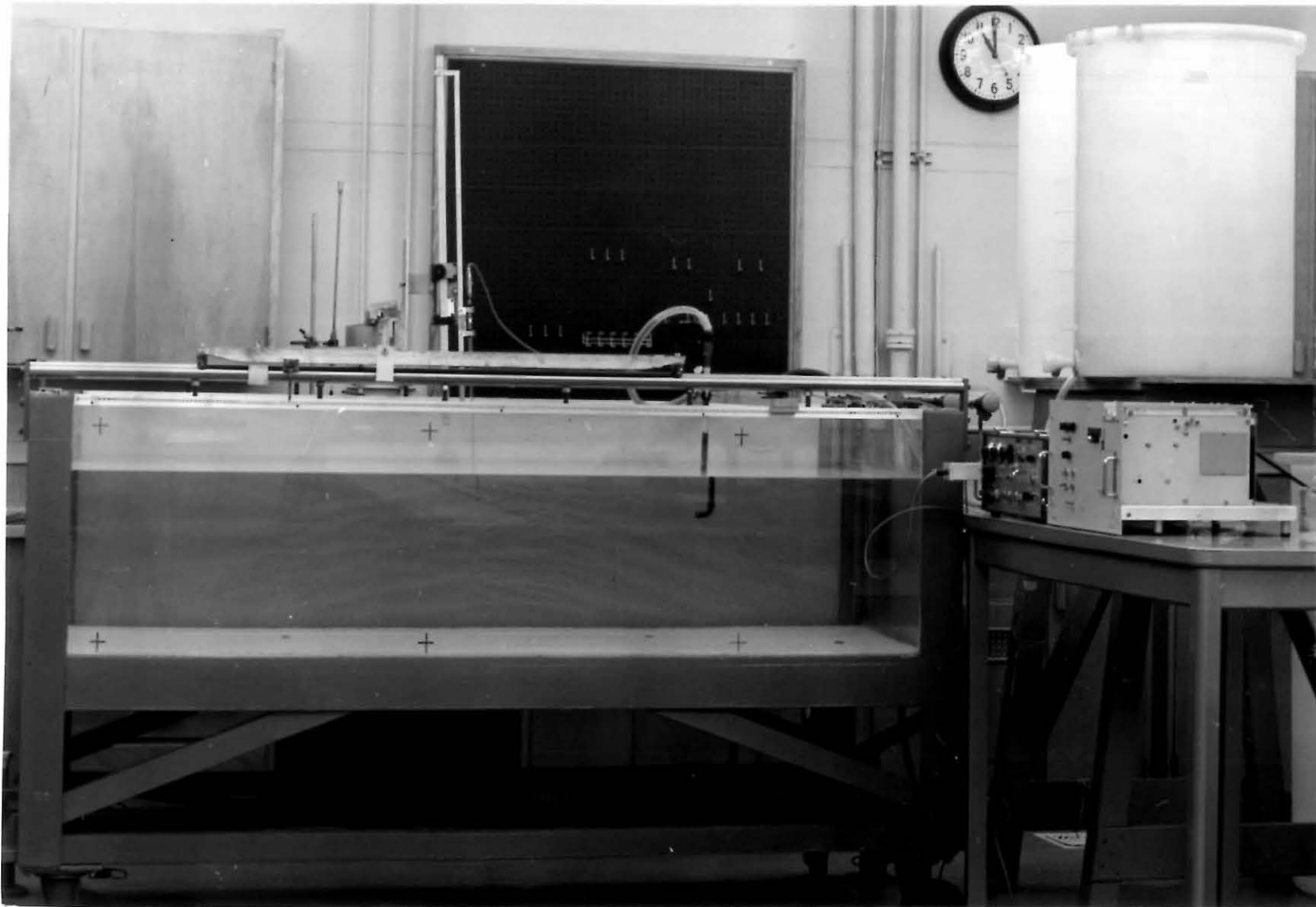


Fig. 16. General experimental setup for jets in stagnant environments

The density of the fluid was checked by a calibrated hydrometer. Then the fluid was transferred into the tank gently through a plastic tube on a circular platform floating on the water surface. The fluid being added in this manner, spread out horizontally on top of the layers of heavier fluids already in the tank. Each layer was 3 to 5 cm thick. The resulting density profiles would not be step-like because of molecular diffusion as well as the mixing introduced by the disturbance caused by filling. The density profiles were found to be smoothed out before running the experiments. Six different density gradients were obtained; the values of  $-\frac{1}{\rho_0} \frac{d\rho_a}{dy}$  ranged from 7.6 to  $50 \times 10^{-5}/\text{cm}$ .

The density stratification in the tank was determined by hydrometer measurements of the fluids withdrawn from different levels of the tank. The fluids were withdrawn through a 2mm wide slit at very small flowrate. For the last two fillings concentration measurements were made to determine the density profiles. The technique and apparatus for concentration measurements by conductivity probe are described in detail in Section VII-B. The measured density profiles were found to be very close to the intended stratification. Two of the profiles are shown in Fig. 17. All of the profiles measured had layers of homogeneous fluid near the free surfaces. But these layers were thin and were avoided by setting the nozzle at a lower level.

All the experiments except one run (Jet No. 16) were made by jetting heavier fluids into ambient of lighter fluids. The amount of

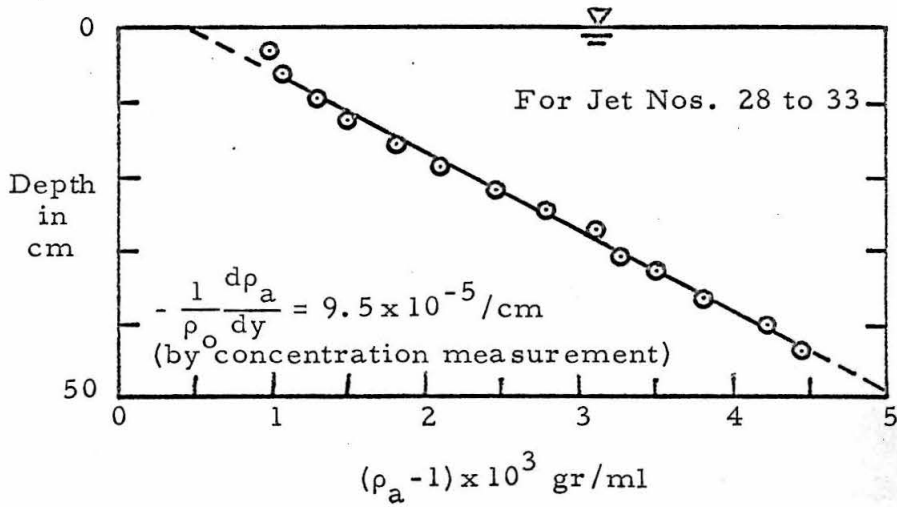
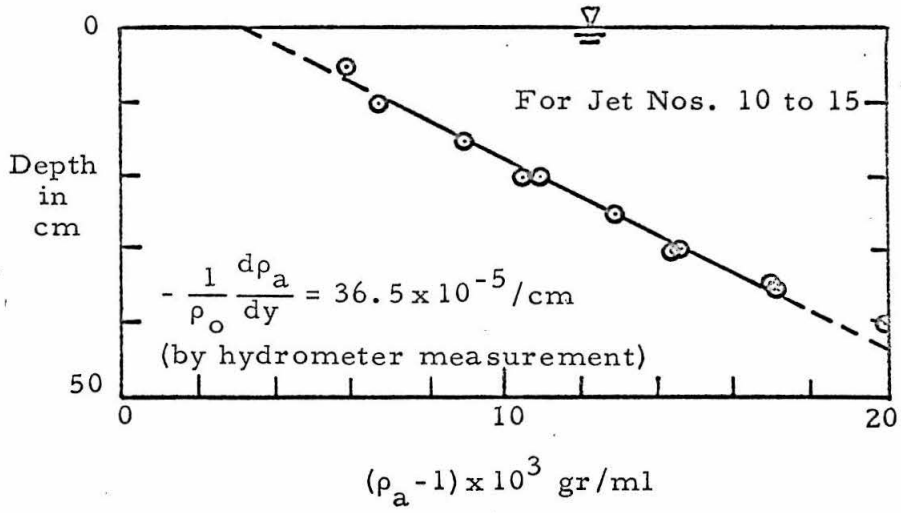


Fig. 17. Two measured density profiles

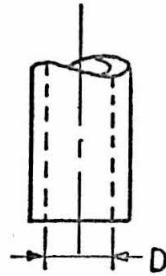


salt and labor used in mixing was greatly saved because the volume of jet fluid was much smaller than the volume of the receiving fluid. It was also beneficial to the concentration measurements as discussed in Section VII-B. The positive y-axis was then pointing downwards in these experiments.

Different nozzle types and sizes were used in the experiments. Fig. 18 shows the nozzles used except No. E and No. F which were used in experiments of jets in cross currents. For those straight tube nozzles the values of  $D$  were taken simply to be the diameters of the tubes. For sharp-edged orifices the  $D$  values were taken to be  $0.8D_o$  (where the  $D_o$ 's were the diameters of the openings) to allow for jet contraction.

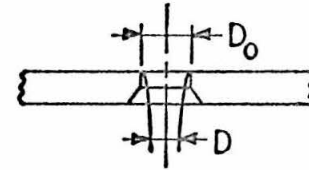
The jet fluid was stored in an 180 liter tank above the receiving tank. The nozzle was connected to the reservoir as shown in Fig. 19. A Fischer-Porter Tri-Flat Tube Flowrator meter was employed to measure the flow rate. The flowmeter was calibrated for fluids of different density used in the experiments. The error was estimated to be less than  $\pm 2\%$ .

The jet flows were established by gravity. Because of the small flow rate (20 cc per second or less in most cases) and the short durations of the runs (about 5 minutes or less) the rates of flow were approximately constant even though no constant head device was provided. Checking of the flowmeter readings during each run revealed very little change. The corresponding change in flow rate was less than 3%.



NOZZLE NO.	A	B	C
$D^{cm}$	0.462	0.223	0.686

STRAIGHT TUBES



NOZZLE NO.	D	E	F
$D^{cm}$	0.254	0.762	0.508
$D_o^{cm}$	0.317	0.952	0.635

SHARP-EDGED ORIFICES

Fig. 18. Nozzles and orifices used in the experiments

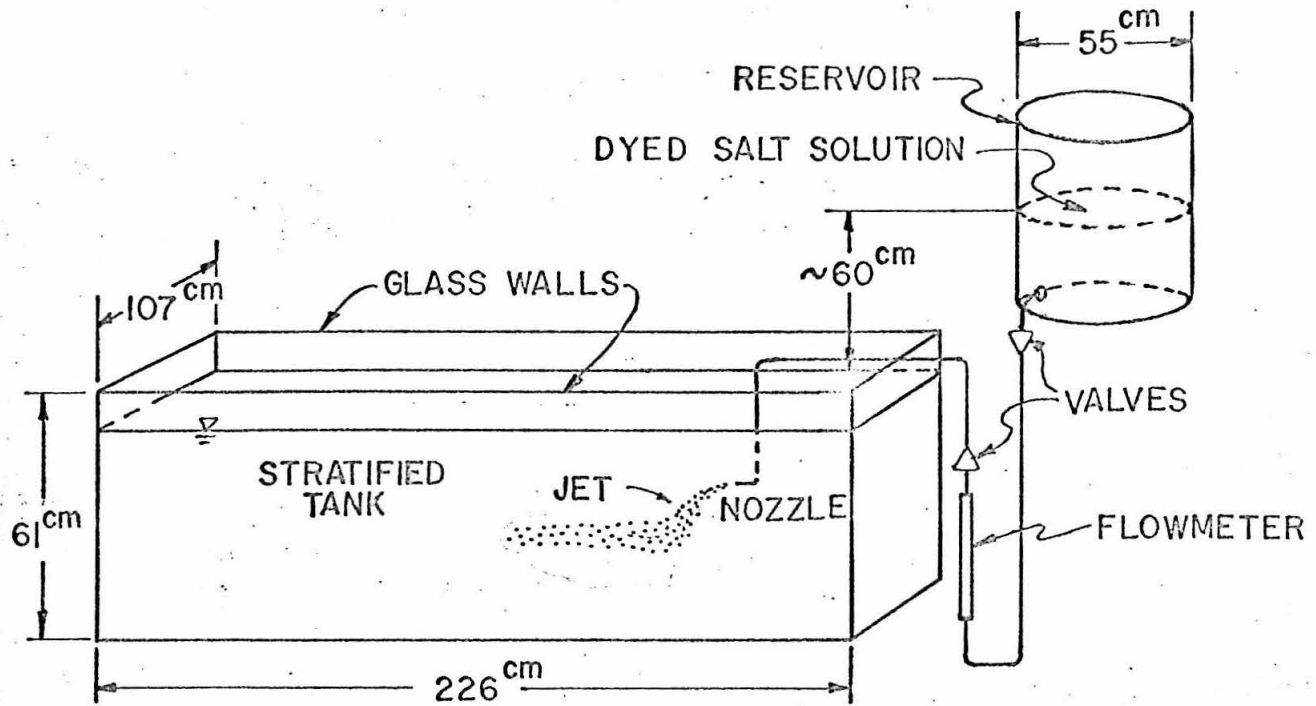


Fig. 19. Schematic flow diagram for jet experiments in stagnant environments

To trace the jet trajectories photographically, the jet fluids were mixed with concentrated blue vegetable dye (Blue A-5-G-3) produced by Krieger Color and Chemical Company. The dye concentration used was from 30 to 50 ppm. The effect of the dye concentration on the density of the injected fluid was not detectable.

A 4 in. x 5 in. Speed Graphic camera was positioned in front of the tank. Lighting was provided from the rear of the tank. Royal Pan black and white films (ASA400) were used to record the dyed trajectories of the jets. The scale was established by taking a photograph of a grid board marked with grids at fixed known distances. The board was set in the center plane of jet motion. By examining the grids from the photograph there was no detectable distortion (less than  $\pm 1\%$ ) of the image in the region of interest.

In each run at least two pictures were taken. Three runs (Jet Nos. 19, 20 and 21) were made to reproduce the dilution ratio along the jet axis of an ordinary momentum jet. The technique is described in Section VII-B. Six runs (Jet Nos. 22 to 27) were made without ambient density stratification to test the trajectories predicted by Fan and Brooks (12).

### V-C. Experimental Results

A total of thirty-three jet experiments were performed as listed in Table 1. Runs except those with Jet Nos. 19 to 27 were carried out in linearly density-stratified environments. Jet Nos. 19, 20 and 21 were simple jets ( $F = \infty$ ) where concentration measurements were

Table 1. Summary of Experiments on Round Jets in Stagnant Environments

Jet Number	Initial Jet Values					Ambient Reference Density ( $\rho_0$ )	Density Gradient $-\frac{1}{\rho_0} \frac{d\rho_a}{dy}$ , $10^{-5}/\text{cm}$	Jet Reynolds Number $R = \frac{U_0 D}{\nu}$	Jet Froude Number Eq. (51)	Stratification Parameter Eq. (52)	Reference for Detailed Results Figure Numbers
	Angle $\theta_0$ deg.	Diameter D cm	Discharge $Q_0$ cc/sec	Velocity $U_0$ cm/sec	Density $\rho_1$ gr/ml						
1	45	0.69	7.9	21	1.0087	1.0004	25	1,500	9.1	48	23, 24a
2	45	0.69	23	62	1.0087	1.0004	25	4,300	26	48	24b
3	0	0.69	17	46	1.0087	1.0005	25	3,200	20	48	--
4	90	0.69	29	79	1.0087	1.0012	25	5,400	35	44	--
5	0	0.22	4.3	110	1.0230	1.0048	50	2,500	55	160	--
6	26.7	0.22	4.3	109	1.0230	1.0036	50	2,400	53	170	--
7	90	0.22	8.2	105	1.0230	1.0046	50	2,300	53	160	--
8	54.5	0.22	8.7	111	1.0230	1.0038	50	2,500	54	170	--
9	-25	0.22	8.9	114	1.0230	1.0046	50	2,500	57	160	--
10	90	0.46	8.4	50	1.0240	1.0070	36.5	2,300	18	100	22
11	43.6	0.46	10.2	61	1.0240	1.0059	36.5	2,800	21	107	25a
12	2.8	0.46	6.4	38	1.0240	1.0052	36.5	1,800	13	110	25b
13	-28.2	0.46	6.4	38	1.0240	1.0082	36.5	1,800	14	93	--
14	-28.2	0.46	10.2	61	1.0240	1.0082	36.5	2,800	23	93	--
15	39.1	0.46	9.7	58	1.0240	1.0062	36.5	2,700	20	106	25c
16	0	0.25	3.1	64	1.0010	1.0249	7.6	1,600	26	1,200	26a
17	0	0.25	4.8	99	1.0175	1.0021	29.5	1,900	51	210	--
18	45	0.25	4.8	99	1.0175	1.0021	29.5	1,900	51	210	21, 26b
19	0	0.25	--	--	1.0030	1.0030	0	--	infinite (2)	--	--
20	0	0.25	~12	~240	1.0015	1.0015	0	~6,000	infinite (2)	--	31
21	0	0.25	~12	~240	1.0015	1.0015	0	~6,000	infinite (2)	--	31
22	0	0.25	2.5	51	1.0101	1.0000	0	1,300	33	infinite (3)	29a
23	0	0.25	5.0	101	1.0101	1.0000	0	2,600	66	infinite (3)	30a
24	0	0.25	10.5	205	1.0101	1.0000	0	5,200	130	infinite (3)	30b
25	0	0.25	2.6	53	1.118	1.000	0	1,300	10	infinite (3)	29b
26	0	0.25	3.5	73	1.118	1.000	0	1,800	13.6	infinite (3)	29c
27	0	0.25	10.6	214	1.118	1.000	0	5,300	40	infinite (3)	28, 30c
28	0	0.25	2.6	53	1.118	1.001	9.5	1,300	10	5,000	--
29	0	0.25	3.5	73	1.118	1.001	9.5	1,800	13.6	5,000	--
30	0	0.25	10.6	214	1.118	1.001	9.5	5,300	40	5,000	26c
31	0	0.25	1.8	36	1.0134	1.0013	9.5	900	20	510	27a
32	0	0.25	3.5	72	1.0134	1.0013	9.5	1,800	40	510	20, 27b
33	0	0.25	5.4	104	1.0134	1.0013	9.5	2,700	60	510	27c

Note:

- 1)  $\rho_0$  is taken to be the ambient density at the level of the nozzle
- 2) F = infinity refers to a simple jet
- 3) T = infinity refers to a buoyant jet in a uniform environment

made along the jet axes. Jet Nos. 22 to 27 were horizontal buoyant jets in uniform environments ( $T = \infty$ ). Three runs (Jet Nos. 9, 13 and 14) were conducted with negative initial angles.

1. Experiments in Linearly Density-Stratified Environments

The experiments in linearly stratified environments covered a range of initial conditions:  $F$  varied from 9 to 60 and  $T$  from 44 to 5,000.

Typical photographs of dyed jets are shown in Figs. 20 to 23. Fig. 20 shows a horizontal jet with  $F = 40$  and  $T = 510$  (Jet No. 32). Fig. 21 shows a jet discharging at  $\theta_0 = 45^\circ$  with  $F = 51$  and  $T = 210$  (Jet No. 18). Fig. 22 shows a vertical jet with  $F = 18$  and  $T = 100$  (Jet No. 10). Fig. 23 is a set of photographs showing the development of a jet in the tank experiment and was used to study the transient effect (Section VIII-A). The total elapsed time was about 2 minutes.

Traces of dyed jet boundaries were obtained directly from the negatives by using an enlarger. The calculated jet trajectories and nominal half widths ( $\sqrt{2}b$ ), obtained based upon  $\alpha = 0.082$  and  $\lambda = 1.16$ , were superimposed on the traces of experimental jet boundaries as shown in Figs. 24 to 27. They agreed well. For vertical buoyant jets ( $\theta_0 = 90^\circ$ ), the observed and calculated values of terminal height of rise  $y'_t/D$  are summarized in Table 2. The calculated values tended to underestimate the height of rise when  $\alpha$  is taken as 0.082. Better agreement for the terminal height of rise is obtained by using  $\alpha = 0.057$ . However this needs more experiments to confirm the choice.



-63-

Fig. 20. A horizontal buoyant jet in a stagnant, linearly stratified environment  
(Jet No. 32,  $F = 40$  and  $T = 510$ , Photo No. 7645.4)



Fig. 21. An inclined ( $\theta_0 = 45^\circ$ ) buoyant jet in a stagnant, linearly stratified environment (Jet No. 18,  $F = 51$  and  $T = 210$ , Photo No. 7642.3)



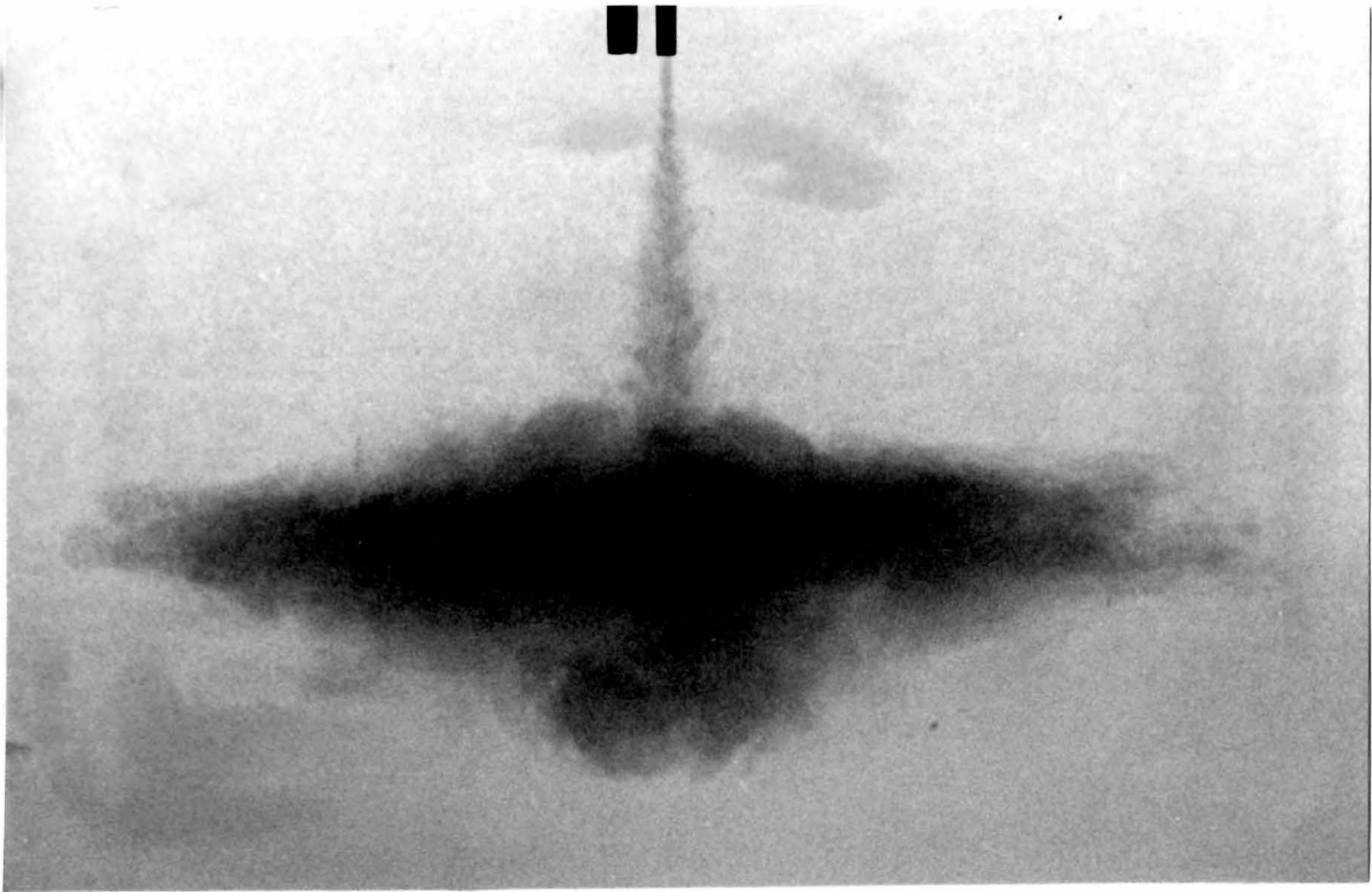
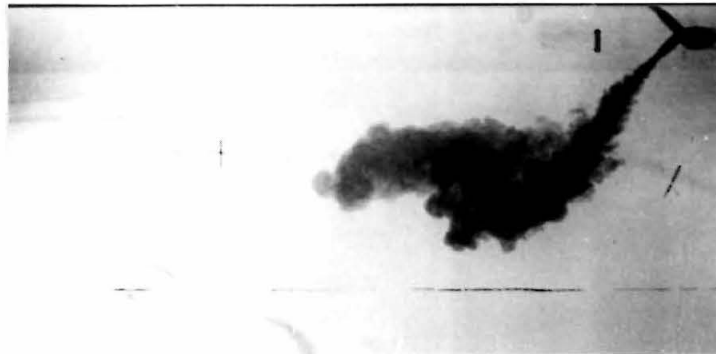
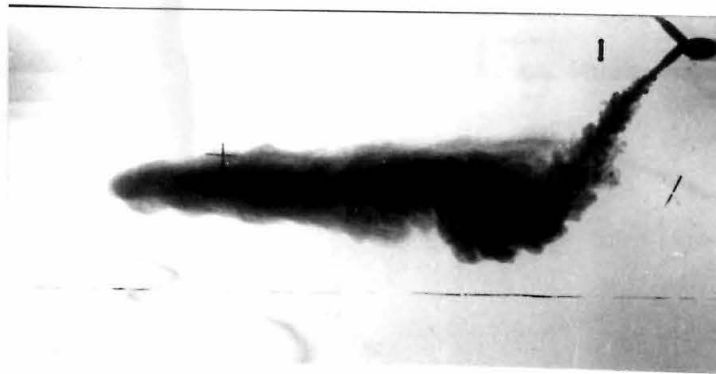


Fig. 22. A vertical buoyant jet in a stagnant, linearly stratified environment  
(Jet No. 10,  $F = 18$  and  $T = 100$ , Photo No. 7660)

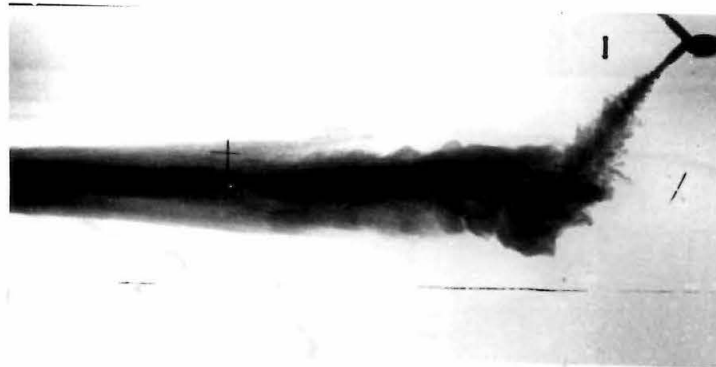
F = 9.1, T = 48,  $\theta_0 = 45^\circ$  (JET NO. 1)



A)

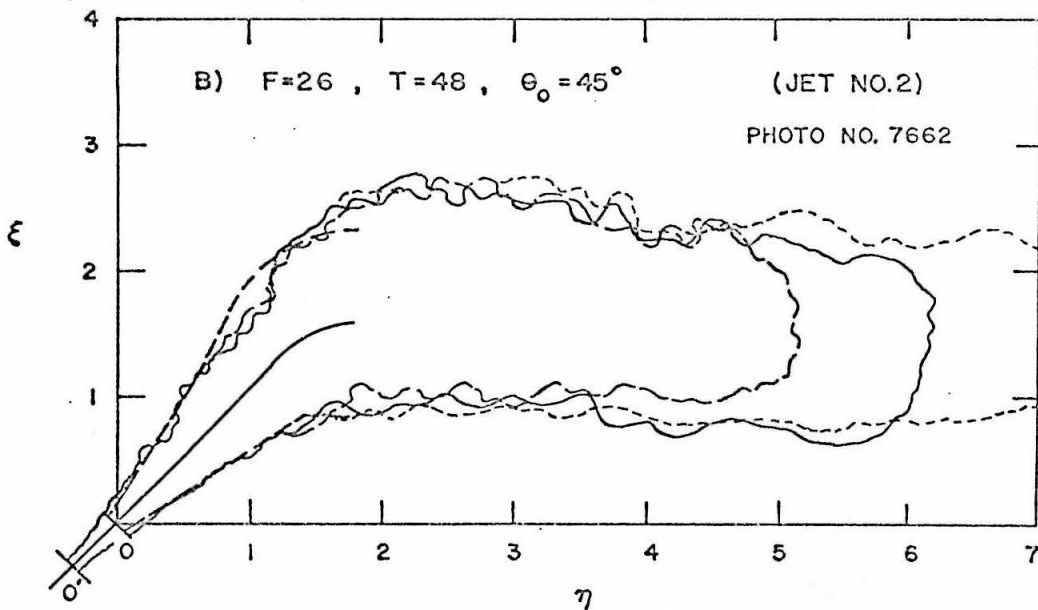
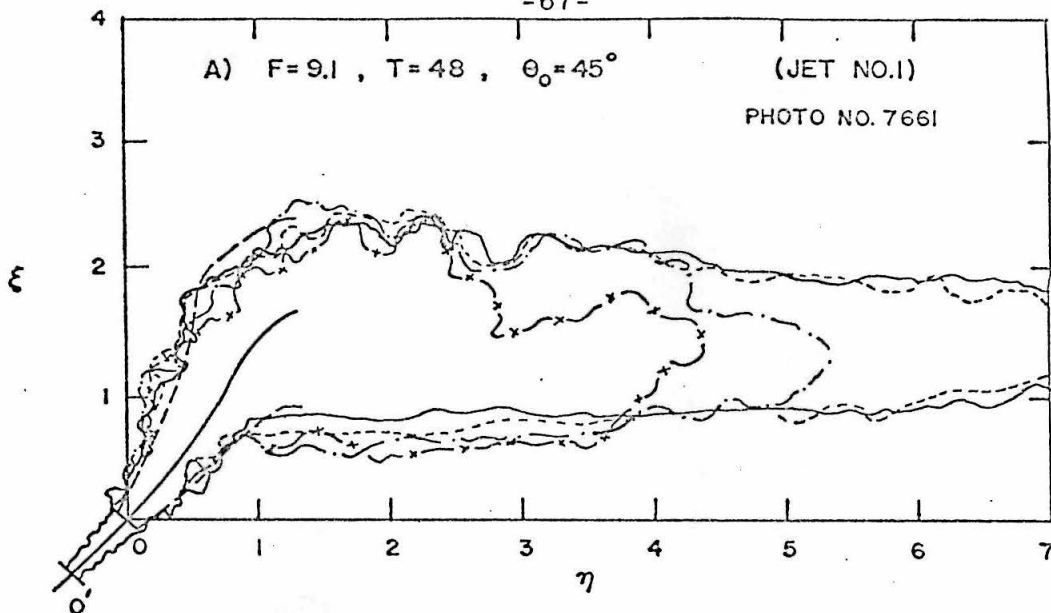


B)



C)

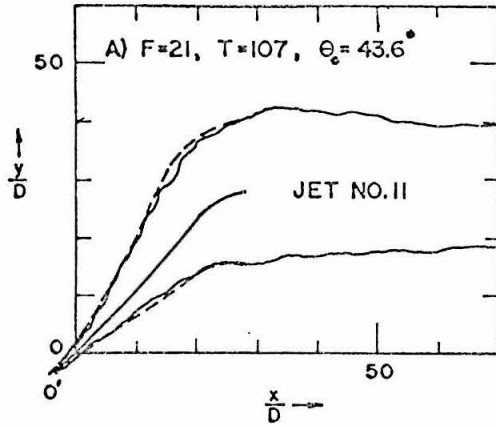
Fig. 23. Development of a round buoyant jet in a linearly stratified environment (Jet No. 1,  $\theta_0 = 45^\circ$ , F = 9.1 and T = 48, Photo No. 7661)



LEGEND

- PREDICTED JET TRAJECTORIES ( $\sigma=0.032, \lambda=1.16$ )
- - - PREDICTED NOMINAL JET BOUNDARIES
- ~~~~~ TRACES OF DYED JET BOUNDARIES
- ~~~~~ (Note: inverted in vertical direction)

Fig. 24. Predicted and observed trajectories and nominal boundaries of buoyant jets in linearly stratified environments



LEGEND

- PREDICTED JET TRAJECTORIES  
( $\alpha=0.082$ ,  $\lambda=1.16$ )
- - - PREDICTED NOMINAL JET BOUNDARIES
- ~~~~ TRACES OF DYED JET BOUNDARIES  
(Note: inverted in vertical direction)

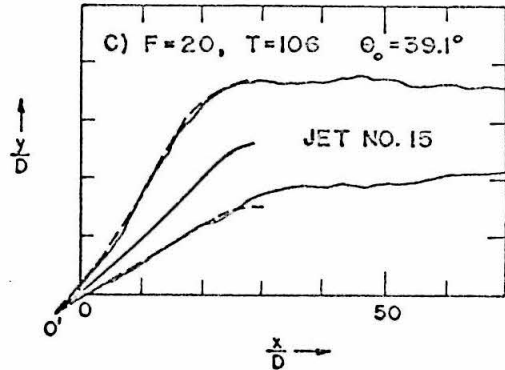
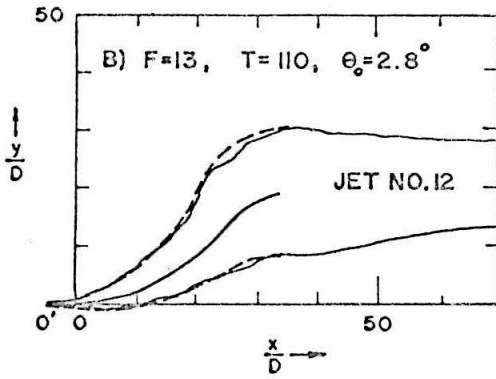


Fig. 25. Predicted and observed trajectories and nominal boundaries of buoyant jets in linearly stratified environments

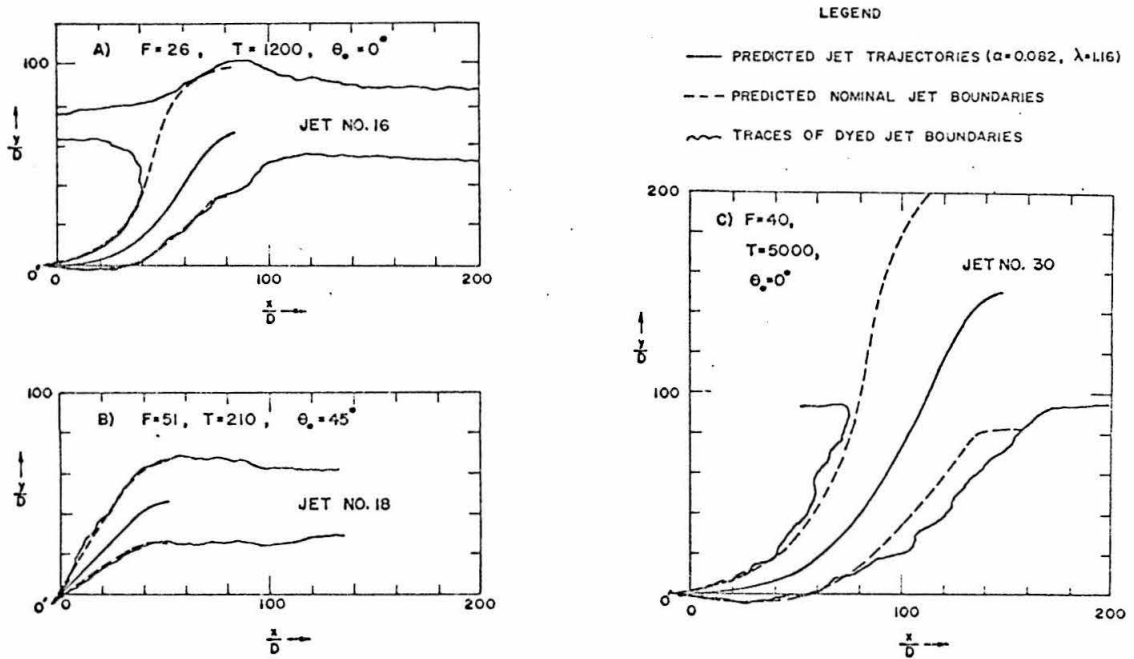
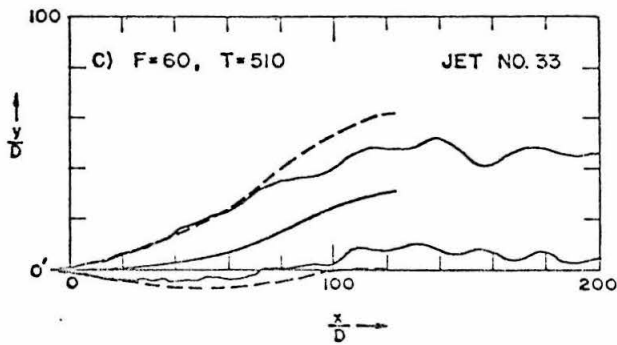
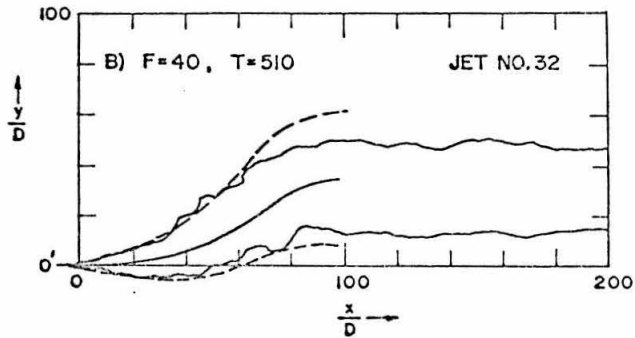
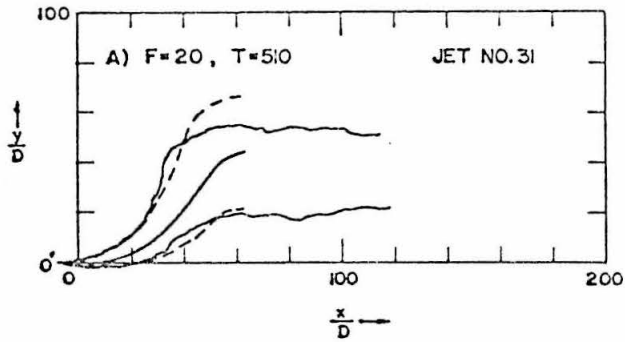


Fig. 26. Predicted and observed trajectories and nominal boundaries of buoyant jets in linearly stratified environments (note: traces inverted in the vertical direction except for Jet No. 16)



LEGEND

- PREDICTED JET TRAJECTORIES ( $\alpha=0.022, \lambda=1.16$ )
- PREDICTED NOMINAL JET BOUNDARIES
- ~ TRACES OF DYED JET BOUNDARIES (inverted in vertical direction)

Fig. 27. Predicted and observed trajectories and nominal boundaries of horizontal buoyant jets in linearly stratified environments

Table 2. Terminal Heights of Rise  $y_t'/D$  of Vertical Buoyant Jets in Linearly Stratified Environments

Jet No.	Froude Number F	Stratification Parameter T	Terminal Height of Rise $y_t'/D$			
			Observed	Predicted		
				$\alpha=0.082$	0.070	0.057
4	35	44	45	36	39	41
7	53	160	81	63	67	74
10	18	100	43	39	42	45

The experiments are not detailed enough to give the sure value of  $\alpha$ . The prediction by using  $\alpha = 0.082$  gives a reasonably good estimate of the jet trajectories and the half widths, although the results are not too sensitive to  $\alpha$ . For vertical jets, the value  $\alpha = 0.057$  gave better results in estimating the terminal heights of rise. More experiments are needed to confirm such choice for vertical jets.

## 2. Experiments in Uniform Environments

Six horizontal buoyant jet runs (Jet Nos. 22 to 27) were conducted in uniform environments. A typical photograph of the dyed jet with  $F = 40$  (Jet No. 27) is shown in Fig. 28. The traces of jet boundaries were compared with theoretical jet trajectories and nominal half widths as shown in Figs. 29 and 30. The observed jet boundaries matched well with theoretical values by using coefficients  $\alpha = 0.082$  and  $\lambda = 1.16$ . In Fig. 29, the jet trajectories given by Abraham's (1) analysis are also shown. His trajectories tended to overestimate the horizontal distance of travel. This may be due to an overstressing of the non-buoyant behavior of the jets in his rate of growth functions.

Concentration measurements taken on the center plane of Jet No. 22 revealed that the maximum concentration values did occur midway between the dyed jet boundaries. The technique of concentration measurement is described in detail in Section VII-B.

## 3. Experiments on Simple Jets

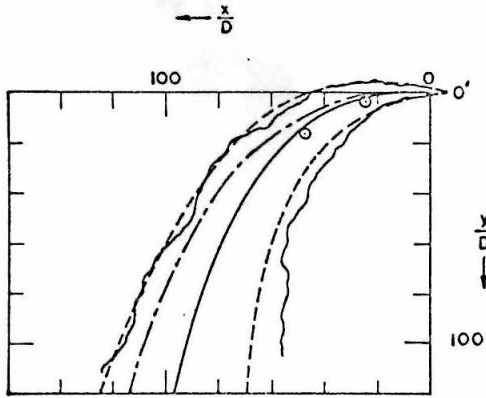
Three runs (Jet Nos. 19, 20 and 21) were made without any density difference. The increase in density of the jet fluid due to salt concentration was balanced by adding a proper amount of sugar to the ambient fluid. Concentration measurements were made along the jet axes. The results are shown in Fig. 31 and agree well with the relation:

$$S_o = 0.185 \frac{x'}{D} \quad (59)$$



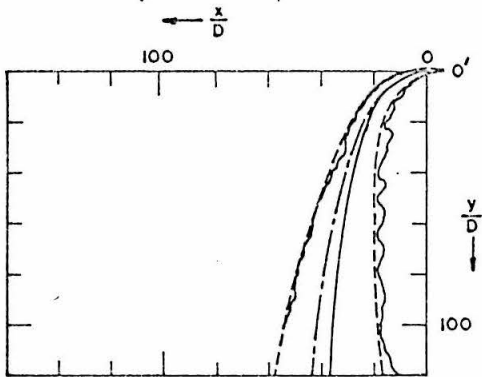


Fig. 28. A horizontal buoyant jet in a stagnant, uniform environment (Jet No. 27,  $F = 40$ , Photo No. 7643-5)

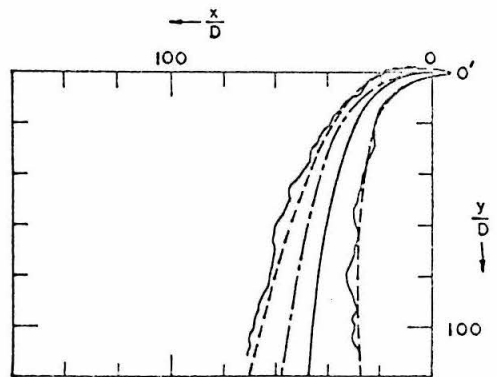


A) F=33 (JET NO. 22)

- LEGEND
- PREDICTED TRAJECTORIES ( $\alpha=0.032, \lambda=1.16$ )
  - - - PREDICTED NOMINAL JET BOUNDARIES
  - ~ TRACES OF DYED JET BOUNDARIES
  - - - ABRAHAM'S ANALYSIS A) F=31.6  
B) F=10  
C) F=14.1
  - JET AXIS BY CONCENTRATION MEASUREMENTS

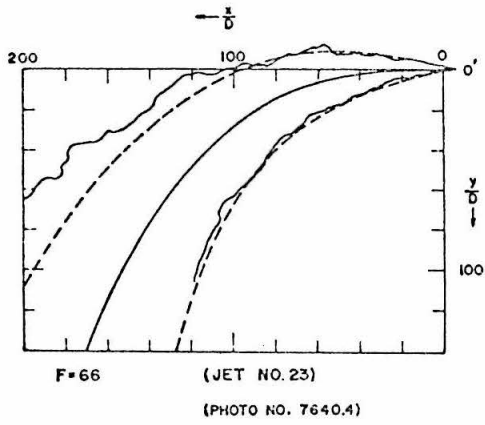


B) F=10 (JET NO. 25)



C) F=13.6 (JET NO. 26)

Fig. 29. Predicted and observed trajectories and nominal boundaries of horizontal buoyant jets in uniform environments



LEGEND

- PREDICTED JET TRAJECTORIES ( $\alpha=0.082$ ,  $\lambda=1.16$ )
- - - PREDICTED NOMINAL JET BOUNDARIES
- ~ TRACES OF DYED JET BOUNDARIES

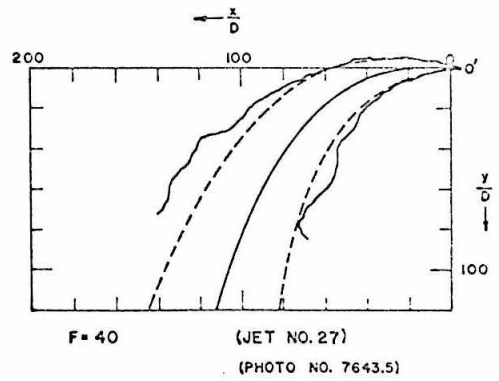
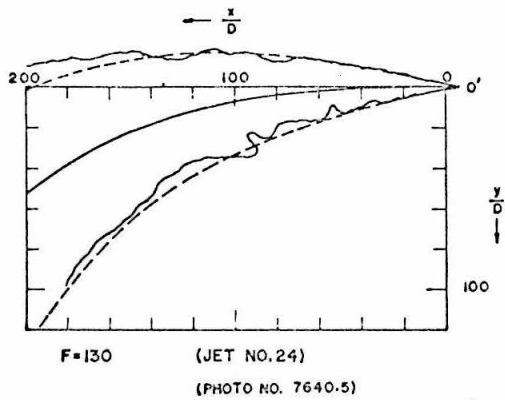


Fig. 30. Predicted and observed trajectories and nominal boundaries of horizontal buoyant jets in uniform environments

which can be derived from Albertson et al's (5) results, eq. (1),  
by taking  $\lambda = 1.16$ , i. e.:

$$S_o = \frac{2\lambda^2}{1+\lambda^2} \frac{\mu}{\mu_o} = \frac{4\lambda^2}{1+\lambda^2} \frac{Q}{Q_o} = 0.185 \frac{x'}{D}$$

The deviation of experimental values of  $S_o$  from this relation ranges  
from +3% to -1%.

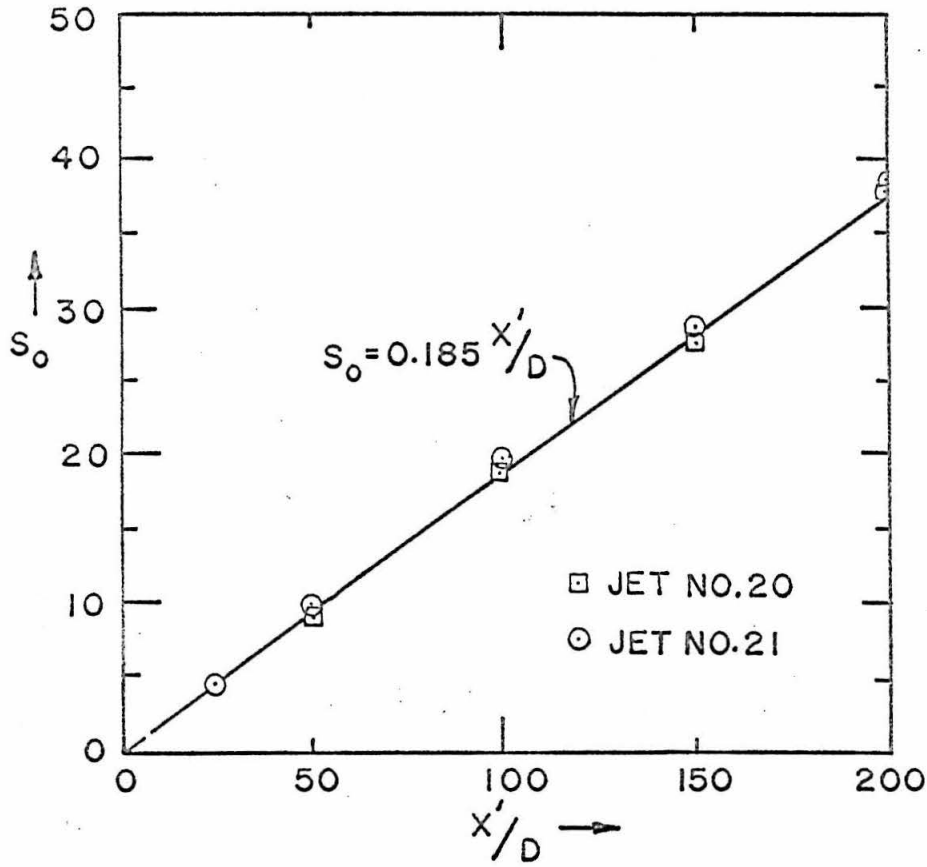


Fig. 31. Dilution ratio  $S_0$  along the axis of a simple jet ( $R \sim 6,000$ )

## CHAPTER VI

### THEORETICAL ANALYSIS FOR A ROUND BUOYANT JET IN A UNIFORM CROSS STREAM OF HOMOGENEOUS DENSITY

In this chapter theoretical solutions are obtained for a round buoyant jet injected normally into a stream of homogeneous density. The problem is formulated based upon the assumptions listed in Chapter III. The equations are solved numerically after normalization. Solutions are presented for some specific cases. Those solutions corresponding to ten experimental cases are given in Section VII-C. Limitations of the theoretical solutions are discussed in Section VIII-B.

#### VI-A. Formulation of the Problem

##### 1. Conservation equations

The basic assumptions are listed in Chapter III. The velocity and buoyancy profiles are assumed to be:

$$u^*(s, r, \varphi) = U_a \cos \theta + u(s) e^{-r^2/b^2} \quad (18)$$

and

$$\rho_a - \rho^*(s, r, \varphi) = [\rho_a - \rho(s)] e^{-r^2/b^2} \quad (19)$$

A schematic diagram of a jet in a cross stream is shown in Fig. 32. The jet boundary is defined to be  $\sqrt{2} b$  from the jet axis.

The continuity relation, based upon the entrainment mechanism represented by eq. (17), can be expressed as:

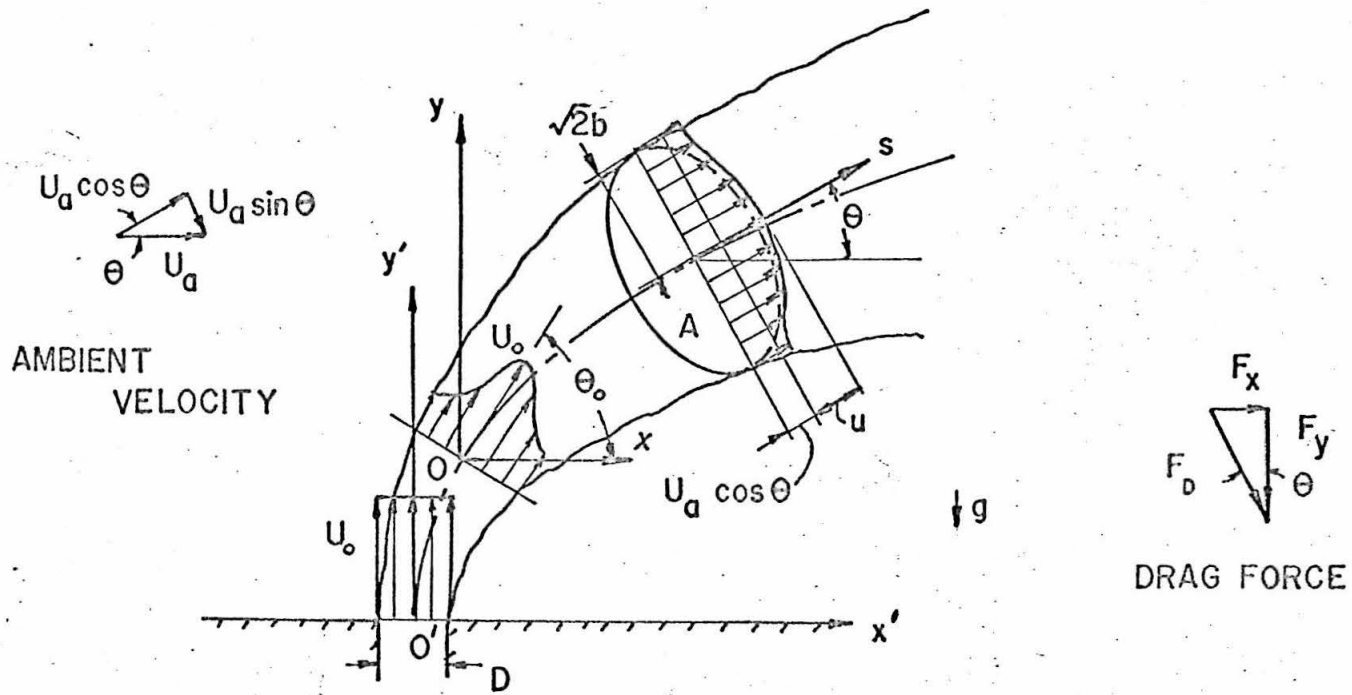


Fig. 32. Schematic diagram for the analysis of a round buoyant jet in a cross stream

$$\begin{aligned} \frac{d}{ds} \int_A u^* dA &= 2\pi \alpha b |\bar{U}_j - \bar{U}_a| \\ &= 2\pi \alpha b (U_a^2 \sin^2 \theta + u^2)^{1/2} \end{aligned} \quad (60)$$

The left-hand side of eq. (60), by substituting eq. (18) for  $u^*$ , becomes

$$\begin{aligned} \frac{d}{ds} \int_A (U_a \cos \theta + u e^{-r^2/b^2}) dA \\ = \frac{d}{ds} \int_0^{\sqrt{2}b} 2\pi r (U_a \cos \theta + u e^{-r^2/b^2}) dr, \end{aligned}$$

which, for simplicity, is approximated by:

$$\begin{aligned} \frac{d}{ds} \int_A u^* dA &\simeq \frac{d}{ds} \int_0^{\sqrt{2}b} 2\pi r U_a \cos \theta dr + \int_0^{\infty} 2\pi r u e^{-r^2/b^2} dr \\ &= \frac{d}{ds} [\pi b^2 (2U_a \cos \theta + u)] \end{aligned}$$

Thus eq. (60) can be written as,

$$\begin{aligned} \frac{d}{ds} [b^2 (2U_a \cos \theta + u)] &= 2\alpha b (U_a^2 \sin^2 \theta + u^2)^{1/2} \\ &\quad \text{(continuity)} \end{aligned} \quad (61)$$

The momentum equations can be written in integral forms by assuming a gross drag term with a drag coefficient  $C_d$ . In the x-direction, the rate of change of momentum flux is equal to the rate of entrainment of ambient momentum flux plus the drag force acting on the jet:



$$\frac{d}{ds} \int_A \rho^* u^* (u^* \cos \theta) dA = \rho_a 2\pi \alpha b U_a |\bar{U}_j - \bar{U}_a| + F_D \sin \theta \quad (62)$$

where  $F_D$  is the drag force assumed to be:

$$F_D = C_d \frac{\rho_a U_a^2 \sin^2 \theta}{2} 2\sqrt{2}b \quad (63)$$

The left-hand side of eq. (62), by substituting eq. (18), becomes:

$$\begin{aligned} & \frac{d}{ds} \int_0^{\sqrt{2}b} \rho^* 2\pi r (U_a \cos \theta + u e^{-r^2/b^2})^2 \cos \theta dr \\ \simeq & \rho_a \frac{d}{ds} \int_0^{\sqrt{2}b} 2\pi r U_a^2 \cos^2 \theta dr + \int_0^{\infty} 2\pi r (2U_a \cos \theta + u e^{-r^2/b^2}) u e^{-r^2/b^2} dr \cos \theta \\ = & \rho_a \frac{d}{ds} \left[ 2\pi b^2 U_a^2 \cos^2 \theta + 2\pi b^2 U_a u \cos \theta + \frac{\pi b^2 u^2}{2} \cos \theta \right] \\ = & \rho_a \frac{d}{ds} \left[ \frac{\pi}{2} b^2 (2U_a \cos \theta + u)^2 \cos \theta \right] \end{aligned}$$

By substituting the entrainment eq. (17) and dividing by  $\rho_a \pi$ , eq. (62) can be written as:

$$\begin{aligned} \frac{d}{ds} \left[ \frac{b^2}{2} (2U_a \cos \theta + u)^2 \cos \theta \right] &= 2\alpha b U_a (U_a^2 \sin^2 \theta + u^2)^{1/2} \\ &+ \frac{C_d \sqrt{2}}{\pi} U_a^2 b^2 \sin^3 \theta \end{aligned}$$

(x-momentum)

(64)

In the y-direction, the rate of change of the momentum flux is equal to the gravity force acting on the jet cross section less the y-component of the drag force:

$$\frac{d}{ds} \int_A \rho^* u^* (u^* \sin \theta) dA = \int_A g(\rho_a - \rho^*) dA - F_D \cos \theta \quad (65)$$

Integrating and dividing by  $\rho_a \pi$ ,

$$\frac{d}{ds} \left[ \frac{b^2}{2} (2U_a \cos \theta + u)^2 \sin \theta \right] = b^2 g \frac{\rho_a - \rho}{\rho_a} - \frac{C_d \sqrt{2}}{\pi} U_a^2 b^2 \sin^2 \theta \cos \theta$$

(y-momentum) (66)

The density deficiency flux, induced by heat content or salt deficiency, should be conserved since the ambient fluid is homogeneous:

$$\frac{d}{ds} \int_A u^* (\rho_a - \rho^*) dA = 0 \quad (67)$$

By substituting eqs. (18) and (19) into eq. (67):

$$\begin{aligned} & \frac{d}{ds} \int_0^{\sqrt{2}b} 2\pi r (U_a \cos \theta + u e^{-r^2/b^2}) (\rho_a - \rho) e^{-r^2/b^2} dr \\ & \simeq \frac{d}{ds} \int_0^{\infty} 2\pi r (U_a \cos \theta + u e^{-r^2/b^2}) (\rho_a - \rho) e^{-r^2/b^2} dr \\ & = \frac{d}{ds} \left[ \frac{\pi b^2}{2} (2U_a \cos \theta + u) (\rho_a - \rho) \right] \\ & = 0 \end{aligned}$$

Then,

$$\frac{d}{ds} \left[ b^2 (2U_a \cos \theta + u) (\rho_a - \rho) \right] = 0$$

(density deficiency) (68)

The flux of any specific tracer of concentration  $c^*$  contained in the jet flow should also be conserved, i. e.

$$\frac{d}{ds} \int_A c^* u^* dA = 0$$

(69)

Integrating by substituting eqs. (18) and (20),

$$\frac{d}{ds} \left[ b^2 (2U_a \cos \theta + u) c \right] = 0$$

(continuity of a tracer) (70)

## 2. Geometric relations

The jet trajectories are determined by solving the following two equations with the set of equations listed above:

$$\frac{d}{ds} x = \cos \theta \quad \text{(geometry)} \quad (71)$$

and

$$\frac{d}{ds} y = \sin \theta \quad \text{(geometry)} \quad (72)$$

Therefore the problem has seven unknowns:  $u$ ,  $b$ ,  $\theta$ ,  $\rho_a - \rho$ ,  $c$ ,  $x$  and  $y$  to be solved from seven simultaneous ordinary differential equations (61), (64), (66), (68), (70), (71) and (72).

### 3. Initial conditions

The initial conditions given at the beginning of the zone of established flow at  $O$  are:

$$\begin{aligned} u(0) &= u_0, \quad b(0) = b_0, \quad \rho(0) = \rho_1, \quad \theta(0) = \theta_0, \\ c(0) &= c_0, \quad x = 0, \quad \text{and } y = 0 \text{ at } s = 0 \end{aligned} \quad (73)$$

where the initial angle  $\theta_0$  is no longer 90 degrees as stated in Section III-C.

Eqs. (68) and (70) can be integrated immediately. The conservation of density deficiency is then expressed as:

$$b^2(2U_a \cos \theta + u) (\rho_a - \rho) = \text{const.} \quad (\text{density deficiency}) \quad (74)$$

This equation, with appropriate initial conditions, may be used to eliminate  $(\rho_a - \rho)$  in eq. (66). Furthermore, the continuity of the tracer substance is:

$$b^2(2U_a \cos \theta + u) c = \text{const.} \quad (\text{continuity of a tracer}) \quad (75)$$

Therefore both  $(\rho_a - \rho)$  and  $c$  values can be determined easily from the solutions of the term  $b^2(2U_a \cos \theta + u)$ . Thus there are only five unknowns remaining in the solution of a system of five simultaneous ordinary differential equations.

VI-B. Normalized Equations and Dimensionless Parameters

The set of equations are then normalized by defining dimensionless parameters as follows, using initial values:

Volume flux parameter:

$$\mu = b^2 (2U_a \cos \theta + u) / [b_o^2 (2U_a \cos \theta_o + u_o)] \quad (76)$$

Momentum flux parameters:

$$m = \frac{b^2 (2U_a \cos \theta + u)^2}{b_o^2 (2U_a \cos \theta_o + u_o)^2} \quad (\text{s-direction})$$

$$h = m \cos \theta \quad (\text{x-direction}) \quad (77)$$

$$v = m \sin \theta \quad (\text{y-direction})$$

$$\text{Velocity ratio: } k = (u_o + U_a \cos \theta_o) / U_a = U_o / U_a \quad (78)$$

$$\text{Buoyancy parameter: } f = b_o g \frac{\rho_a - \rho}{\rho_a} / (k^2 U_a^2) \quad (79)$$

Coordinates:

$$\text{s: } \zeta = \frac{2\alpha}{b_o} s$$

$$\text{x: } \eta = \frac{2\alpha}{b_o} x \quad (80)$$

$$\text{y: } \xi = \frac{2\alpha}{b_o} y$$

Equations (61), (64), (66), (71) and (72) are then normalized in terms of these dimensionless parameters:

$$\frac{d\mu}{d\zeta} = \frac{1}{k'} \mu \psi / m \quad (81)$$

$$\frac{dh}{d\zeta} = \frac{1}{k'^2} \frac{\mu}{m} [2\psi + C_d' \sin^3 \theta] \quad (82)$$

$$\frac{dv}{d\zeta} = f \frac{\mu}{m} - \frac{C_d'}{k'^2} \frac{\mu}{m} \sin^2 \theta \cos \theta \quad (83)$$

$$\frac{d\eta}{d\zeta} = \cos \theta \quad (84)$$

$$\frac{d\xi}{d\zeta} = \sin \theta \quad (85)$$

where,

$$k' = k + \cos \theta_0$$

$$\psi = [\sin^2 \theta + (m/\mu - 2 \cos \theta)^2]^{1/2}$$

and

$C_d' = C_d \sqrt{2}/\alpha\pi$  is defined as a reduced drag coefficient.

The initial conditions at  $\zeta = 0$  are:

$$\mu(0) = 1, m(0) = 1, \theta(0) = \theta_0, \xi(0) = 0 \text{ and } \eta(0) = 0 \quad (86)$$

The initial angle of jet inclination  $\theta_0$ , must be evaluated at the end of the zone of flow establishment. In Section VI-E it will be shown that  $\theta_0$  may be considered as a function of the velocity ratio,  $k$ . Thus,

there are two parameters relevant to the problem; namely the velocity ratio  $k$  and the buoyancy parameter  $f$ . The value of  $C_d'$  is to be determined from the experiments as shown in Section VII-C.

#### VI-C. Method of Numerical Solution

The system of ordinary differential equations is similar in nature to the equations for jets in stagnant environments shown in Chapter IV. Hence the numerical solutions were carried out by the same technique as stated in Section IV-C.

For each set of values of  $k$ ,  $f$ , and  $C_d'$  a numerical calculation was made. The  $\theta_0$  values used are based upon eq. (87) shown in Section VI-E. The coefficients  $\alpha$  and  $C_d'$  were determined by comparing experimental and calculated values of dilution ratios and trajectories as presented in Section VII-C.

#### VI-D. Solutions of Gross Behavior of Jets

Fig. 33 shows the calculated variations of the momentum flux parameter  $m$  and volume flux parameter  $\mu$  with the normalized distance along the jet trajectory,  $\zeta$ , for the cases  $k = 4$  and  $f = 0.00269$  at two different drag coefficients  $C_d' = 0.7$  and  $1.2$ . Both  $m$  and  $\mu$  increase steadily with the distance of travel  $\zeta$ . Fig. 34 shows the variations for the case  $k = 8$  and  $f = 0.00103$  at a chosen  $C_d'$  value of  $0.5$ .

Fig. 35 shows the decay of jet velocity along  $\zeta$ -coordinate for both cases of  $k = 4$  and  $8$ . The jet velocities approach the value of

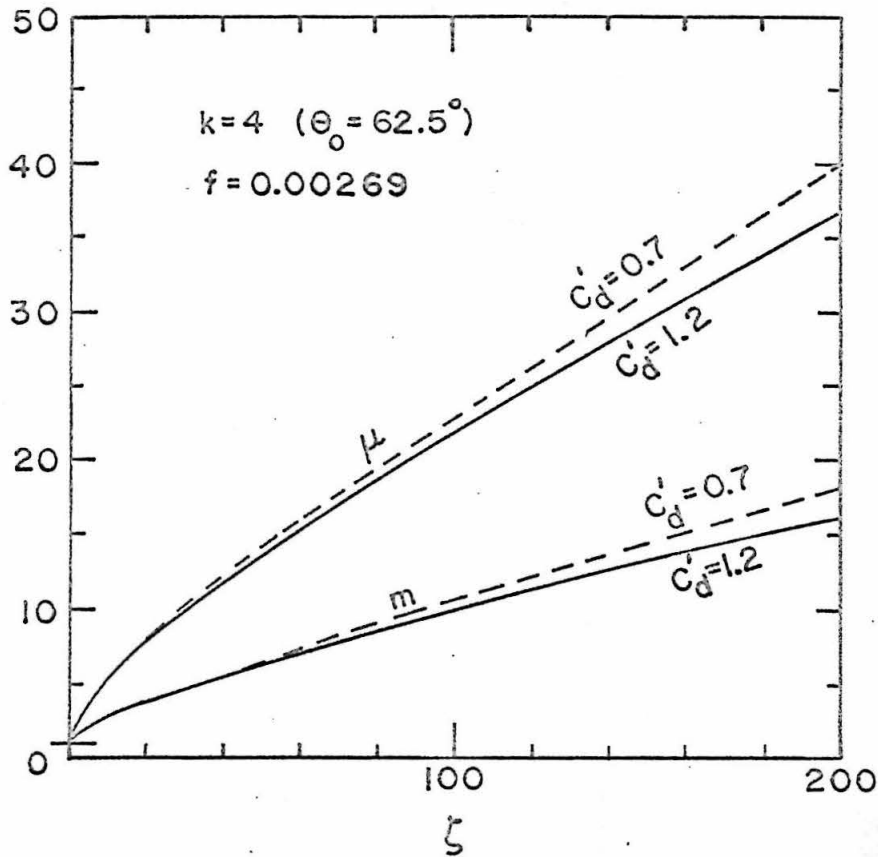


Fig. 33. Variation of volume flux parameter,  $\mu$ , and momentum flux parameter  $m$  along  $\zeta$ -coordinate for a buoyant jet in a uniform cross stream with  $k = 4$  and  $f = 0.00269$  (for  $\alpha = 0.5$ ,  $F = 20$ ).



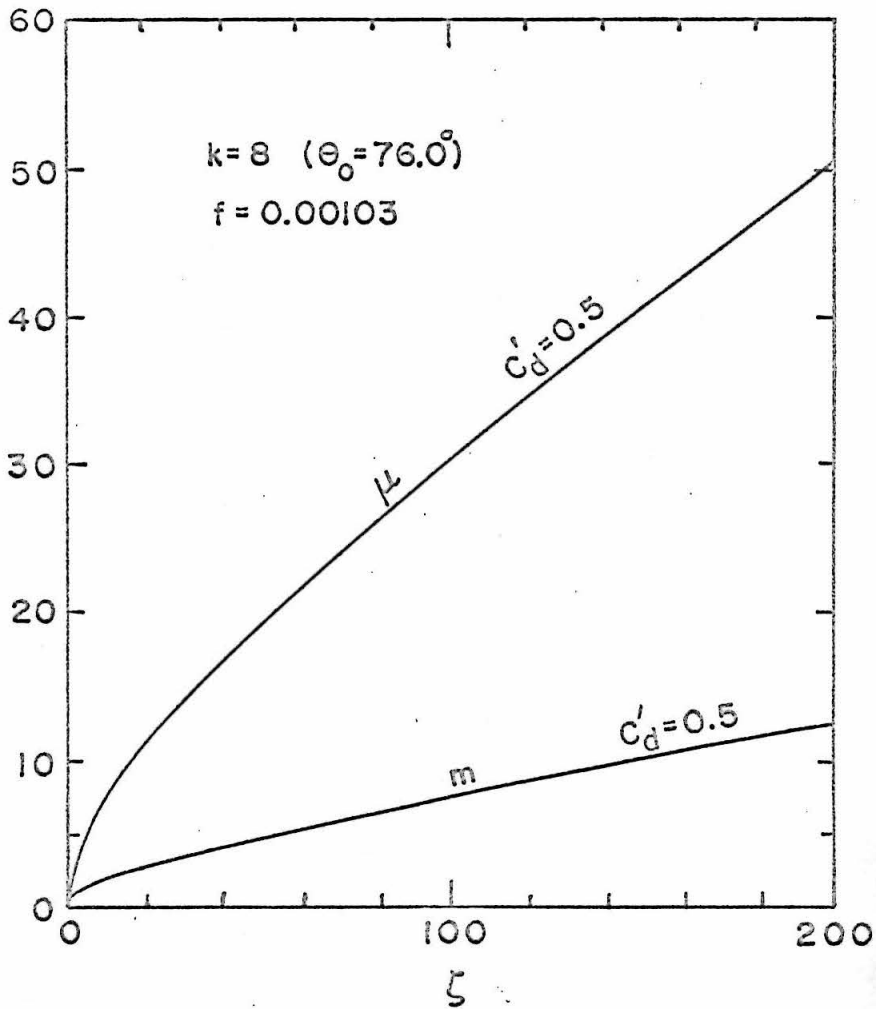


Fig. 34. Variation of volume flux parameter,  $\mu$ , and momentum flux parameter,  $m$ , along  $\zeta$ -coordinate for a buoyant jet in a uniform cross stream with  $k = 8$  and  $f = 0.00103$  (for  $\alpha = 0.4$ ,  $F = 40$ ).

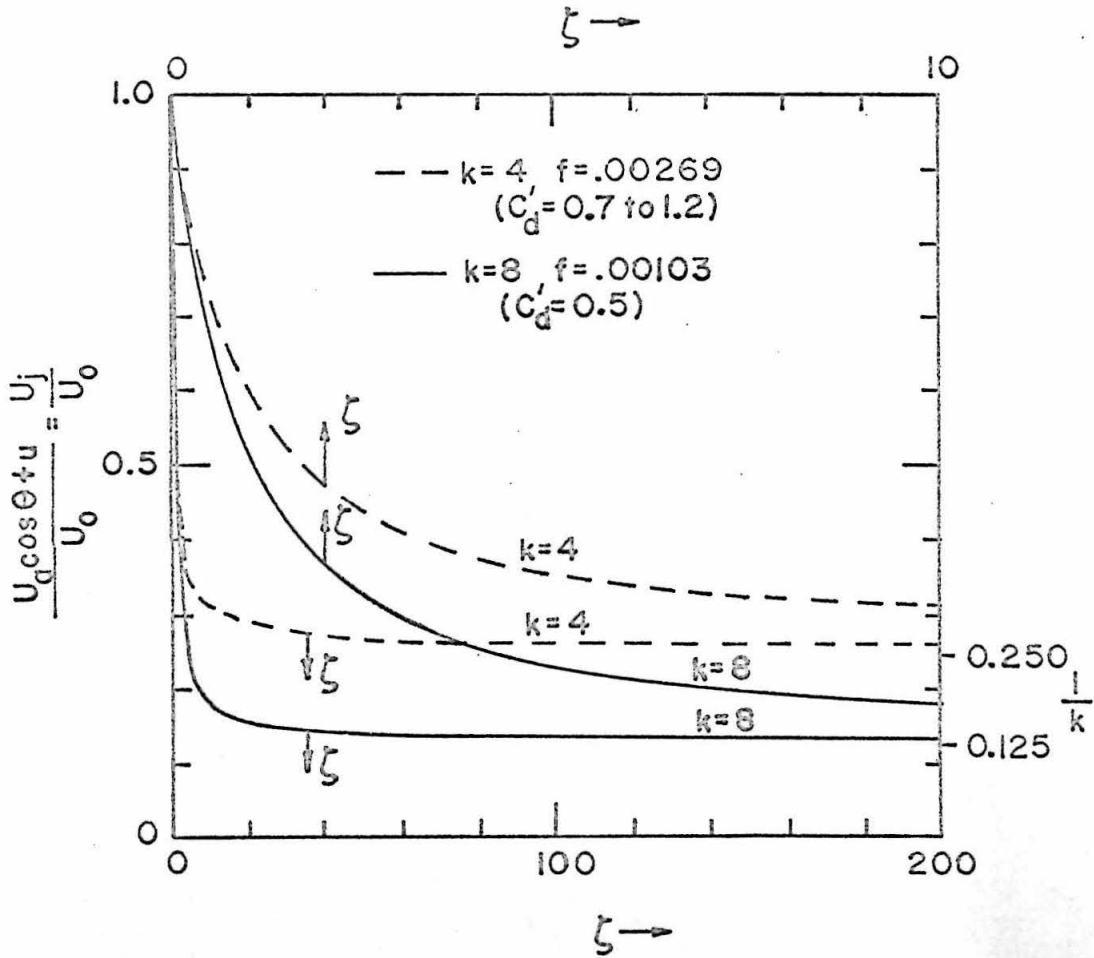


Fig. 35. Variation of the ratio of the jet center line velocity,  $U_j$ , and jet discharge velocity  $U_0$  along  $\zeta$ -coordinate for buoyant jets in uniform cross streams

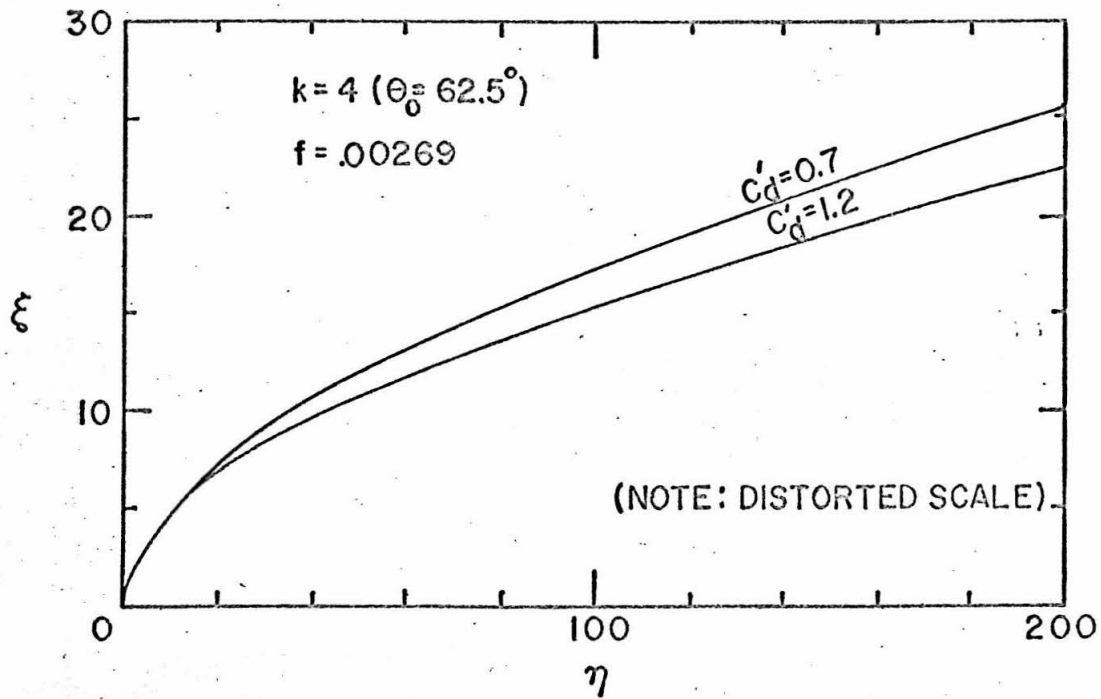


Fig. 36. Trajectory of a buoyant jet in a uniform cross stream with  $k=4$  and  $f=0.00269$  (for  $\alpha = 0.5$ ,  $F=20$ )

the ambient velocity rapidly. Such relations are probably affected little by the choice of the drag coefficient as implied by the case  $k = 4$ .

Jet trajectories for the case  $k = 4$  are shown in Fig. 36 for two different drag coefficients  $C_d'$ . As  $C_d'$  increases the trajectory bends over more rapidly as expected.

Solutions for ten experimental cases are presented in Section VII-C for comparison with the experimental jet trajectories, half widths and dilution ratios.

#### VI-E. Application to Practical Problems

In practical applications the zone of flow establishment has to be defined. A definition sketch and the jet trajectories obtained by Gördier (15), Jordinson (17) and Keffer and Baines (18) near the nozzle  $O'$  are shown in Fig. 37. The results shown were determined by velocity measurements in ordinary (non-buoyant) jets in cross streams. Based upon Gördier's results the length of the zone  $s_e'$  is assumed to follow the relation expressed in Fig. 38. The initial angles  $\theta_o$  were then measured from the trajectories shown in Fig. 37 and expressed as shown in Fig. 39. The relation can be assumed as:

$$\theta_o = 90 - 110/k \quad (\text{in degrees}) \quad (87)$$

The relations are obtained from the experiments on ordinary jets but are assumed to be applicable to buoyant jets as well.

By considering the conservation of the flux of density deficiency at two cross sections at  $O$  and  $O'$ :

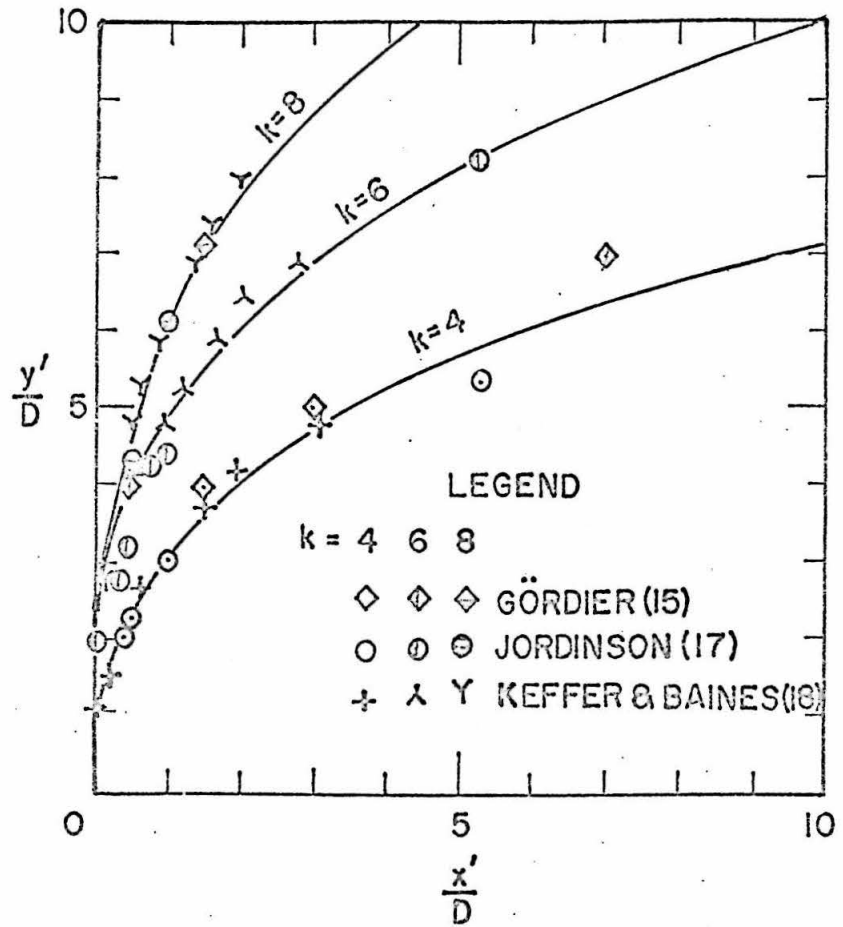
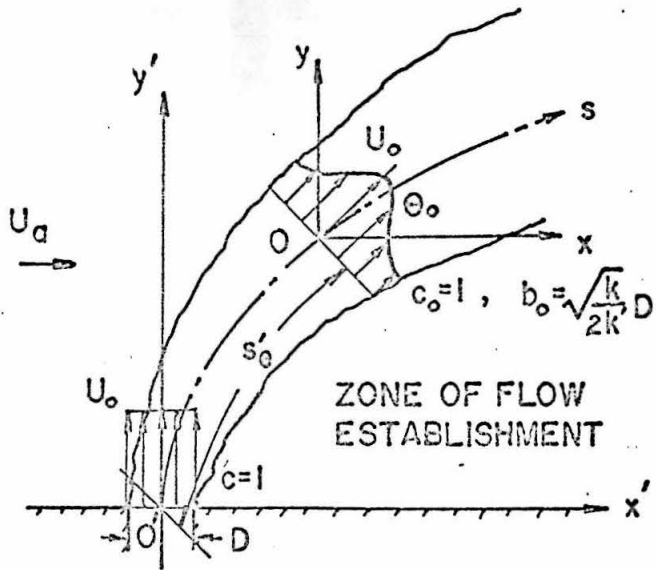


Fig. 37. Definition sketch and measured trajectories for the zone of flow establishment ( $O' \rightarrow O$ ) of round jets in cross streams at  $k=4, 6$  and  $8$

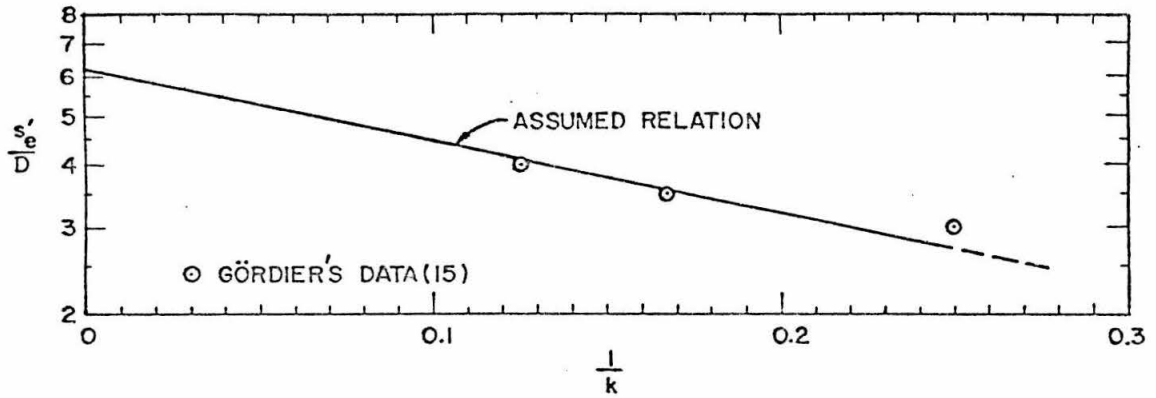


Fig. 38. Values of  $s'_e/D$ , length of the zone of flow establishment, as a function of  $1/k$  for jets in uniform cross streams

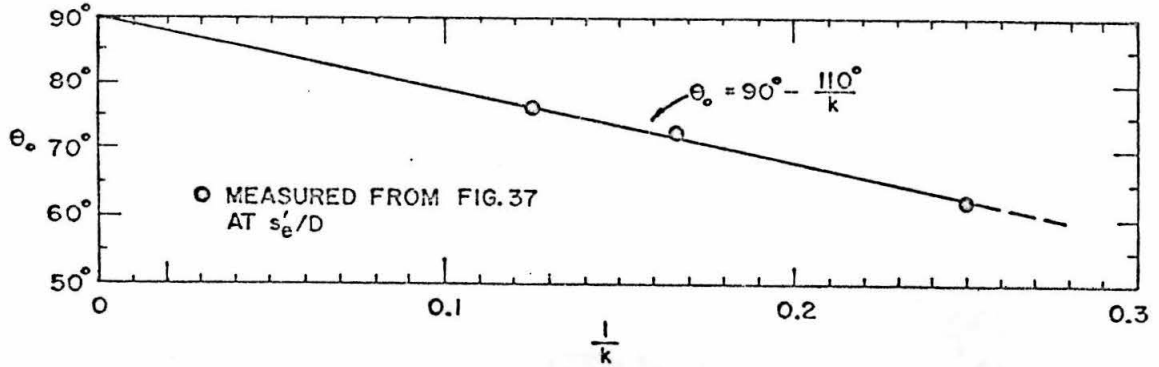


Fig. 39. Initial angle  $\theta_0$  as a function of  $1/k$  for jets in uniform cross streams

$$\frac{1}{2} \pi b_o^3 (2U_a \cos \theta_o + u_o) \frac{\rho_a - \rho_1}{\rho_a} = \frac{\pi D^3}{4} U_o \frac{\rho_a - \rho_1}{\rho_a} \quad (88)$$

the value  $b_o$  is found to be related to the diameter  $D$  by:

$$b_o = D \sqrt{k/2k'} \quad (89)$$

The buoyancy parameter  $f$  is then related to the densimetric Froude number of the jet,  $F$ , defined by eq. (11), by:

$$f = \left[ \frac{1}{2\alpha} \left( \frac{k}{k'} \right)^{5/2} \right] / F^2 \quad (90)$$

or,

$$F = \left\{ \frac{1}{2\alpha f} \left( \frac{k}{k'} \right)^{5/2} \right\}^{1/2} \quad (91)$$

The dilution ratio of a certain tracer substance  $S$  along the jet axis is directly related to the volume flux parameter  $\mu$  by:

$$S \equiv \mu = \frac{c_o}{c} \quad (92)$$

Values of the entrainment coefficients and drag coefficients are determined in the next chapter. By using these values the jet gross behavior can be predicted from the theoretical analysis.

Limitations of the analysis are discussed in Section VIII-B.

## CHAPTER VII

### EXPERIMENTAL STUDY FOR A ROUND BUOYANT JET IN A UNIFORM CROSS STREAM OF HOMOGENEOUS DENSITY

Experiments on buoyant jets in cross streams are described in this chapter. First, the objectives are outlined, and then the experimental procedure and apparatus are described in detail. The results of the experiments are summarized in the final section and discussed in Section VIII-B.

#### VII-A. Objectives of the Experimental Investigation

The objectives of the experimental investigation are:

1. to determine the gross behavior of the jet flows and compare with the theoretical solutions (see Chapter VI),
2. to examine the validity of the assumptions made in the analysis,
3. to provide the numerical values of the entrainment coefficient,  $\alpha$ , and the drag coefficient,  $C_d$ .

The velocity along the jet axis decays rapidly and approaches the value of the ambient velocity in a short distance. The excess of velocity is difficult to measure. Also, it is a vector quantity whose direction should be determined as well as its magnitude. Hence the velocity measurement was not carried out in this study.



Salt concentration in the jet flow, on the other hand, could be determined easily by conductivity measurements. The results of such measurements not only gave the variation of concentration but could also be used to locate the jet axis and the variations of the width of the jets. Therefore, conductivity measurements were made to determine these quantities.

To make the experiments simpler, salt water was injected into the flowing stream of fresh water from the top, thus producing a sinking jet. Because of the very small density difference between the fluids, the analysis for the sinking jet discharged down is the same as for the buoyant jet discharged up, except for reversal of the gravity force. Photographs of a sinking jet may simply be turned upside down to show a buoyant jet.

#### VII-B. Procedure and Apparatus

Experiments were conducted in flows covering a range of initial conditions with different jet densimetric Froude numbers and velocity ratios. The general setup for the experiments is shown in Fig. 40 and explained in detail in the following sections. In each run a jet of heavy fluid was discharged into the flume flow from the free surface. Conductivity measurements were carried out at several cross-sections normal to the jet axis. A set of towed jet experiments was also performed in the flume without flow to determine the effects of ambient turbulence.

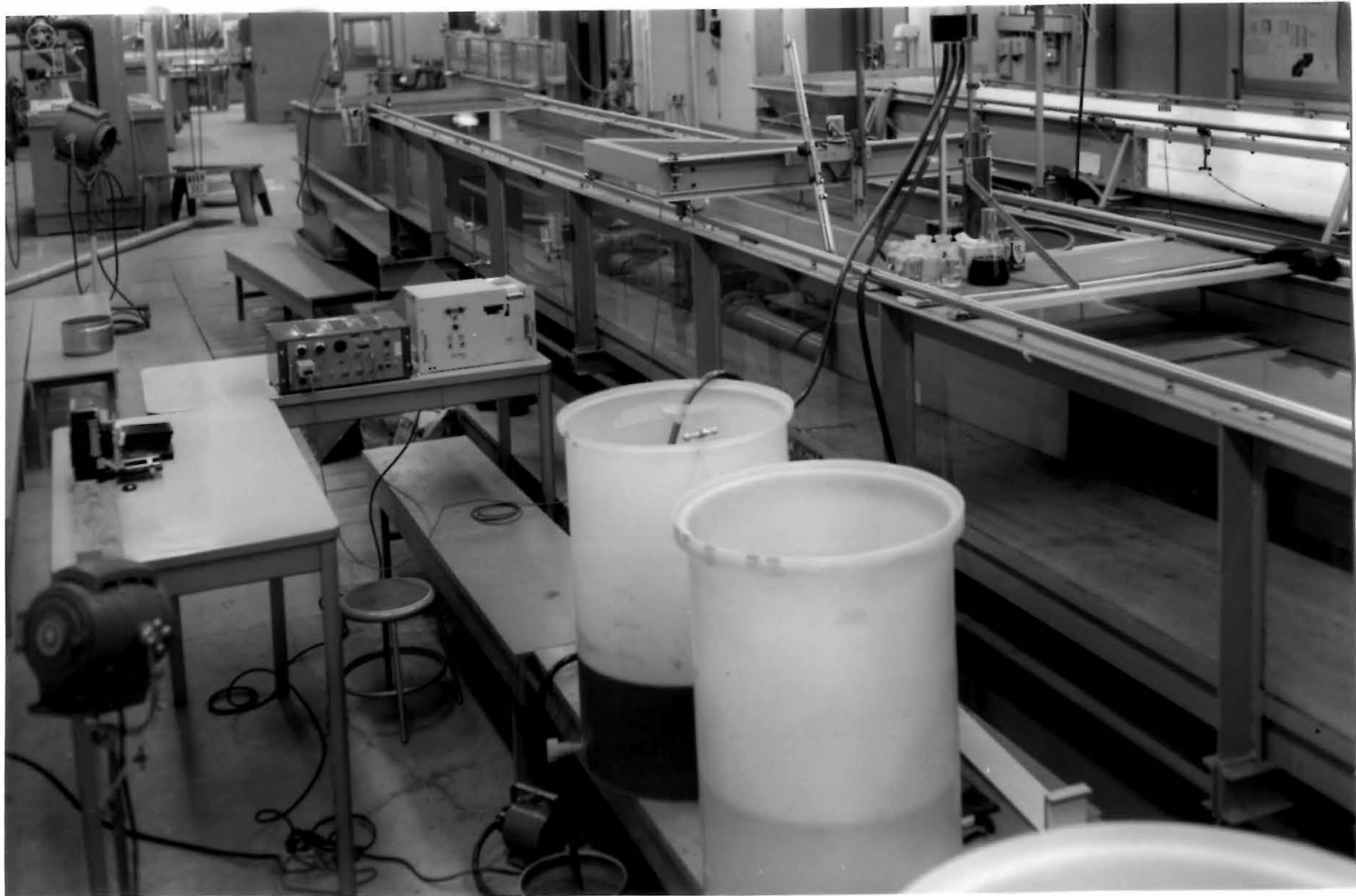


Fig. 40. General experimental setup for buoyant jets in cross streams.

1. The flume and flume flows

The experiments were carried out in the 40-meter precision flume with a cross section of 110 cm wide and 61 cm deep in the W. M. Keck Laboratory of Hydraulics and Water Resources. The side walls are glass plates 1.2 cm thick, and the bottom was lined with smooth stainless steel plates. A schematic diagram of the flume is shown in Fig. 41 (see Vanoni (34) for a detailed description of the flume).

For all the experiments the flume was filled with filtered tap water up to 50 cm deep. The total volume of water in the flume was approximately 33,000 liters. The water was recirculated through the flume by a 30 hp pump. The flume flow rate was determined by a manometer connected to a Venturi meter (laboratory no. Q-39).

Since the object of the experiments was to study a buoyant jet into a uniform ambient stream, not a turbulent shear flow, the main region of the downward jet flow was set at a region of flume flow that was relatively uniform.

To seek such a region, velocity measurements in the flume without jet flow were performed by using a 0.32 cm Prandtl-Pitot tube. A typical measured velocity distribution is shown in Fig. 42. The maximum velocity occurred off the center of the flume to the west side indicating the presence of a counterclockwise (looking downstream) secondary flow. Such behavior was consistent from the upstream to the downstream end of the flume and its cause was unknown. A shaded region where the velocity distribution was relatively uniform was

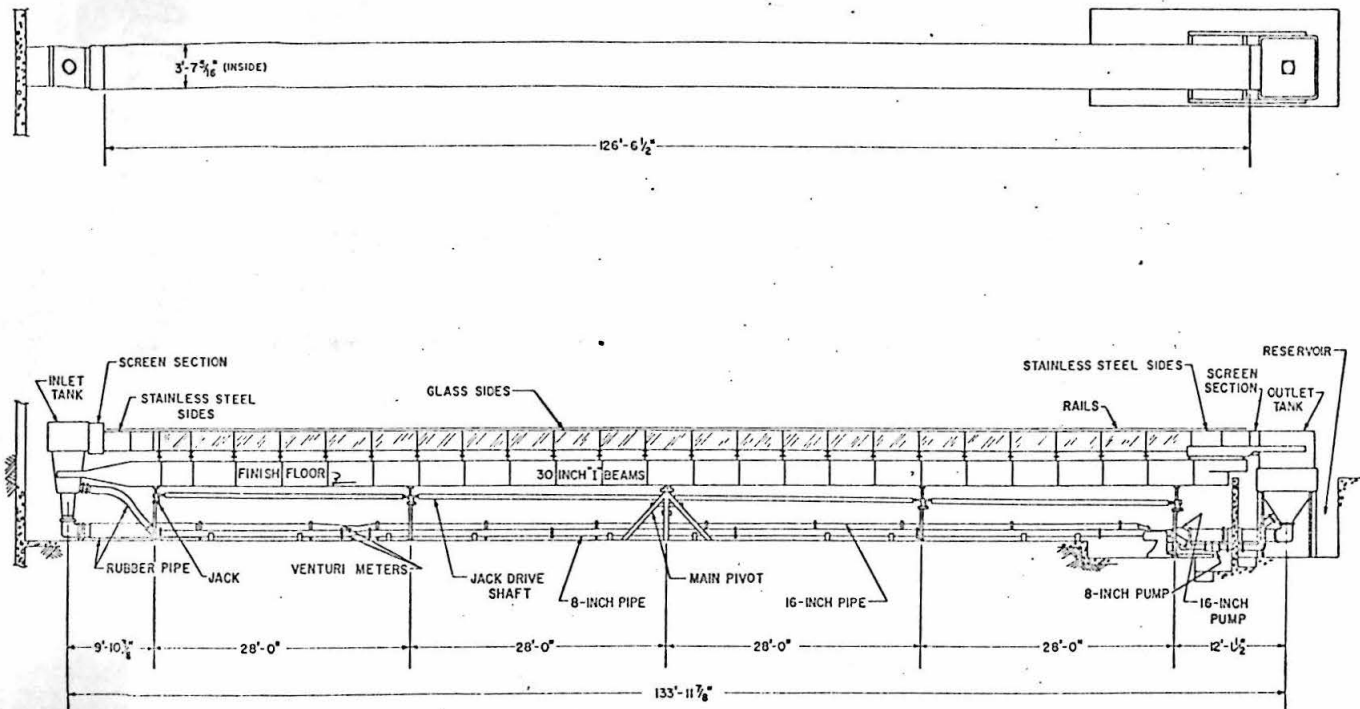


Fig. 41. The 40-Meter Precision Tilting Flume (From Vanoni (34), p. 7)

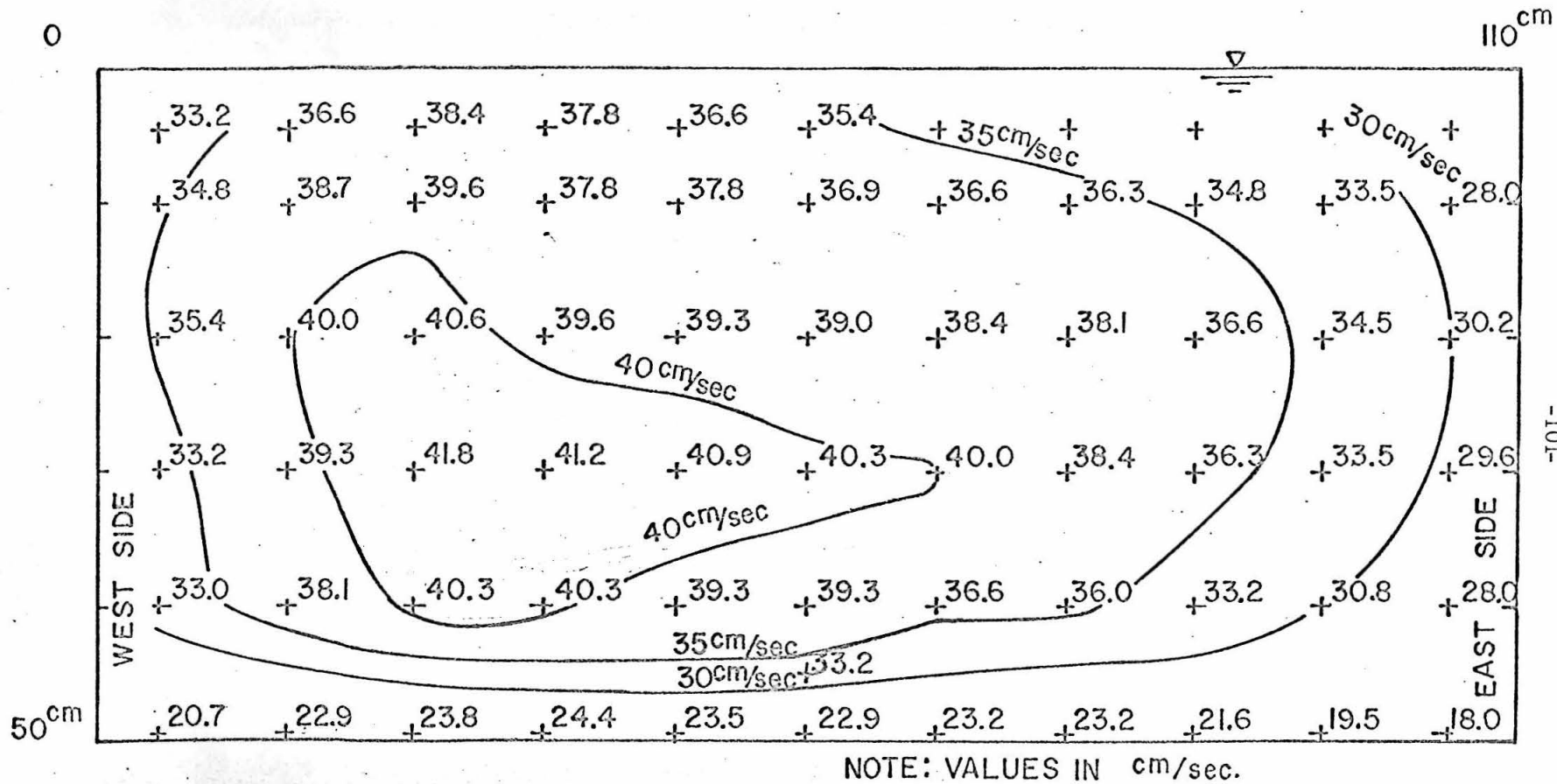


Fig. 42. A measured velocity distribution in flume (cross section looking downstream)

chosen as shown in Fig. 43. The jet discharging point  $O'$  was set off center 15 cm to the west side. The shaded zone was assumed to affect the jet flow most and the average velocity of the region was taken to be the value of the ambient velocity  $U_a$ . The values of  $U_a$  were obtained by velocity measurements in the shaded region and were related to the readings of the Venturi meter on the return pipe from the pump. In each run the ambient velocity  $U_a$  was set by adjusting the pump speed to get the appropriate value of the Venturi meter reading for the desired ambient velocity.

In the region chosen, the extreme deviations from the  $U_a$  values are listed in Table 3. In the main region of the jet flow, the maximum deviations of the mean point velocities from the zonal mean were approximately +6 to -9%.

The flume was set at a fixed slope of 0.00022 for all the runs except the towed jet experiments where the flume was set at a level position. The flow depth was set at 50 cm for all the runs at the test section. The depth probably varied very slightly along the flow direction, but in view of the short length of the test section (less than 1.5 m) the variation over such a distance was neglected.

The turbulence intensities of the flume flow has not been determined. The turbulence intensity is expected to be under 5% over the main region based on Raichlen's (28) data obtained in another flume flow.

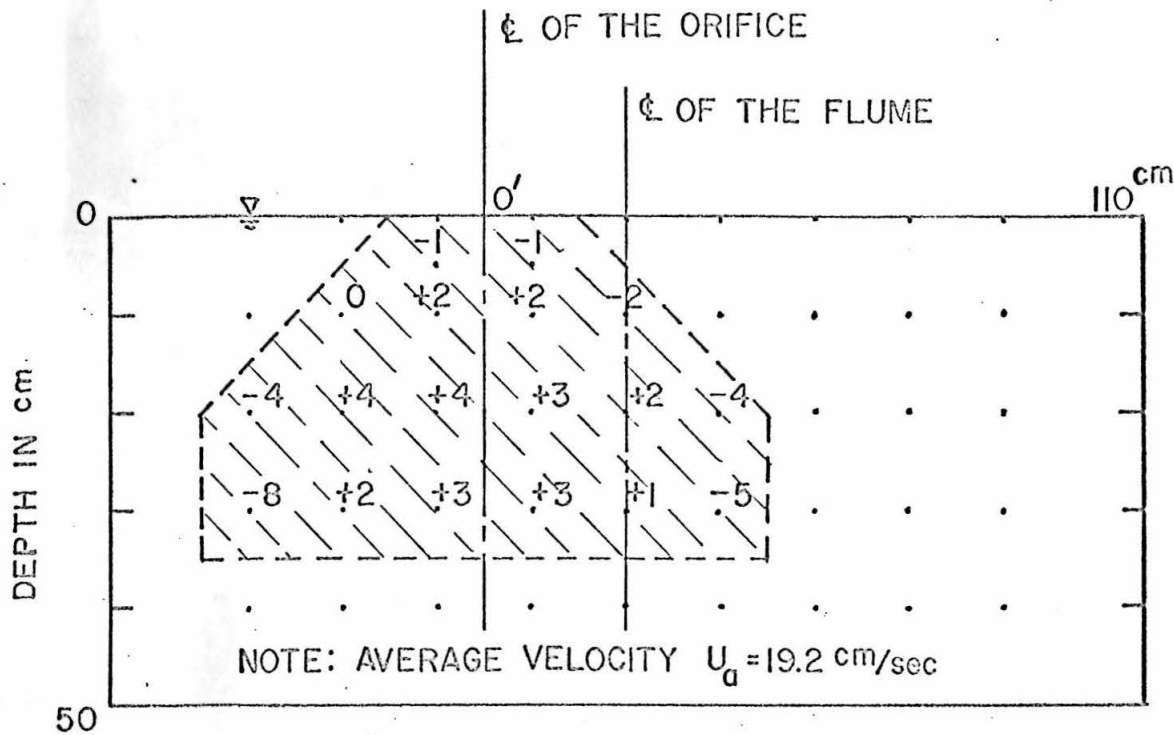


Fig. 43. The location of the jet discharge point  $O'$  relative to the flume center-line and the region assumed to affect the jet flow (shaded zone). The values shown are percentage deviations from the average velocity  $U_a$  when at 19.2 cm/sec.

Table 3. Deviation from ambient mean velocity  $U_a$  in the shaded zone shown in Fig. 43

Average Velocity in the Shaded Zone	Extreme Deviation of Velocity in the Shaded Zone
$U_a$ cm/sec	% of $U_a$
13.2	+6 to -8
19.2	+4 to -8
25.8	+3 to -6
26.7	+5 to -9
32.7	+3 to -4



## 2. Modeling of the gravity effect

The variation of density was modeled by using aqueous solutions of sodium chloride - the same method as mentioned in Section V-B. The base fluid for the jet flow was taken from the flume. The values of density were determined by hydrometer measurements to the nearest 0.0001 gr/ml for  $\rho < 1.038$  gr/ml and 0.001 gr/ml for  $\rho > 1.04$  gr/ml. The specific gravity of the jet fluids used varied from 1.01 to 1.15. The flume water was fresh with a specific gravity around 1.000. The fluids were at temperatures between 20 to 22°C. The effect of the temperature difference was neglected.

## 3. The nozzles and jet flows

The setup of the jetting unit is shown in Figs. 44 and 45. The jet was produced by a sharp-edged orifice either 0.95 cm or 0.64 cm in diameter (see Fig. 18, nozzles E and F, in Section V-B). The jet fluid was pumped from three reservoir tanks with a total volume of 900 liters into a small constant head tank, then into a 15 cm x 15 cm x 20 cm box. Each orifice plate was attached to the bottom of the box facing down and just touching the water surface in the flume. The flow rate was determined by an open ended manometer connected to the side of the jet box. The manometer was calibrated to give the volume flow rate. The initial jet diameter,  $D$ , was taken to be  $0.8 D_0$  to allow jet contraction. The nozzles E and F are hereafter denoted by the contracted jet diameters, namely 0.76 cm and 0.51 cm respectively. The calibration curves for the manometer reading vs discharge

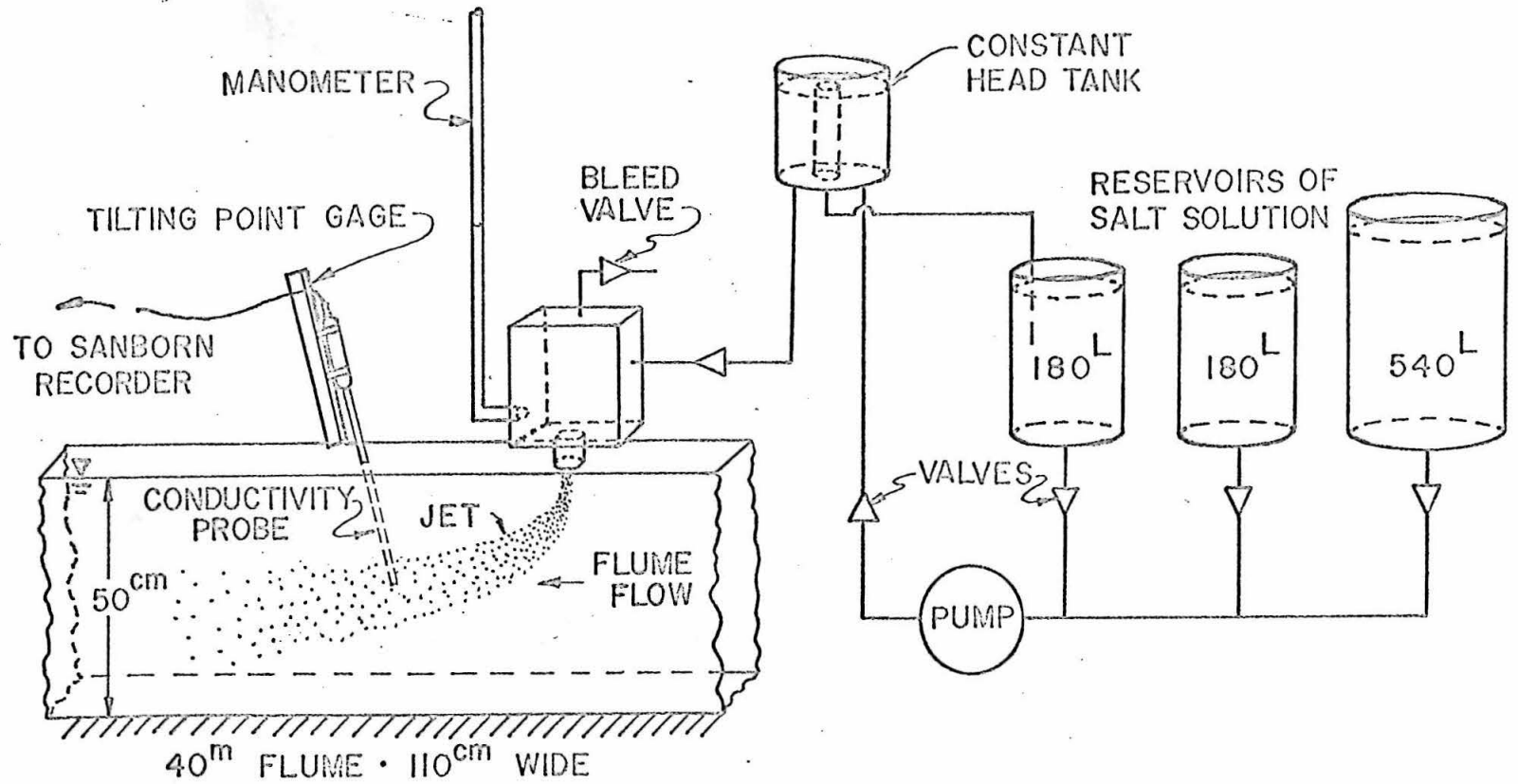


Fig. 44. Schematic flow diagram of buoyant jet experiments in flowing environments.



Fig. 45. The constant head tank and the jetting box

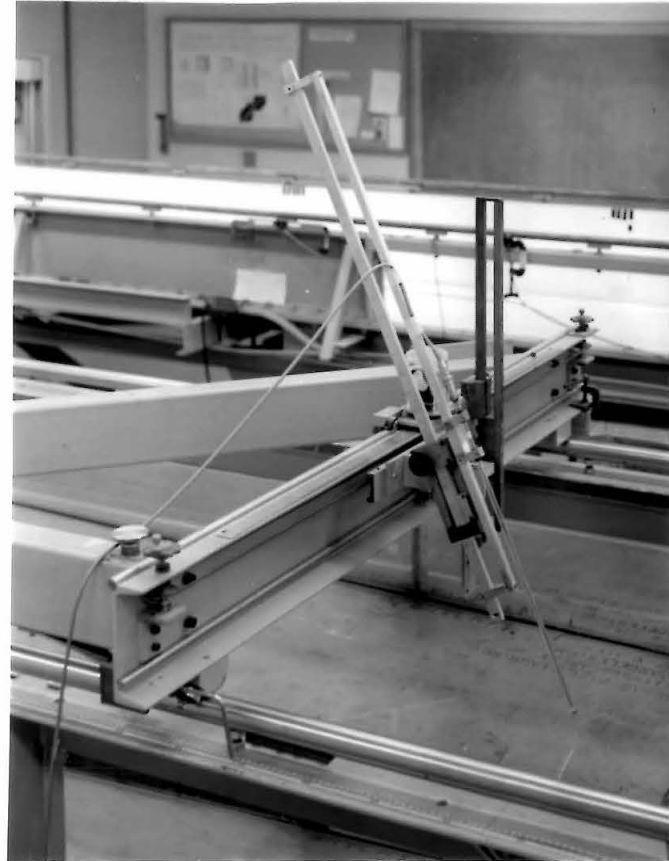


Fig. 46. The instrument carriage, the tilting point gage and the probe

velocity, based upon the flow rate divided by the initial contracted jet cross-sectional area, were identical for both nozzles.

The jet flow was controlled by a set of valves. The jet discharge velocity could be adjusted to within 1% of the desired value.

In each run the density difference between the flume water and the jet fluid was determined first. Then the required jet discharge velocity was calculated from the jet Froude Number  $F$  desired. The intended velocity ratio determined the ambient velocity  $U_a$ . The error in control of the velocities was estimated to be less than  $\pm 2\%$  for  $U_o$ , and  $\pm 1\%$  for  $U_a$ . The range of the jet discharge velocity was from 104 to 296 cm/sec.

#### 4. Conductivity measurements and apparatus

The salt in solution in the jet fluid not only served to model the gravity effect but also was convenient as a tracer for the conductivity measurements.

A conductivity probe (45.5 cm long) developed by the Hydrodynamics Laboratory at the Massachusetts Institute of Technology was used. The electrodes were 0.32 cm x 0.32 cm x 30 mil platinum plates 0.32 cm apart as described by Koh (19). The conductivity measurement technique was similar to Koh's method. Fig. 47 shows the probe both schematically and photographically. A single channel Sanborn recorder (Model 150) with 1100 AS Carrier Pre-Amplifier were used. The bridge circuit used in conjunction with the Sanborn recorder for the measurement of the conductivity is shown in Fig. 48.

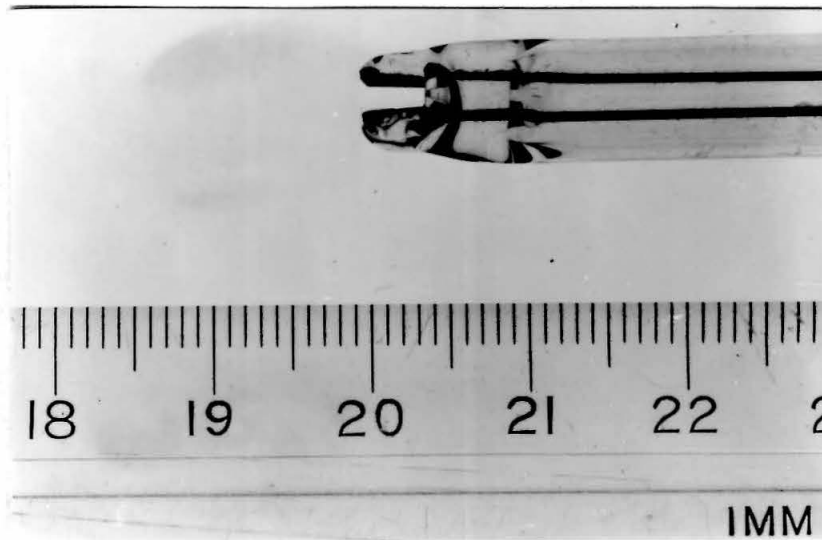
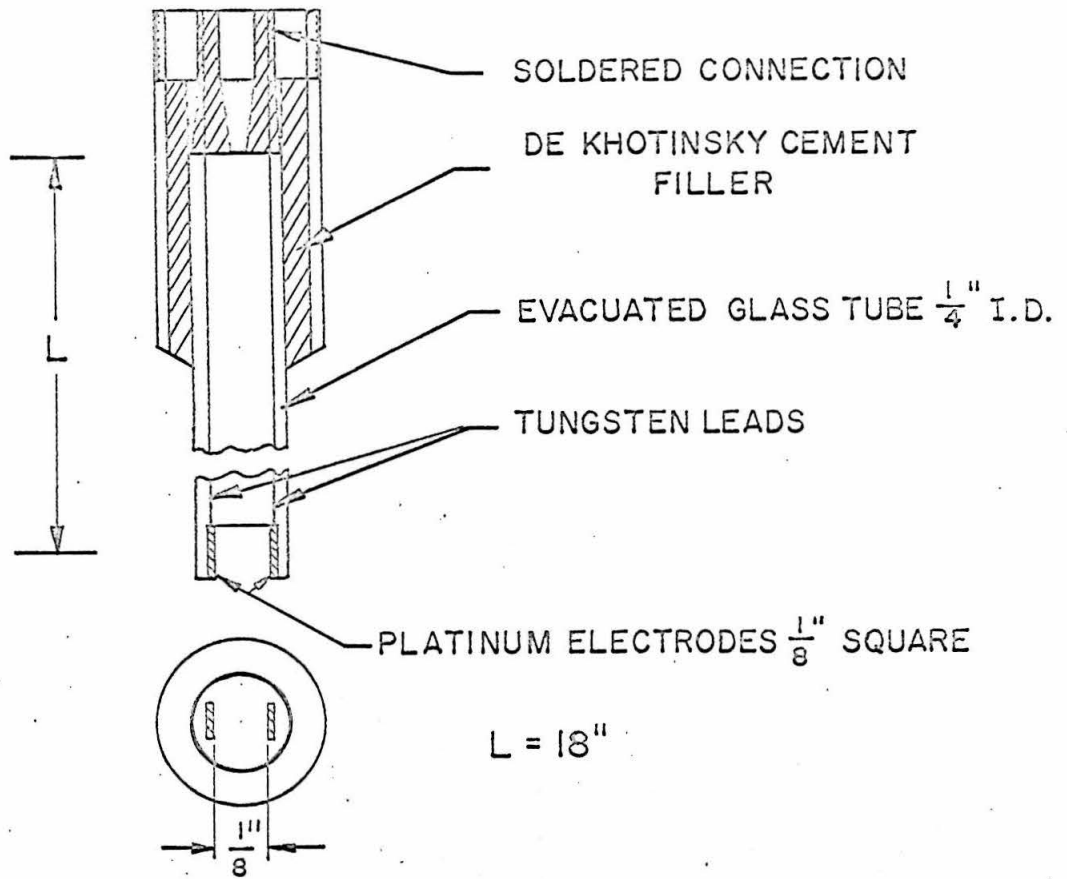


Fig. 47. The conductivity probe (From Koh (19), p. 57)

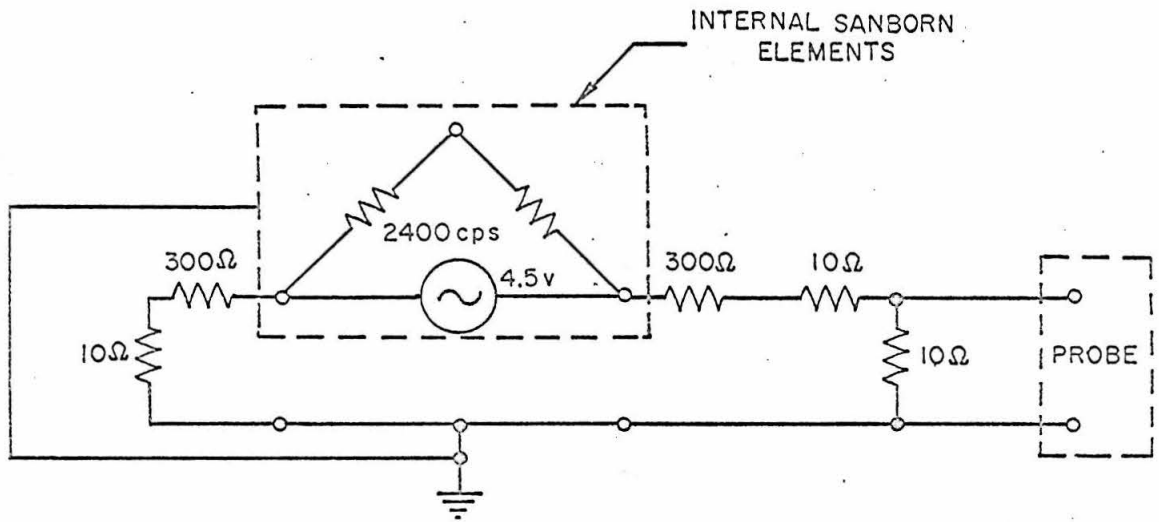


Fig. 48. The bridge circuit used in conjunction with the Sanborn recorder for the measurement of the conductivity. (From Koh (19), p. 59)

The probe was mounted on a tiltable point gage as shown in Fig. 46. The gage could move in the transverse direction on the carriage.

Since the purpose of the probe was to measure concentration  $c^*$  of the original jet fluid in a mixture of jet fluid and flume water, the calibrations were determined in terms of standard reference mixtures prepared from the jet fluid and flume water for each run. It was not necessary to relate recorder readings to absolute salt concentration or electrical conductivity. Calibration of the probe was obtained by immersing the probe into these standard solutions of different concentrations of the jet fluid in mixtures with flume water and reading the corresponding deflections on the Sanborn recorder. Since the calibration drifted slightly with time in each run, several calibrations were made during the run. Fig. 49 shows the calibration curves for a typical run. Note that all concentrations  $c^*$  used hereafter are not salt concentrations, but are jet fluid concentrations, whereby the original jet is represented as  $c^* = 1$ . The curves were nearly linear, but curved slightly at large concentrations.

By visual observation of the dyed jet, the probe was first lined up normal to the jet axis at the section to be measured. The location of the probe relative to the jet was determined from a photograph taken with the probe set at a known point gage reading. The photographic technique was the same as mentioned in Section V-B. The concentration distribution across the section was then measured point by point. The measuring time for each point was about 100 seconds when the fluctuation was large and less time was allowed in case of

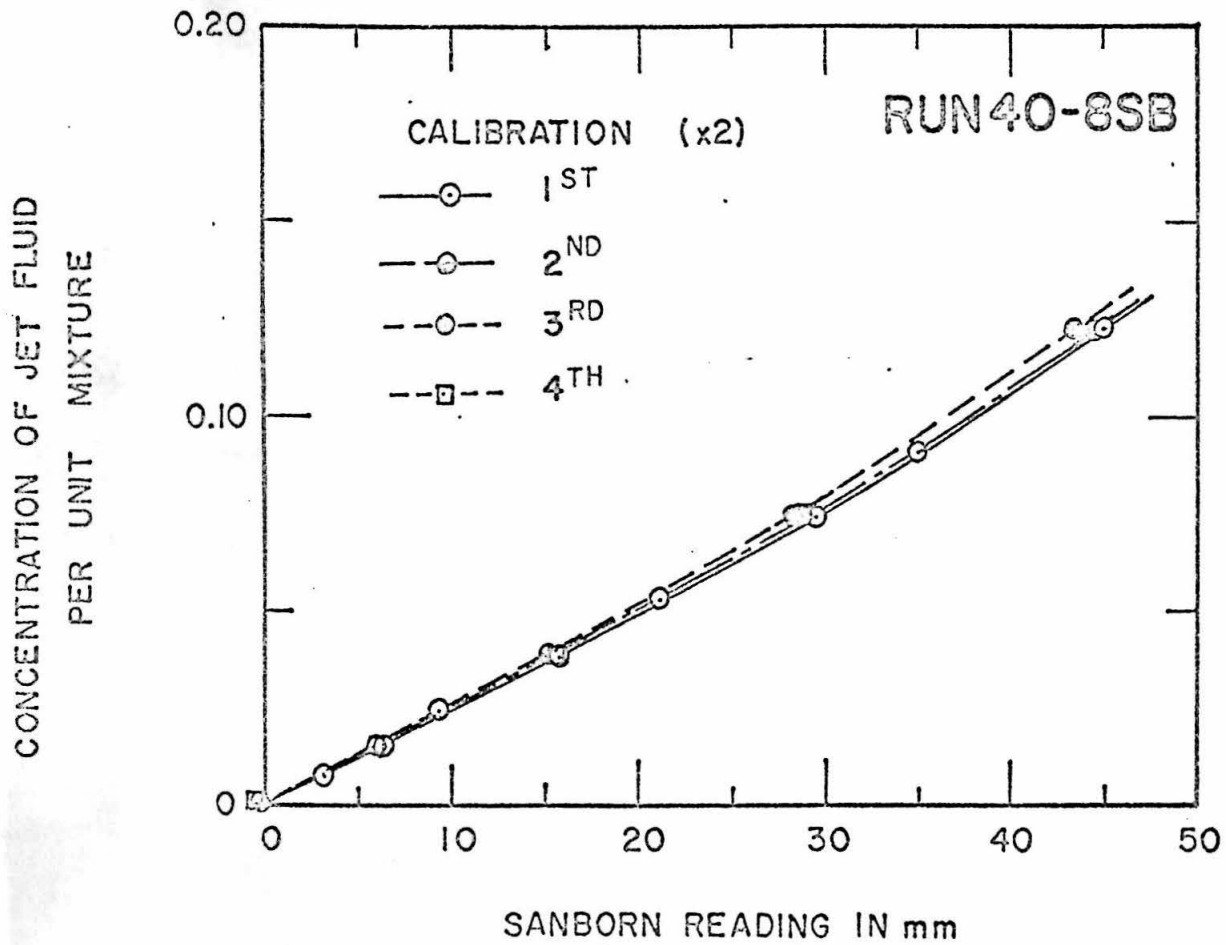


Fig. 49. Typical calibration curves of the conductivity probe



small fluctuations. A sample of the record is shown in Fig. 50. The average value of the reading was obtained by visual estimation. The error in  $c^*$  was estimated to be less than  $\pm 2\%$  near the jet axis and  $\pm 10\%$  near the jet edge.

#### 5. Correction for the change of ambient salt content

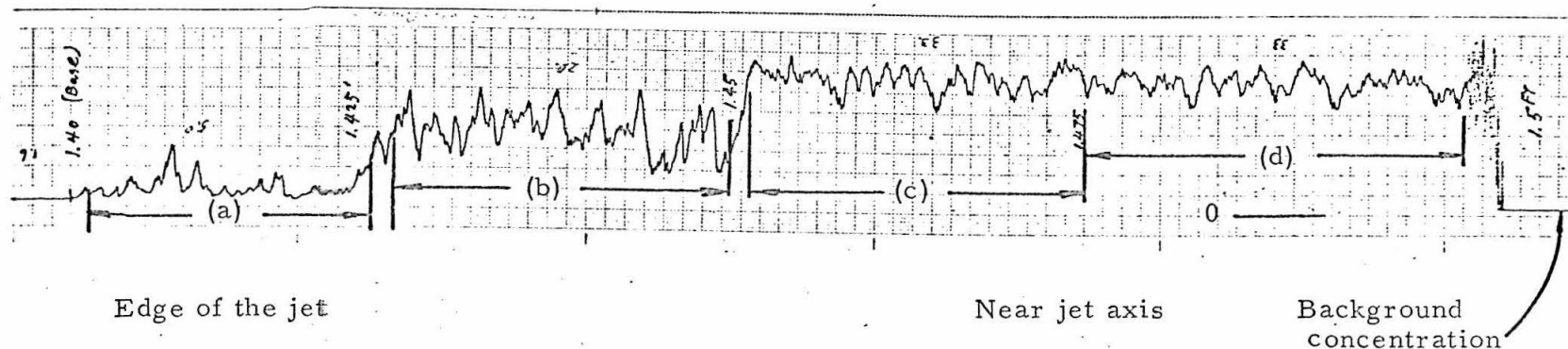
Since the flume water was recirculated, the salt content of the flume increased slowly during the run. The measured apparent concentration  $c_m$  was reduced to the actual concentration of jet fluid in flume water ( $c^*$ ) by the formula:

$$c^* = \frac{c_m - c_b}{1 - c_b} \approx (c_m - c_b)(1 + c_b) \quad (93)$$

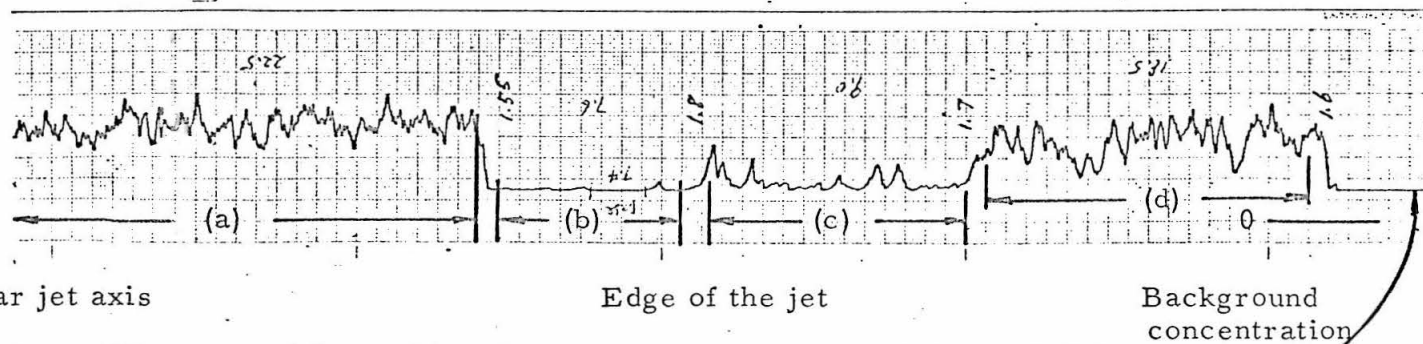
where  $c_b$  was the apparent background concentration inferred from the calibration curves, such as Fig. 49. The error of the formula was estimated to be of the order of  $c_m c_b^2$ . The value of  $c_b$  for all the runs was less than 3%; thus the error involved was extremely small. The change of the Froude number due to increase of ambient density was then less than 1.5% and neglected.

The concentration measurements were made mostly on the vertical center plane to locate the jet axis and the width. The maximum concentration values of these vertical profiles were used as the  $c(s)$  values in the analysis. Several complete concentration profiles were also obtained to examine the distributions over whole cross sections. The results are presented in the next section.

RUN 20-4, paper speed = 1 division(mm) per second from right to left



A)  $s_e'/D=9.5$ ; at different positions with point gage readings: (a) 1.425 ft, (b) 1.45 ft, (c) 1.475 ft, and (d) 1.5 ft.



B)  $s_e'/D=123$ ; at different positions with point gage readings: (a) 1.55 ft, (b) 1.8 ft, (c) 1.7 ft, and (d) 1.6 ft.

Fig. 50. A sample of the record of the concentration measurements

## 6. Photographic techniques

The same photographic technique was used here as described in Section V-B. The technique served one more purpose here, that being to determine the location and the inclination of the probe at each section measured.

The jet fluid was mixed with the concentrated blue dye at a concentration of about 50 ppm. The density of the jet fluid was not affected by the dye concentration. The dyed solutions were used only for photographic purposes and in aligning the probe positions. In actual concentration measurements solutions without the dye were used.

For each experimental case, at least two photographs of the dyed jet were taken. Motion pictures were also taken for specific runs.

## 7. Towed jet experiments

Runs were made with the jetting device mounted on the motorized carriage, moving along the flume at a constant speed. The flume was set at horizontal slope and used as a towing tank. The towing distance was about 32 m. A Minarik speed control was used to set the speed of the D.C. motor drive on the carriage. The speed was established to within  $\pm 1\%$  of the desired values to simulate previous runs. The jet fluid was pumped to the jetting unit through a long hose.

Photographs were taken for the dyed jets. Concentration measurements were made at several sections with the probe mounted

on the carriage at fixed positions. Each towing yielded the concentration value at one point. Motion pictures were also taken to compare visually with the runs with fixed jet into flowing water in the flume.

### VII-C. Experimental Results

Twenty-six runs were conducted in this investigation as shown in Table 4. The run numbers were designated by two numerals: first, the jet Froude number,  $F$ , and second, the velocity ratio,  $k$ . The letter S was used to denote the runs where complete concentration profiles over the cross-sections were made; and T for the towed jet runs. The range of Froude number was from 10 to 80, the velocity ratios from 4 to 16.

The results are presented in the following sequence: photographs of dyed jets; concentration profiles and maximum concentration values  $c(s)$ ; the location of the jet axes, trajectories, dilution  $S$ , and half widths,  $r_{0.5}$ ; values of the coefficient of entrainment,  $\alpha$ , and the drag coefficients,  $C'_d$  (or  $C_d$ ).

#### 1. Photographs of the dyed jets

A set of photographs of dyed jets with  $k = 4, 6, 8, 12$  and  $16$  at  $F = 20$  are shown in Figs. 51(a) to (e) demonstrating the effect of the ambient current. Figs. 52(a) and (b) show the cases of  $F = 10$  and  $20$  at  $k = 8$ . Figs. 53(a) to (c) show the cases of  $F = 20, 40$  and  $\infty$  at  $k = 16$ . These two sets of pictures demonstrate the effect of gravity on the jets. All these jets were issued from the  $0.76$  cm orifice. Figs. 54(a) and (b) are cases for  $k = 12$  and  $8$  at  $F = 40$  using the

Run	Jet Froude No.	Velocity Ratio	Jet Discharge Vel.	Ambient Velocity	Jet Diameter	Density Ratio	Jet Reynolds No.	Position of the Jet Axis			Concentration	Dilution Ratio	Jet Half Width	Reference for Figure Nos.			
	$F = \frac{U_0}{\sqrt{\frac{\rho_a}{\rho_a} g D}}$	$k = \frac{U_0}{U_a}$	$U_0$ (cm/sec)	$U_a$ (cm/sec)	D (cm)	$\frac{\rho_a}{\rho_a} \frac{U_0^2 D^3}{\rho_a}$	$R = \frac{U_0 D}{\nu}$	$x'$ D	$x'$ D	$y'$ D	c (%)	$S = \frac{1}{c}$	$r_{0.5}/D$	Graph(s)	Photo(s)		
10-4	10	4.0	105	26.4	0.76	0.148	8,200	7.2	4.1	5.8	0.167	6.0	1.04	60a	--		
								17.8	14.3	9.0	0.066	15	2.2				
								43.8	39.0	13.6	0.033	30	3.0				
								67.6	62.2	16.5	0.026	39	4.4				
								94.0	89.0	20.8	0.018	57	5.9				
125	119	24.8	0.014	69	8.8												
10-8	10	8.0	105	13.2	0.76	0.148	8,200	12.1	4.8	11.0	0.120	8.3	2.7	60b	52a		
								27.6	18.0	20.0	0.044	23	2.6				
								56.8	45.6	30.8	0.013	75	5.9				
								74.2	62.3	35.9	0.0079	120	5.5				
								122	109	49.5	0.0054	180	6.6				
10-8B	10	8.0	104	13.1	0.76	0.146	8,200	44.0	34.5	24.8	0.015	65	3.8	60b	52a		
								97.0	85.0	42.0	0.0063	160	7.0				
20-4	20	4.0	111	27.8	0.76	0.0415	8,700	9.5	6.0	6.5	0.147	6.8	1.5	56,59,60c	51a		
								22.0	18.5	8.6	0.106	9.4	2.3				
								52.8	49.0	12.0	0.059	17	3.4				
								89.2	85.2	15.2	0.041	24	4.2				
								123	119	17.5	0.029	34	4.8				
20-4B	20	4.0	116	29.0	0.76	0.0451	9,100	75.0	71.0	13.7	0.042	24	4.0	60c	51a		
								97.0	92.8	15.7	0.031	32	4.5				
								123	119	17.3	0.026	38	5.7				
20-8	20	8.0	110	13.7	0.76	0.0405	8,600	11.1	4.5	10.2	0.121	8.3	1.4	60d	51c, 52b		
								18.8	11.4	14.5	0.053	19	2.5				
								44.8	36.5	21.0	0.034	29	4.4				
								70.0	61.5	25.5	0.023	44	5.9				
								85.7	76.5	28.6	0.018	54	7.0				
128	118	37.4	0.012	85	6.7												
20-8B	20	8.0	116	14.5	0.76	0.0451	9,100	73.5	64.0	27.0	0.029	35	5.6	60d	51c, 52b		
								112	103	34.5	0.014	73	8.4				
								132	122	39.2	0.0115	87	7.4				
20-8C	20	8.0	131	16.3	0.51	0.0850	6,800	113	103	37	0.017	64	6.3	60d	--		
								155	144	45	0.010	100	7.5				
								200	190	47.5	0.0068	150	8.8				
20-8S <sup>(2)</sup>	20	8.0	110	13.7	0.76	0.0405	8,600	37.0	28.5	20.0	0.036	28	4.1	57,60d	51c, 52b		
								100	90.5	32.0	0.020	50	6.2				
20-12	20	12	208	17.4	0.76	0.146	16,200	17.0	6.0	16.3	0.142	7.1	2.8	60e	51d		
								26.8	14.0	22.4	0.068	15	4.8				
								47.1	33.5	30.7	0.045	22	--				
								103	87.3	46.3	0.021	47	--				
20-16	20	16	208	13.1	0.76	0.148	16,200	17.8	3.5	17.2	0.157	6.4	--	--	51e, 53a		
								26.5	9.0	24.0	0.083	12	3.1				
								41.2	20.8	34.0	0.040	25	7.8				
								59.0	37.5	40.5	0.020	50	--				
40-4	40	4.0	163	40.8	0.76	0.0224	12,700	9.2	6.7	5.5	0.141	7.1	1.8	60f	--		
								21.6	19.1	7.8	0.108	9.3	2.4				
								48.8	45.8	10.0	0.071	14	3.3				
								79.0	76.5	12.0	0.054	18	4.4				
								114	111	13.0	0.038	26	4.5				
40-8	40	8.0	163	20.4	0.76	0.0224	12,700	10.7	3.7	10.0	0.184	5.4	2.0	60g	--		
								17.5	9.2	13.8	0.098	10	2.4				
								42.0	31.5	18.8	0.048	19	4.4				
								58.0	49.4	21.2	0.041	24	4.2				
40-8S	40	8.0	161	20.1	0.76	0.0221	12,600	9.6	3.0	9.0	0.159	6.3	1.8	60g	--		
								54.0	45.7	20.6	0.039	27	4.6				
								136	128	30.0	0.017	59	7.3				

Table 4. Summary of buoyant jet experiments in flowing environments.

Run	Jet Froude No.	Velocity Ratio	Jet Dia-charge Vel.	Ambient Velocity	Jet Diameter	Density Ratio	Jet Reynolds No.	Position of the Jet Axis			Concentration	Dilution Ratio	Jet Half Width	Reference for Figure Nos.	
	$F = \frac{U_o}{\sqrt{\frac{\rho_a \rho_a}{N} g D}}$	$k = \frac{U_o}{U_a}$	$U_o$ (cm/sec)	$U_a$ (cm/sec)	D (cm)	$\frac{\rho_a}{\rho_a}$	$R = \frac{U_o D}{\nu}$	$x'$ D	$x'$ D	$y'$ D	c (%)	$S = \frac{1}{c}$	$r_{0.5}/D$	Graph(s)	Photo(s)
40-8SB	40	8.0	115	14.4	0.76	0.0110	9,000	32.5	24.1	18.2	0.059	16	3.5	56,59,60g	--
								87.0	79.2	24.9	0.039	26	5.8		
								119	111	29.0	0.032	31	7.0		
40-8SC	40	8.0	117	14.6	0.76	0.0115	9,100	88.0	81.5	24.5	0.035	29	6.6	60g	--
40-8B	40	8.0	116	14.5	0.76	0.0113	9,000	48.0	40.1	20.9	0.045	22	4.0	60g	--
								92.2	83.0	26.1	0.030	33	6.5		
								113	104	27.9	0.026	39	7.0		
40-8D	40	8.0	133	16.6	0.51	0.0220	6,900	100	91.0	29.1	0.019	53	6.4	60g	51a
								140	131	33.0	0.014	70	7.5		
								192	184	38.2	0.011	91	9.0		
40-8T <sup>(3)</sup>	40	8.0	148	18.5	0.51	0.0275	7,800	208	199	40.1	0.0098	100	9.6	60g	--
								145	137	30.7	0.016	63	--		
								240	232	42.7	0.011	91	--		
40-12	40	12	222	18.6	0.76	0.0415	17,300	18.0	6.0	16.0	0.146	6.8	3.0	59,60h	--
								41.9	28.2	26.0	0.051	20	5.6		
								83.8	70.0	33.5	0.027	37	--		
								107	92.6	37.6	0.024	41	--		
								133	119	39.0	0.021	48	--		
40-12B	40	12	261	21.8	0.51	0.0850	13,600	120	106	39.0	0.017	58	8.5	60h	51b
								160	147	44.5	0.014	73	9.3		
								206	191	50.5	0.011	91	10.5		
40-12T	40	12	148	12.3	0.51	0.0275	7,800	151	137	43.0	0.018	55	--	60h	--
								246	232	48.5	0.084	120	--		
40-16	40	16	219	13.7	0.76	0.0405	17,100	25.4	8.2	22.8	0.098	10	3.9	60i	53b
								33.5	15.0	28.0	0.057	17	5.0		
								74.0	53.8	41.0	0.027	37	--		
40-16B	40	16	219	13.7	0.76	0.0405	17,100	44.2	25.0	32.0	0.049	20	6.6	59,60i	53b
								67.2	47.0	38.5	0.030	33	9.6		
40-16C	40	16	261	16.3	0.51	0.0850	13,600	52.0	31.5	35.5	0.032	31	7.8	60i	--
								85.5	65.0	44.5	0.020	50	8.8		
								110	89.0	50.5	0.015	65	12		
								147	124	57.5	0.011	91	12		
								189	166	66.0	0.0096	100	11		
								215	192	67.5	0.0073	140	12		
80-16	80	16	232	14.6	0.76	0.0113	18,000	31	13.0	26.2	0.078	13	5.6	60j	--
								44	25.5	32.1	0.041	24	8.0		
								57	38.2	34.3	0.034	30	8.0		
								72	52.0	37.0	0.026	38	9.2		
								81.5	61.5	40.5	0.019	52	8.0		
80-16B	80	16	266	16.6	0.51	0.0220	13,900	116	96.2	45.0	0.013	74	9.6	60j	55a
								163	142	51.2	0.012	85	9.9		
								209	187	56.0	0.010	100	--		
								254	232	60.0	0.011	91	--		
80-16T	80	16	296	18.5	0.51	0.0275	15,400	254	232	60.0	0.011	91	--	60j	55b

Note: (1) c = Volume of initial jet fluid per unit volume of mixture

(2) S : runs where complete concentration profile(s) was taken

(3) T : towed jet runs (injector towed at speed  $U_a$ , actual velocity in flume = 0)

Table 4 (continued)

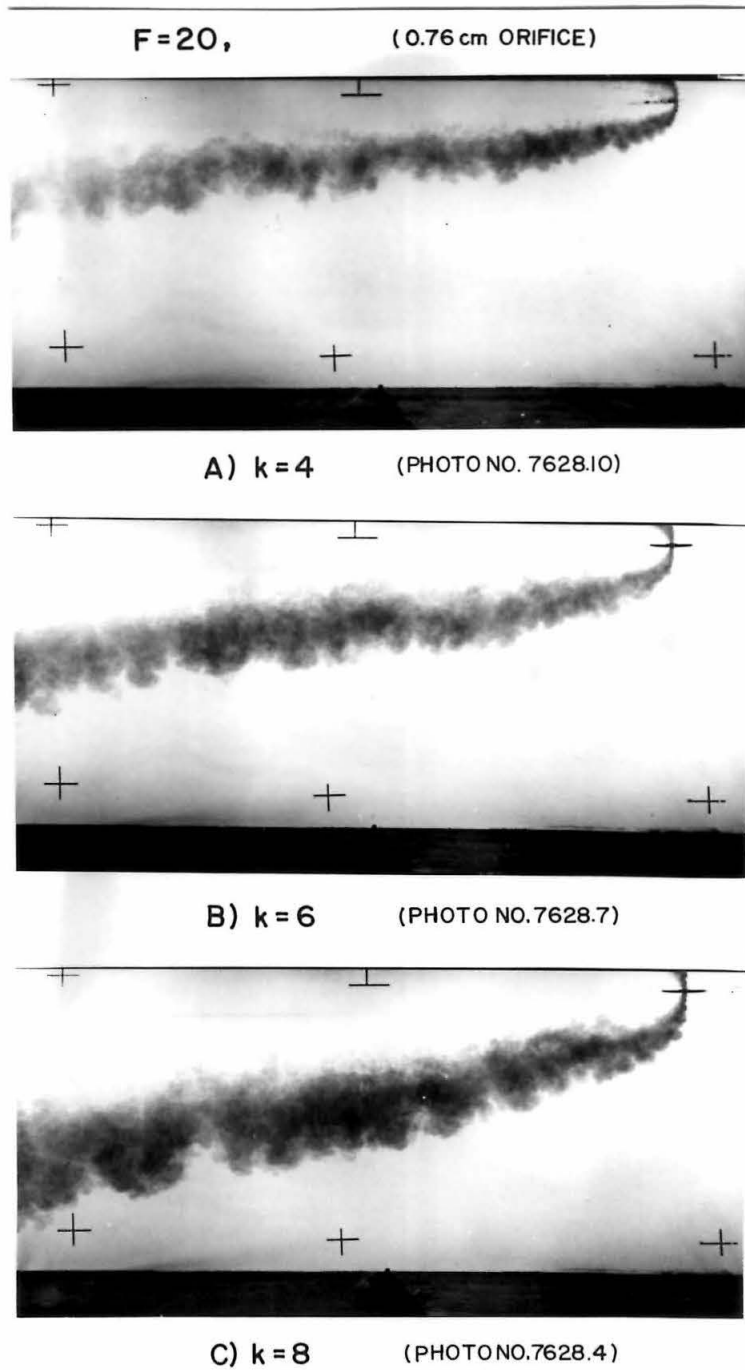
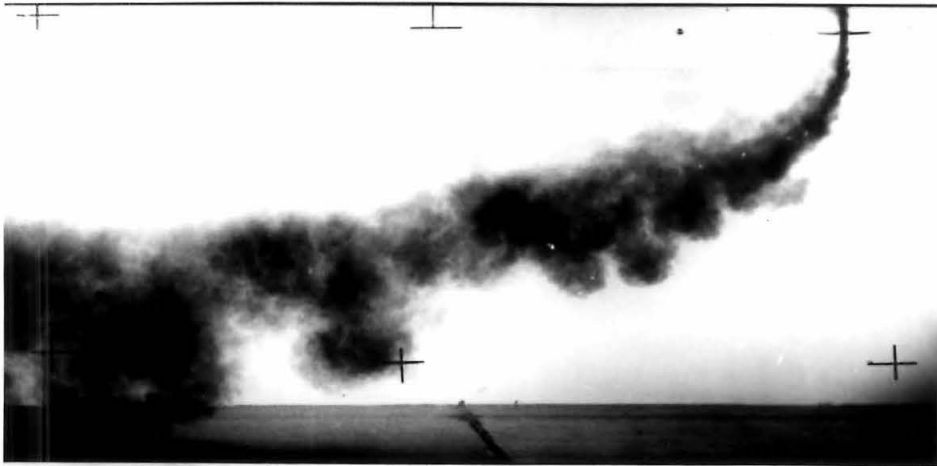


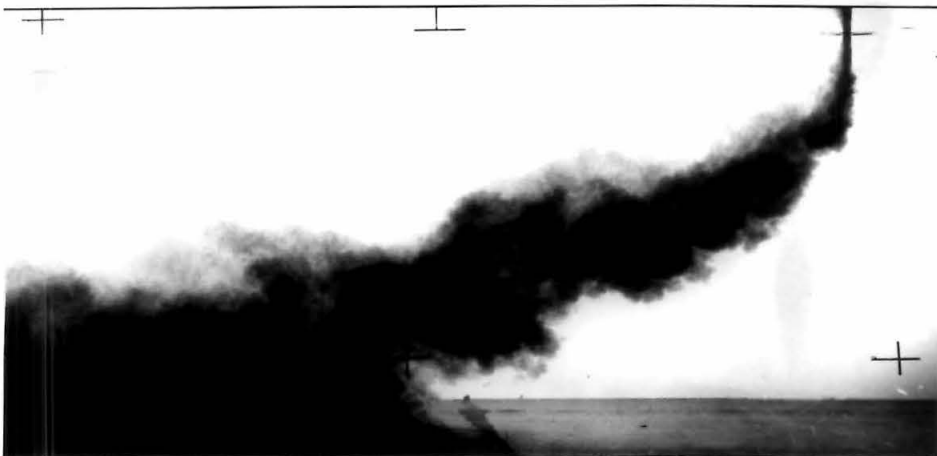
Fig. 51. Buoyant jets in cross streams with  $F = 20$  at various velocity ratios  $k = 4, 6$  and  $8$

**F=20,**

**(0.76 cm ORIFICE)**



**D) k=12 (PHOTO NO. 7620.3)**



**E) k=16 (PHOTO NO. 7620.5)**

Fig. 51. Buoyant jets in cross streams with  $F = 20$   
at various velocity ratios  $k = 12$  and  $16$



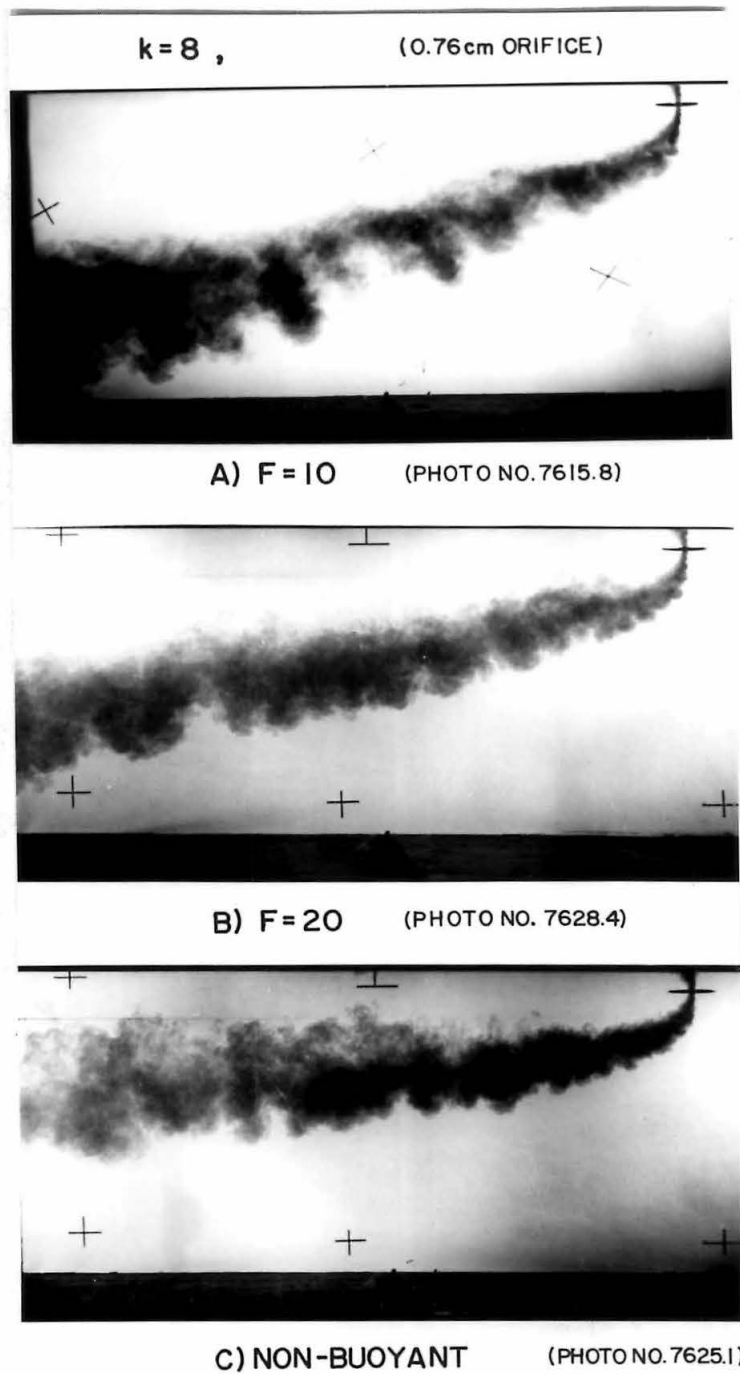


Fig. 52. Buoyant jets in cross streams with  $k = 8$  at various Froude numbers  $F = 10, 20$  and infinity

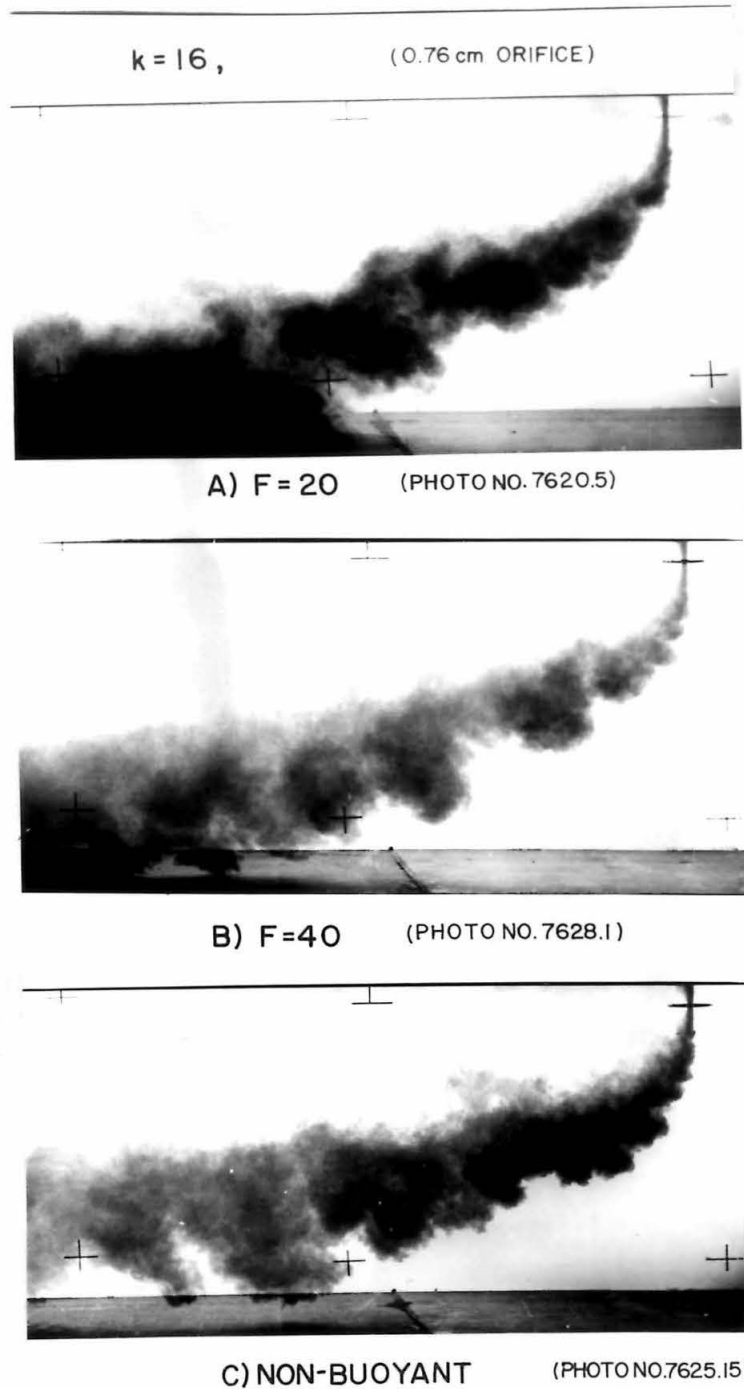
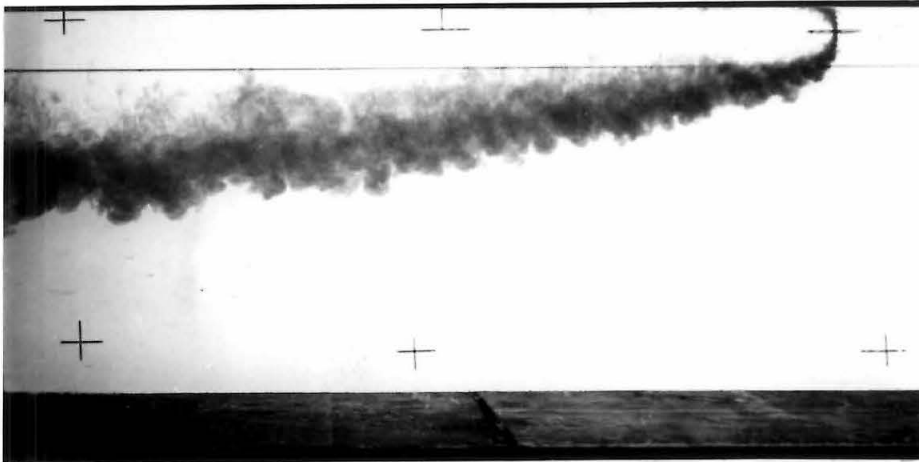


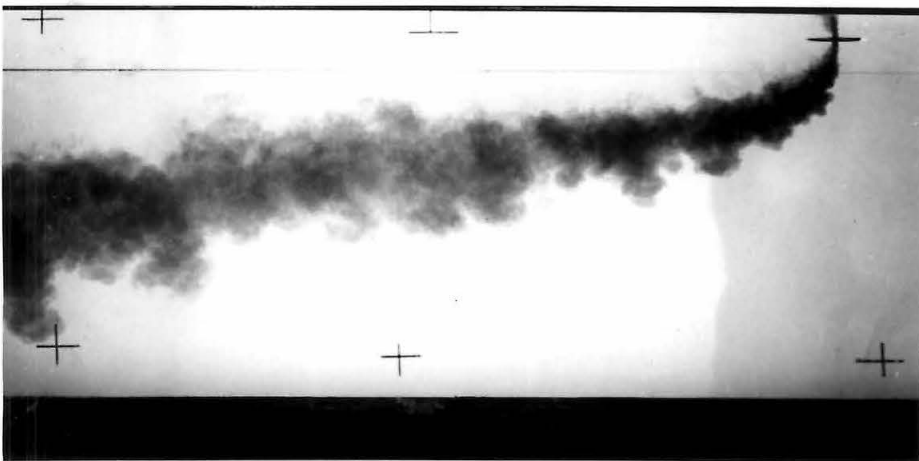
Fig. 53. Buoyant jets in cross streams with  $k = 16$  at various Froude numbers  $F = 20, 40$  and infinity

**F=40,**

(0.51cm ORIFICE)



**A) k=8** (PHOTO NO. 7655.6)



**B) k=12** (PHOTO NO. 7650.5)

Fig. 54. Buoyant jets in cross streams with  $F = 40$   
at velocity ratio  $k = 8$  and  $12$

0.51 cm orifice. Fig. 55(a) and (b) are respectively stationary and towed jet cases at  $F=80$  and  $k=16$ . The photograph of the dyed jets revealed no detectable difference between the stationary and the towed jet cases.

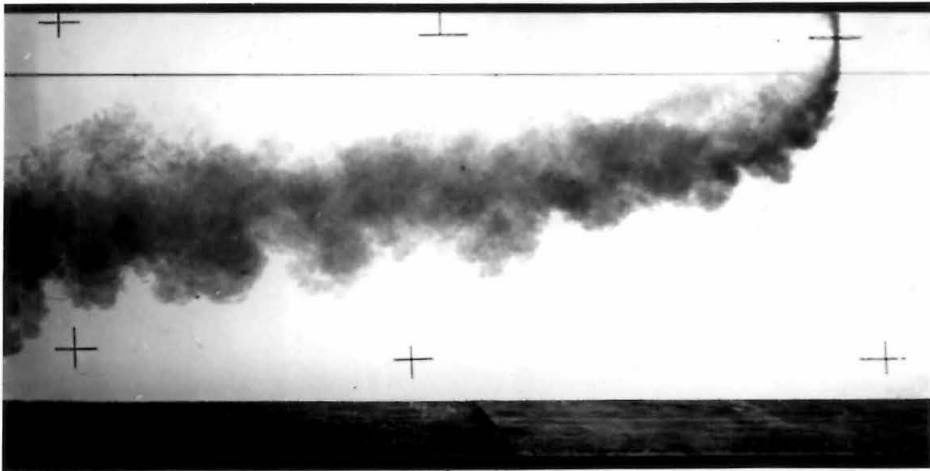
The dyed jet boundaries were traced directly from the negatives by using an enlarger. These were superimposed on the jet trajectories based on concentration measurements as shown in Figs. 60 (a) to (j).

## 2. Concentration profiles and the location of the jet axis

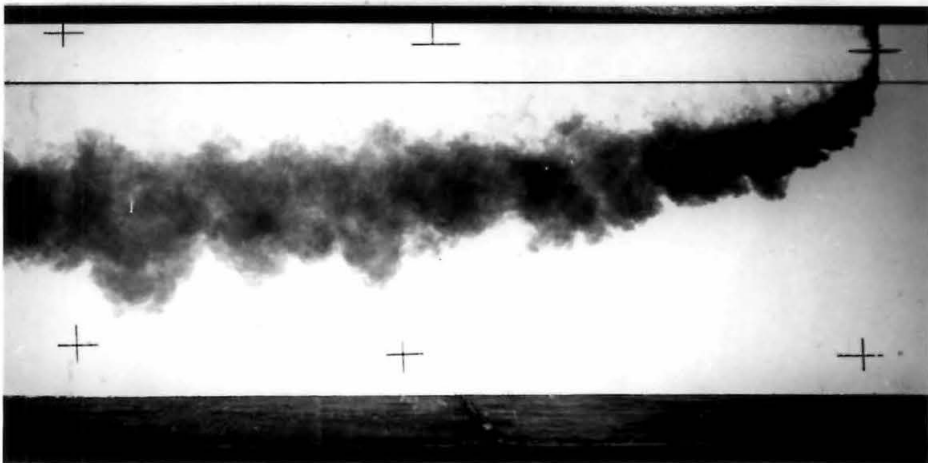
The concentration profile measured across the jet in a vertical center-line plane was first plotted for each section as shown in Fig. 56. A curve was then fitted through the data points by inspection. The center-line concentration of original jet fluid,  $c$ , was obtained as the maximum  $c^*$  value from the curve. The location of the point was taken as the axis of the jet and later laid out on the trace of the photographs of the probe locations. The jet half width  $r_{0.5}$  was here taken to be the distance from the axis to the point where  $c^*=0.5c$  and designated as  $r_{0.5}$  as shown in Fig. 56. The value of  $r_{0.5}$ , based upon a Gaussian distribution, is equal to  $0.833b$ .

The profiles show little skewness at the plane of symmetry. A complete profile of the concentration distribution over a cross section is shown in Fig. 57. The overall maximum concentration has peaks on each side of the plane of symmetry and showed an excess over the  $c$ -value chosen of more than 75%. The jet half width  $r_{0.5}$  was only one half of the transverse half width  $r'_{0.5}$  as shown in Fig. 57.

**F=80, k=16** (0.51 cm ORIFICE)



**A) STATIONARY JET** (PHOTO NO. 7655.2)



**B) TOWED JET** (PHOTO NO. 7657.4)

Fig. 55. Stationary and towed buoyant jets for the case  $F = 80$  and  $k = 16$

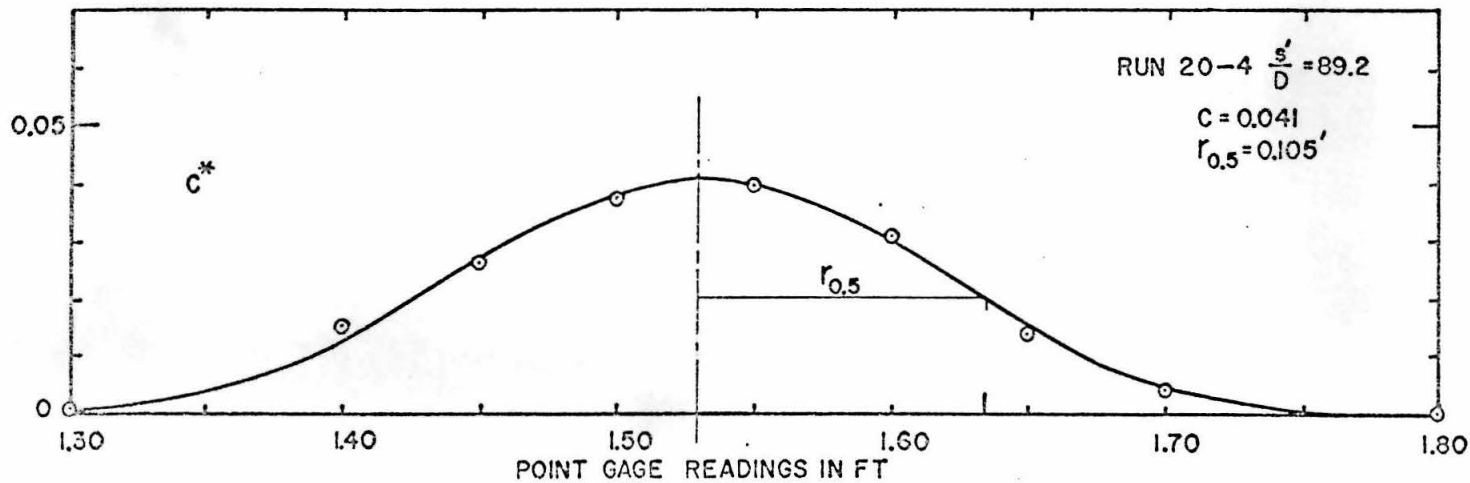
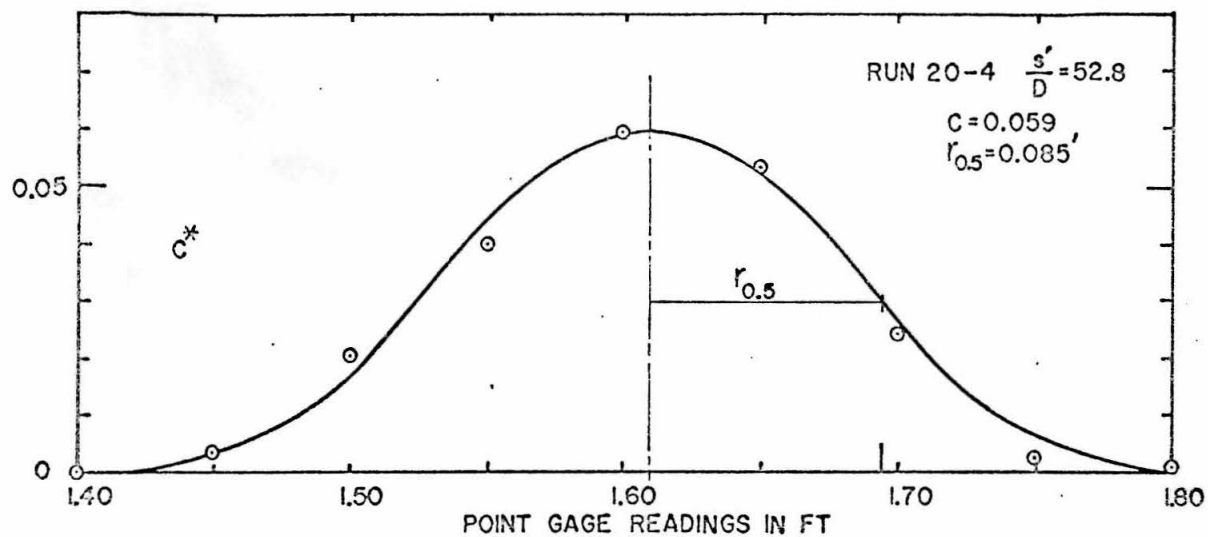


Fig. 56. Two measured concentration profiles for the case  $F = 20$  and  $k = 4$  (0.76 cm orifice)

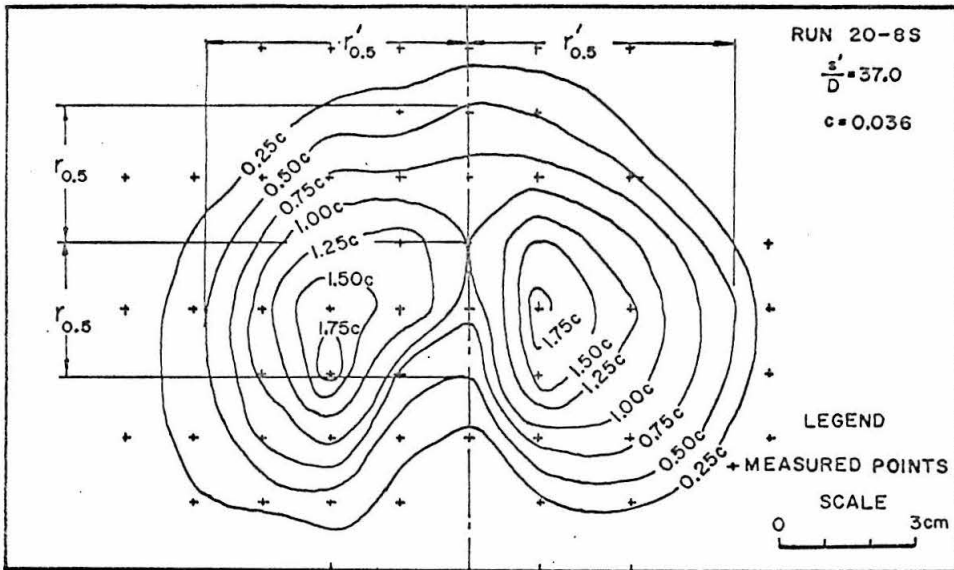


Fig. 57. A complete concentration profile for the case  $F = 20$  and  $k = 8$  (0.76 cm orifice). As shown, the ambient flow component is from the top, and the wake is below

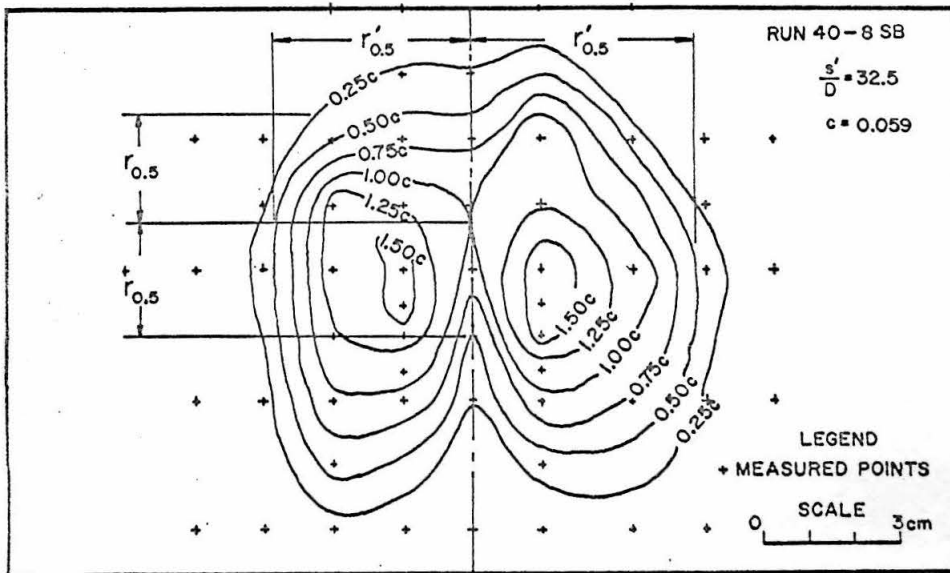


Fig. 58. A complete concentration profile for the case  $F = 40$  and  $k = 8$  (0.76 cm orifice). As shown, the ambient flow component is from the top, and the wake is below

Similar results were obtained for the case of  $F = 40$  and  $k = 8$ , as shown in Fig. 58. The excess over the  $c$ -value was slightly less (60%), but the overall shapes were similar and the transverse half widths  $r_{0.5}$  were nearly always twice the value of  $r_{0.5}$  as shown in these two figures.

The concentration profiles on the planes of symmetry were normalized by  $c$  and  $r_{0.5}$  and presented as shown in Fig. 59. The distributions were close to a Gaussian error curve.

### 3. Trajectories, dilution ratios, $S$ , and half widths, $r_{0.5}$

Measured trajectories with the dyed jet forms traced from the photographs are shown in Figs. 60(a) to (j). Since a photograph is an instantaneous view, the irregular boundary sketched is just one sample of the jet boundary. Figs. 60(a) to (j) show also the variation of the dilution ratio,  $S = \frac{1}{c}$ , and half width,  $r_{0.5}$ , along the distance of travel,  $s'/D$ .

The theoretical solutions were computed over a range of  $C_d'$  and  $\alpha$  values for each case to compare with the trajectory and the dilution ratios. An approximate best fit was obtained by a choice of  $C_d'$  and  $\alpha$  for each run. The corresponding  $r_{0.5}/D$  values fitted the solutions fairly well for each case.

### 4. Entrainment coefficients, $\alpha$ , and drag coefficients, $C_d'$ (or $C_d$ )

The values of the coefficients of entrainment and pressure coefficients obtained are summarized in Table 5.



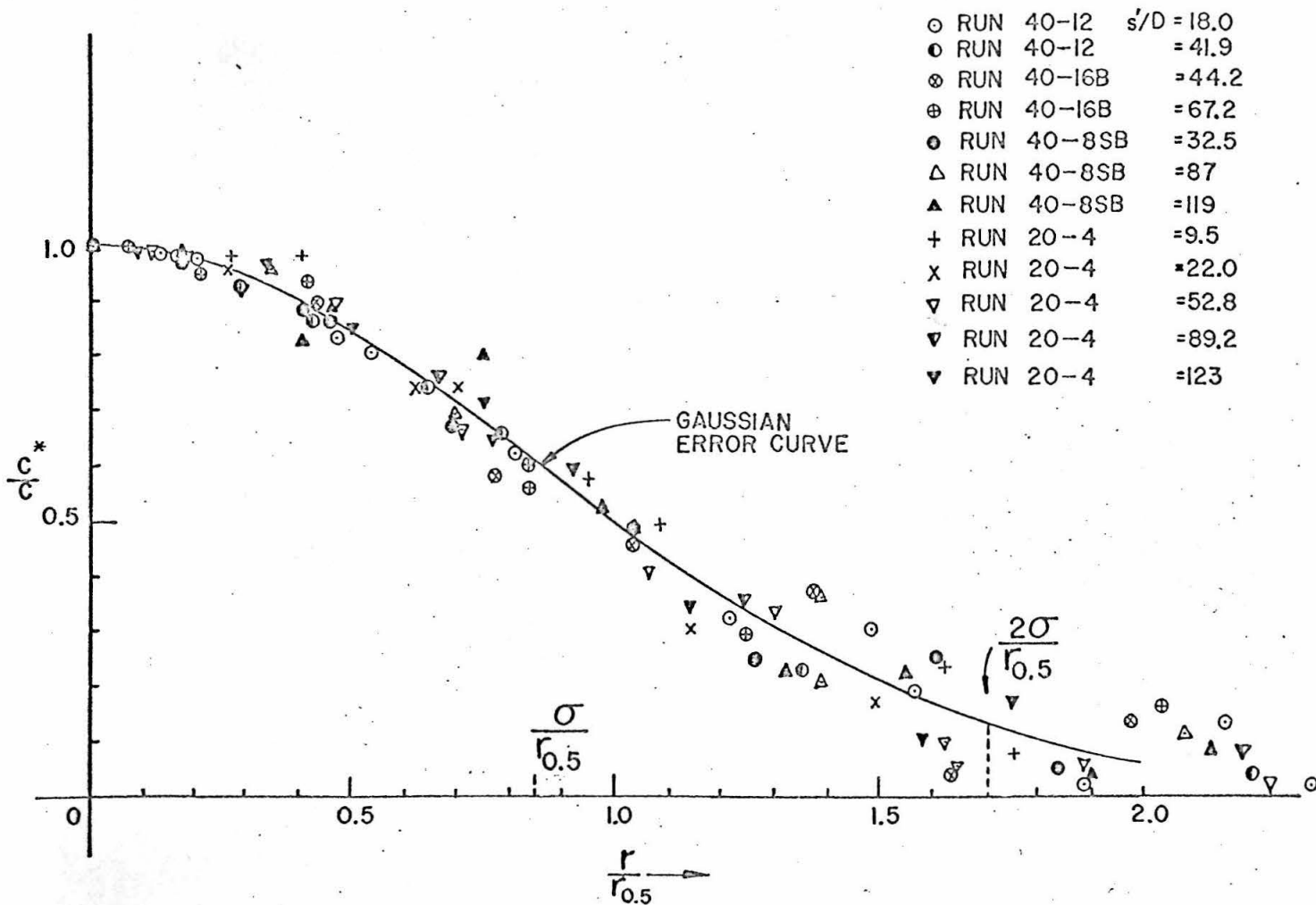
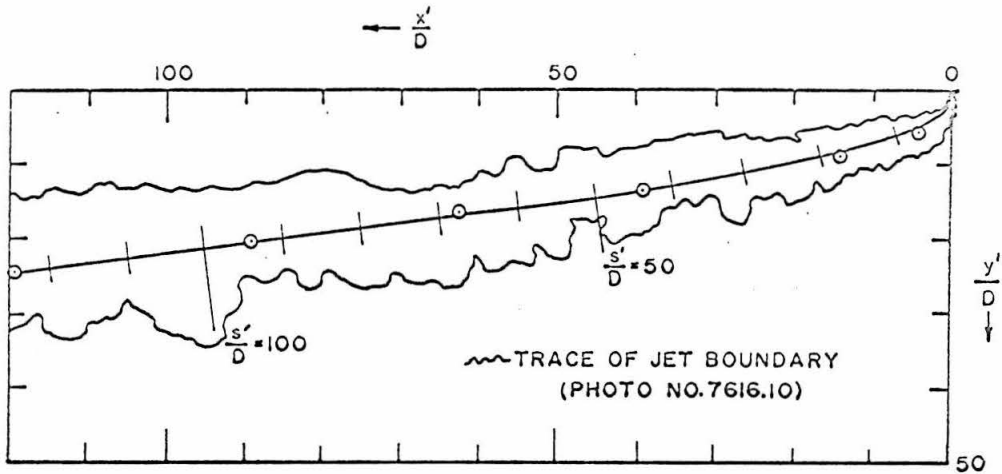


Fig. 59. Normalized concentration distribution on the plane of symmetry



F=10 k=4

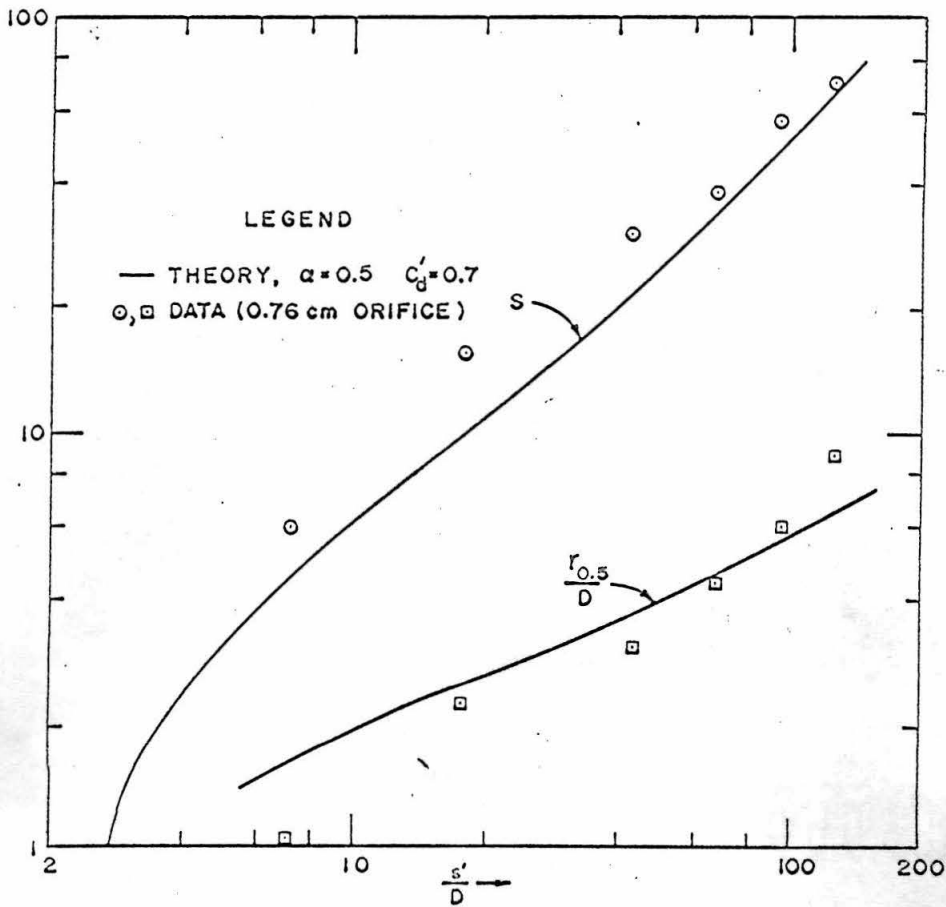
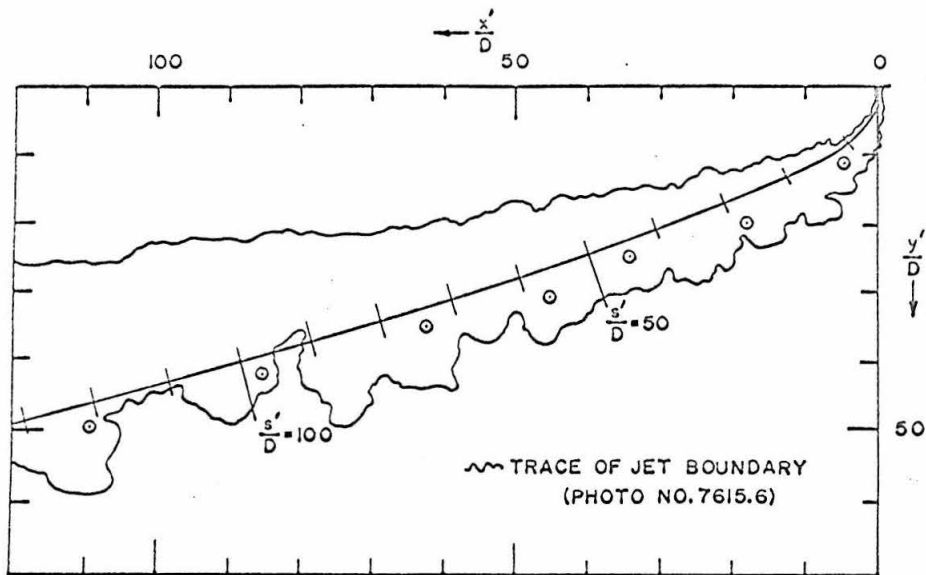


Fig. 60. Comparison of observed and theoretical trajectory, half widths,  $r_{0.5}/D$ , and center-line dilution ratios,  $S$ , of a buoyant jet in a uniform cross stream.  
(a)  $F = 10$  and  $k = 4$



F=10 k=8

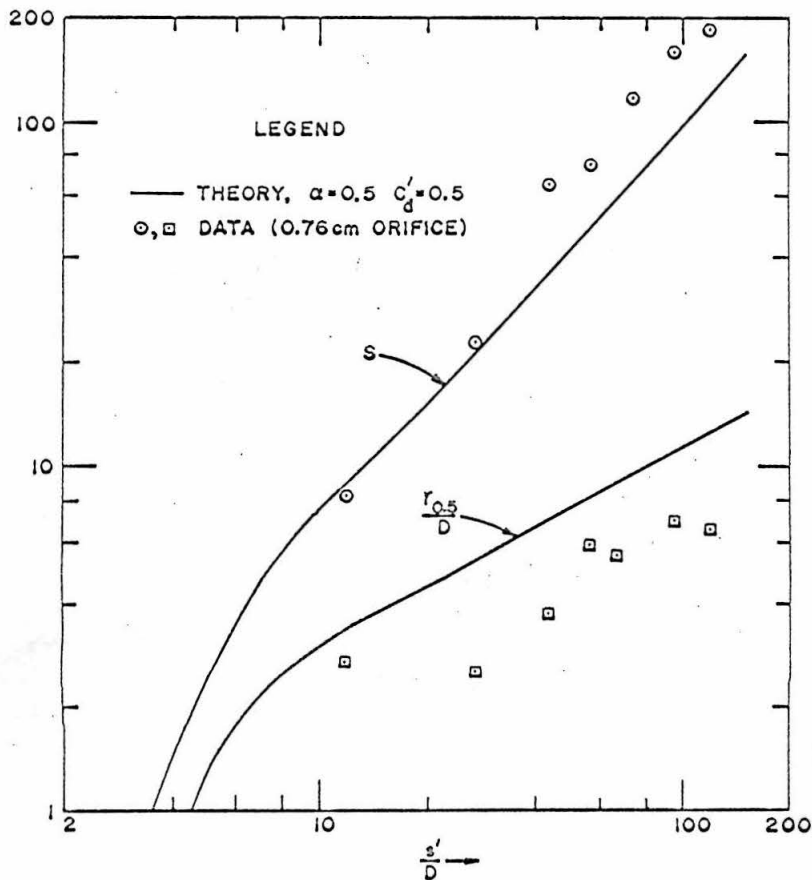
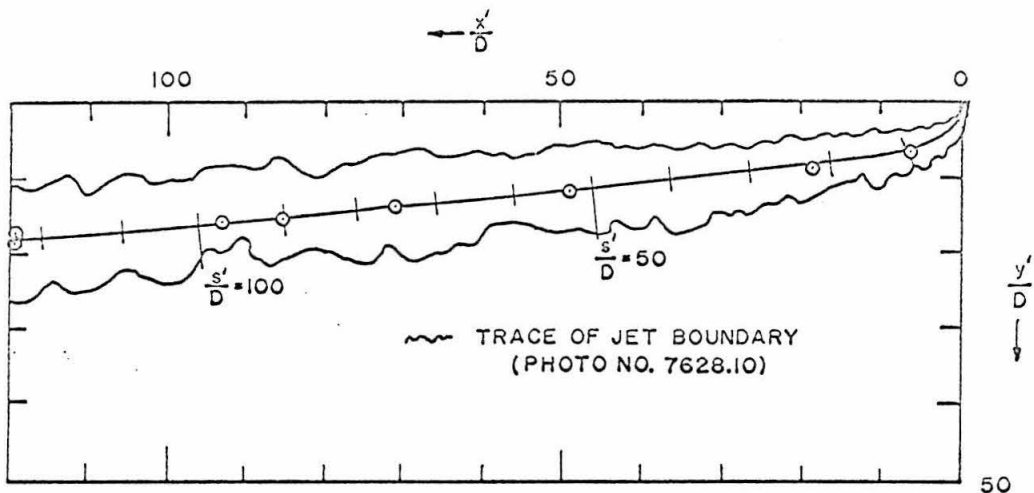


Fig. 60. Comparison of observed and theoretical trajectory, half widths,  $r_{0.5}/D$ , and center-line dilution ratios,  $S$ , of a buoyant jet in a uniform cross stream.  
(b)  $F = 10$  and  $k = 8$



$F=20 \quad k=4$

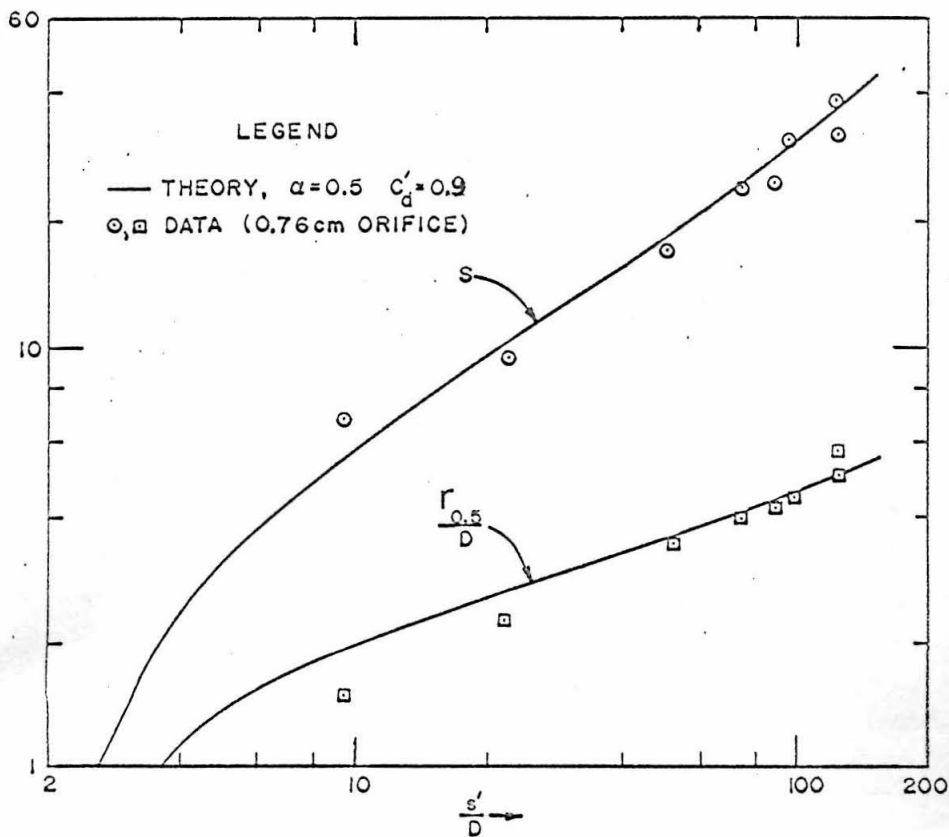
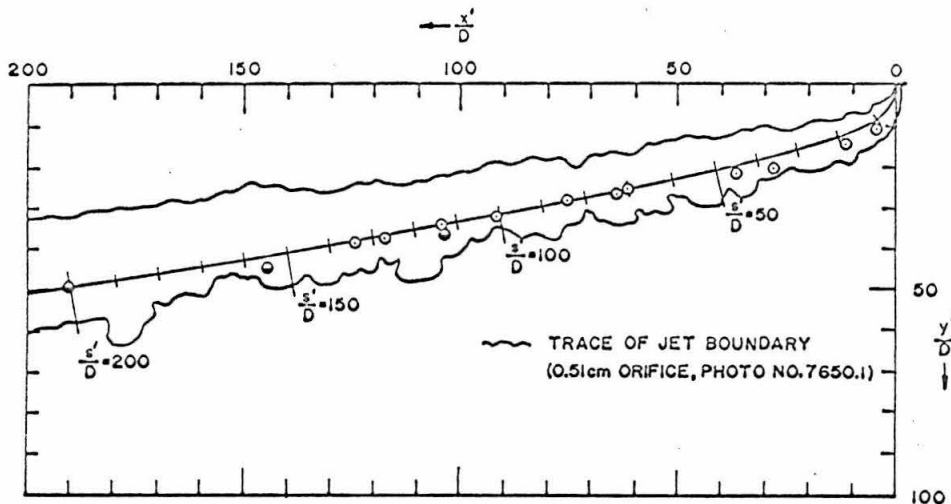


Fig. 60. Comparison of observed and theoretical trajectory, half widths,  $r_{0.5}/D$ , and center-line dilution ratios,  $S$ , of a buoyant jet in a uniform cross stream. (c)  $F = 20$  and  $k = 4$



$F=20 \quad k=8$

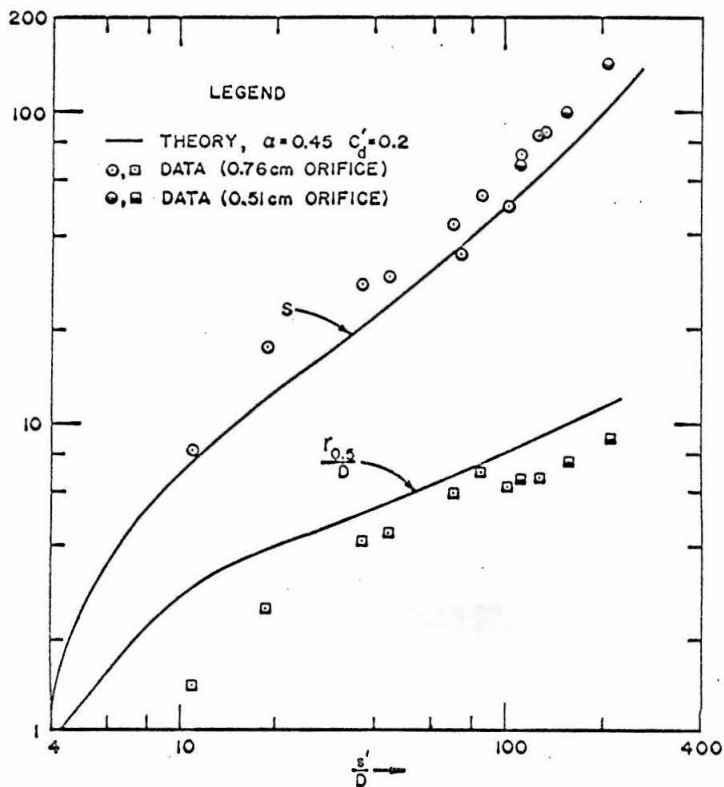
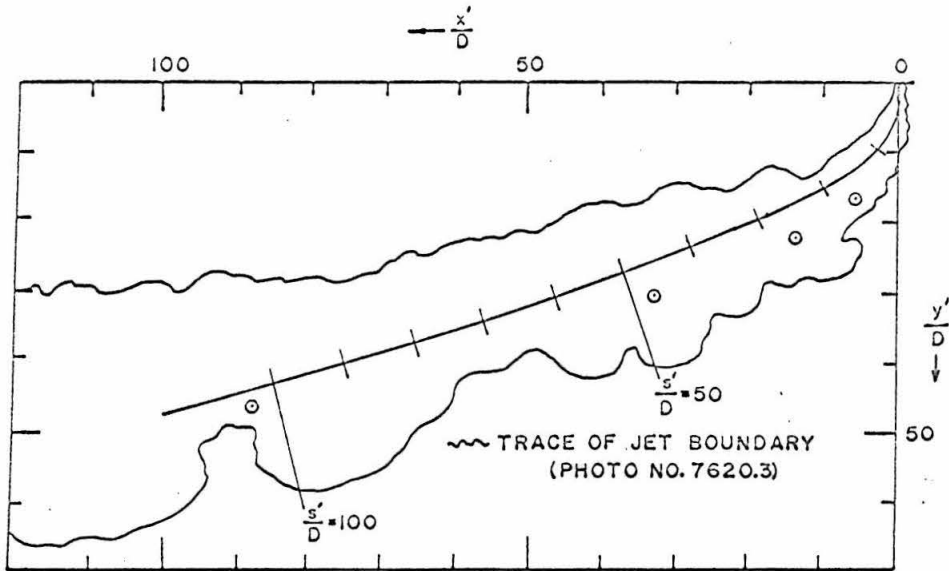


Fig. 60. Comparison of observed and theoretical trajectory, half widths,  $r_{0.5}/D$ , and center-line dilution ratios,  $S$ , of a buoyant jet in a uniform cross stream. (d)  $F = 20$  and  $k = 8$



$F=20 \quad k=12$

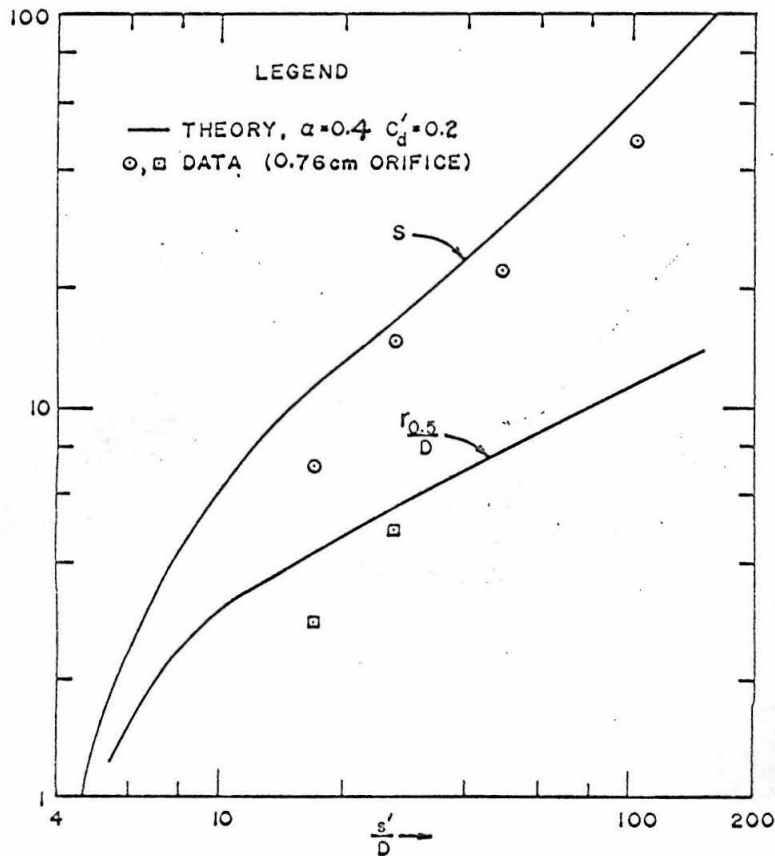
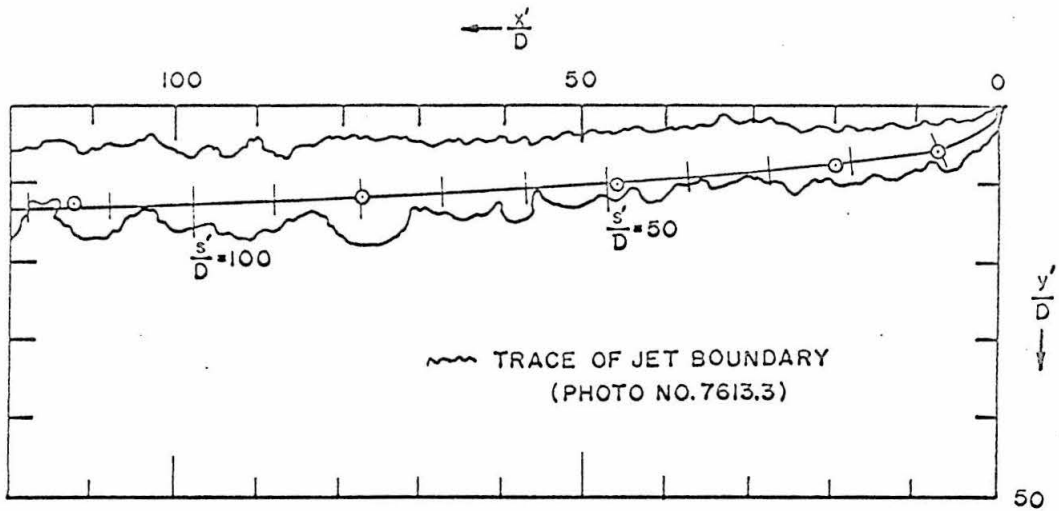


Fig. 60. Comparison of observed and theoretical trajectory, half widths,  $r_{0.5}/D$ , and center-line dilution ratios,  $S$ , of a buoyant jet in a uniform cross stream.  
(e)  $F = 20$  and  $k = 12$



F=40 k=4

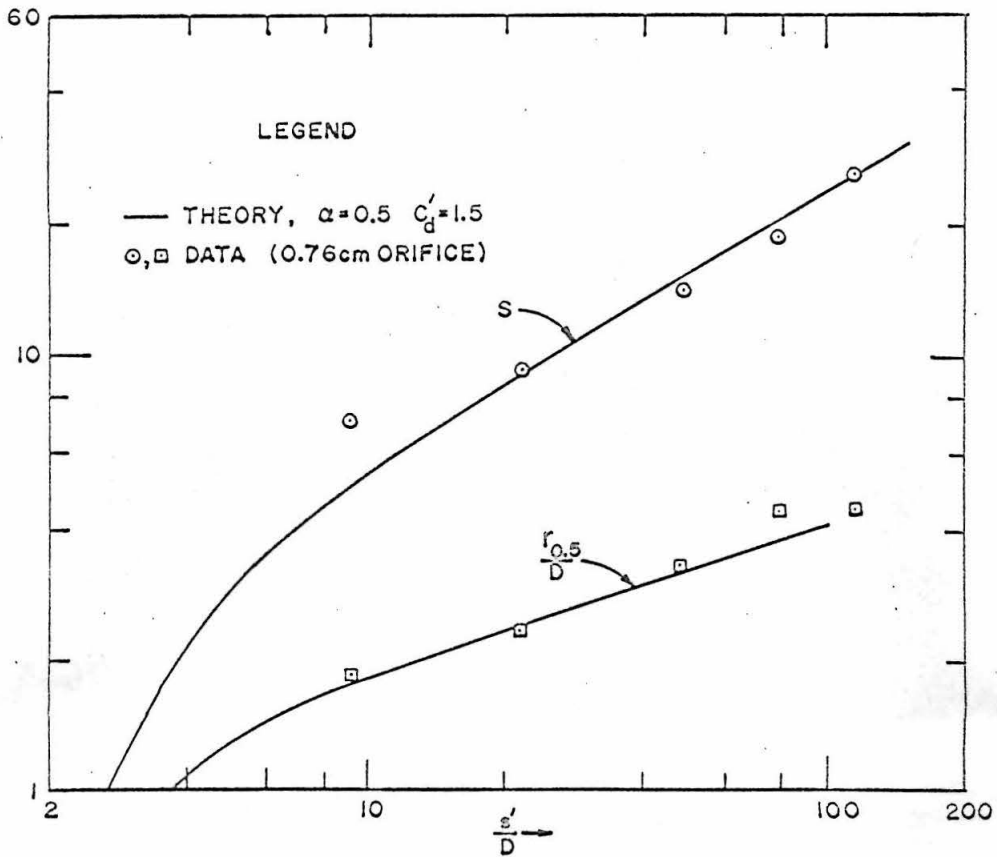
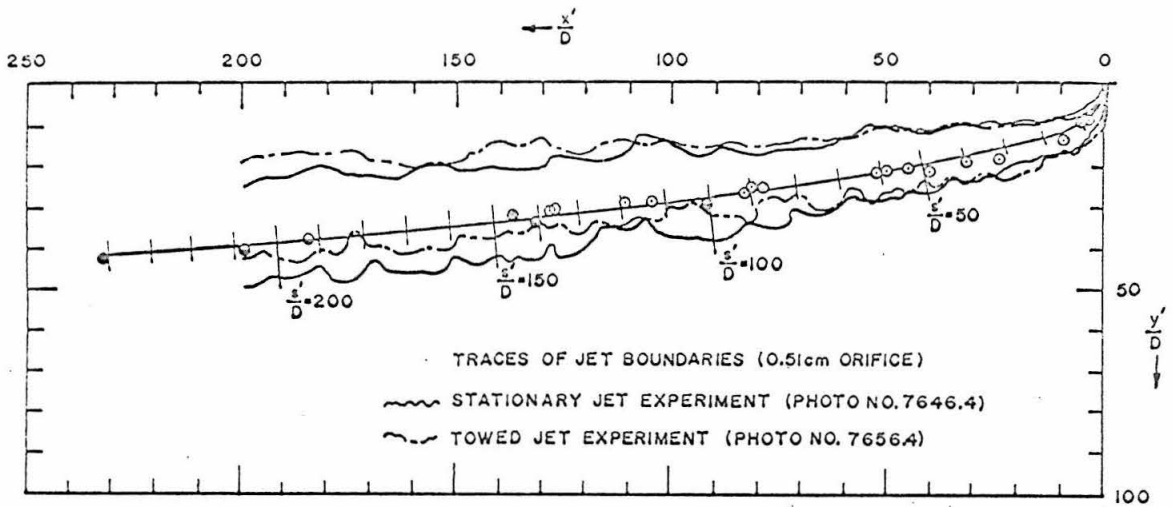


Fig. 60. Comparison of observed and theoretical trajectory, half widths,  $r_{0.5}/D$ , and center-line dilution ratios,  $S$ , of a buoyant jet in a uniform cross stream. (f)  $F = 40$  and  $k = 4$



$F=40$   $k=8$

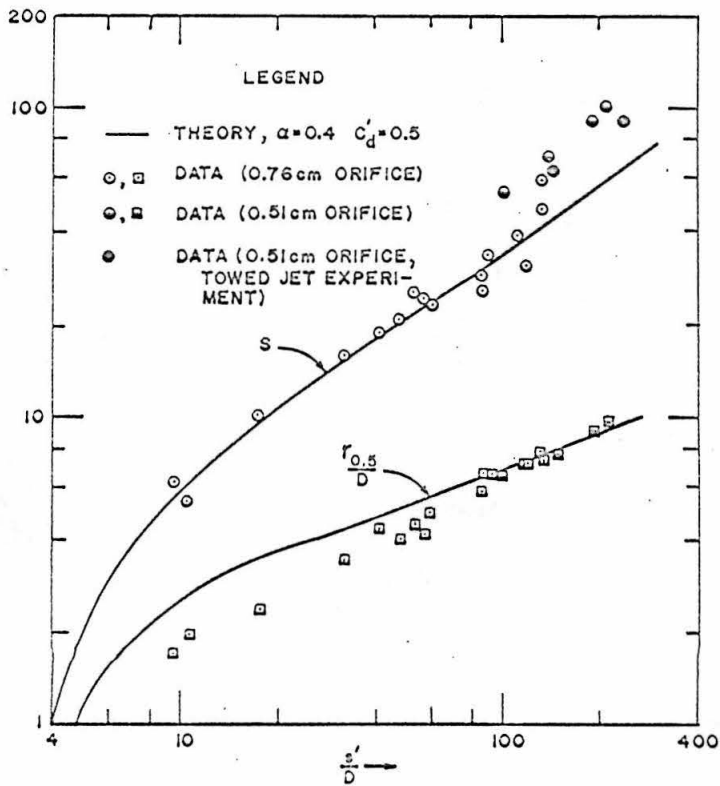
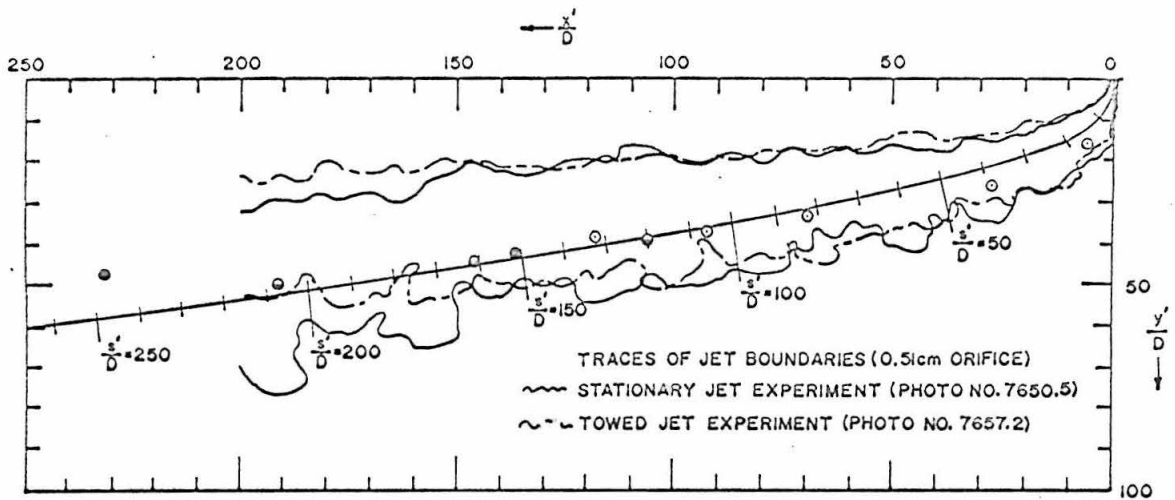


Fig. 60. Comparison of observed and theoretical trajectory, half widths,  $r_{0.5}/D$ , and center-line dilution ratios,  $S$ , of a buoyant jet in a uniform cross stream. (g)  $F = 40$  and  $k = 8$





F=40 k=12

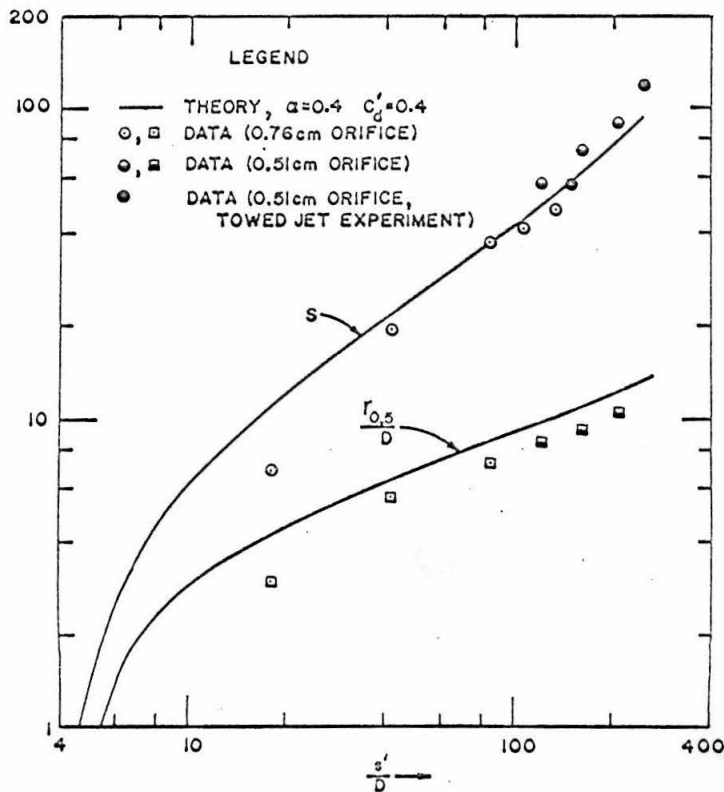
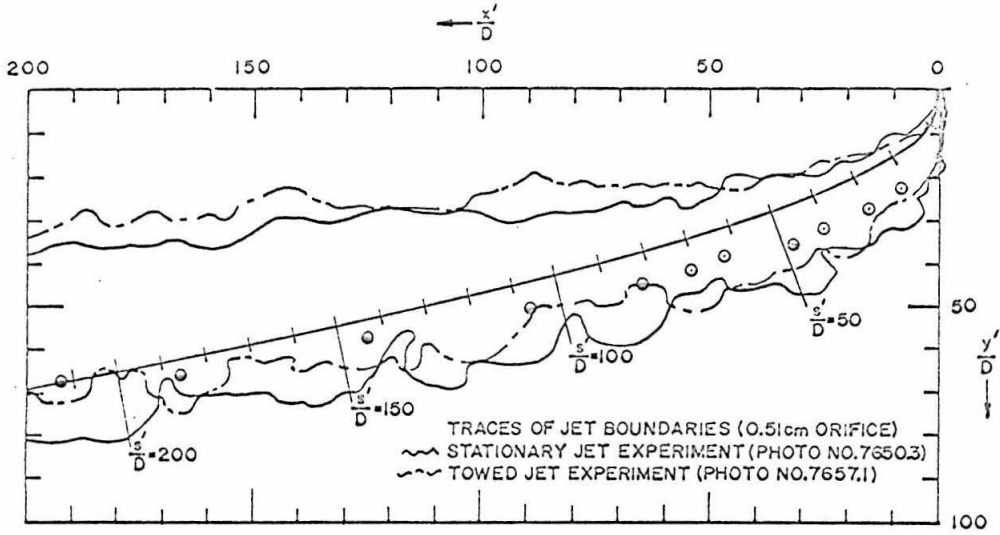


Fig. 60. Comparison of observed and theoretical trajectory, half widths,  $r_{0.5}/D$ , and center-line dilution ratios,  $S$ , of a buoyant jet in a uniform cross stream.  
 (h)  $F = 40$  and  $k = 12$



$F=40$   $k=16$

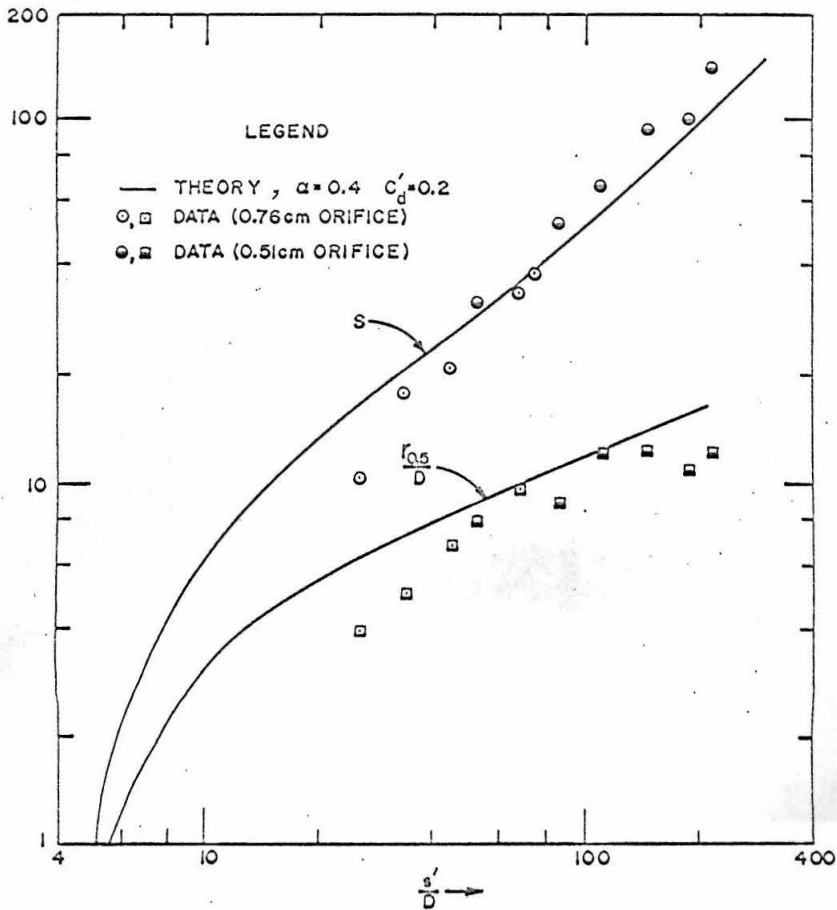
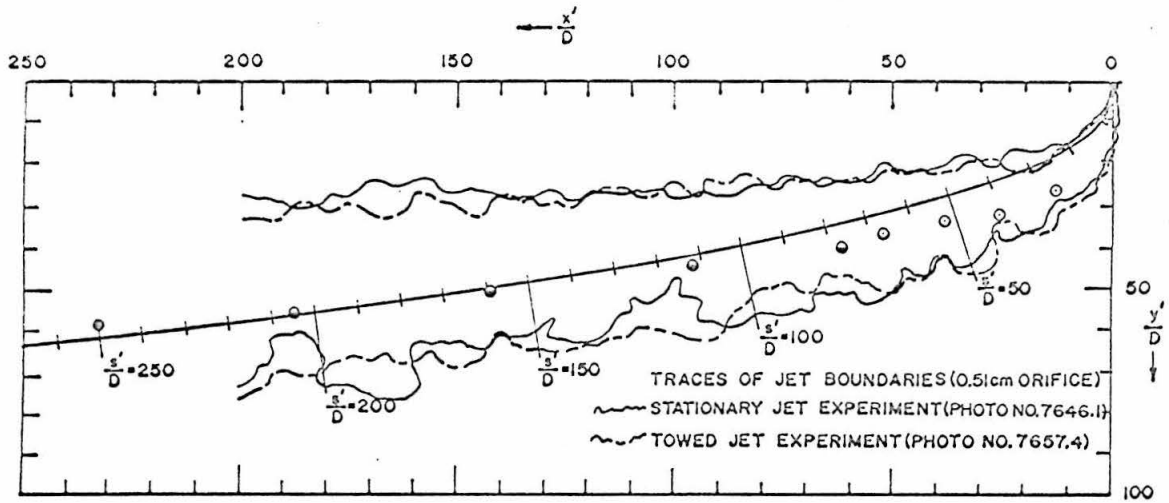


Fig. 60. Comparison of observed and theoretical trajectory, half widths,  $r_{0.5}/D$ , and center-line dilution ratios,  $S$ , of a buoyant jet in a uniform cross stream.  
(i)  $F = 40$  and  $k = 16$



F=80 k=16

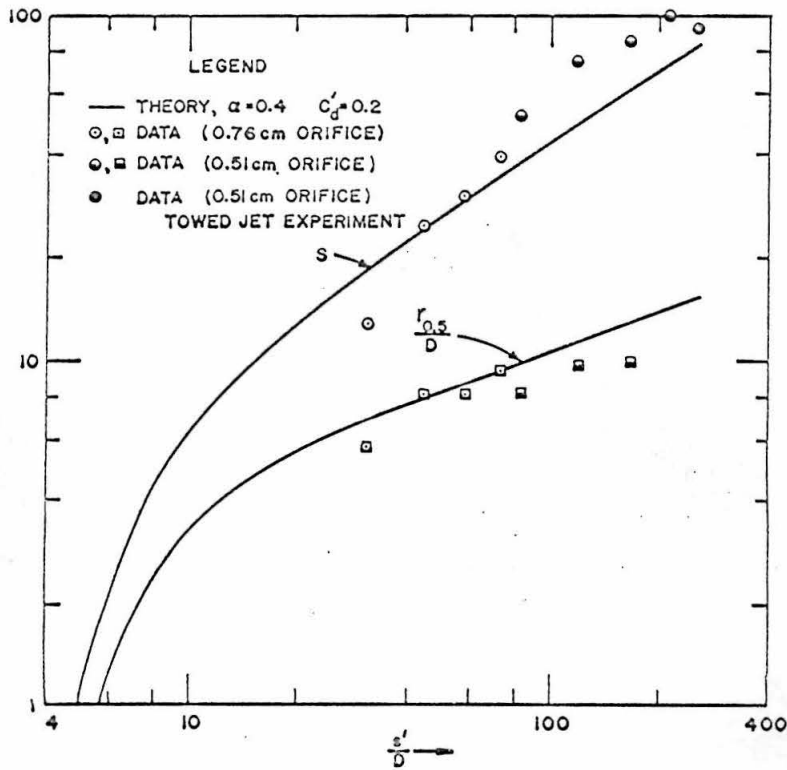


Fig. 60. Comparison of observed and theoretical trajectory, half widths,  $r_{0.5}/D$ , and center-line dilution ratios,  $S$ , of a buoyant jet in a uniform cross stream.  
 (j)  $F = 80$  and  $k = 16$

Table 5. Values of the Entrainment Coefficients,  $\alpha$ , and Drag Coefficients,  $C_d'$  and  $C_d$ , Determined from the Experimental Results

k \ F	10	20	40	80
4	$\alpha = 0.5$ $C_d' = 0.7$ $C_d = 0.8$	0.5 0.9 1.0	0.5 1.5 1.7	-
8	$\alpha = 0.5$ $C_d' = 0.1$ $C_d = 0.1$	0.45 0.2 0.2	0.4 0.5 0.4	-
12	-	$\alpha = 0.4$ $C_d' = 0.2$ $C_d = 0.2$	0.4 0.4 0.4	-
16	-	-	$\alpha = 0.4$ $C_d' = 0.1$ $C_d = 0.1$	0.4 0.2 0.2

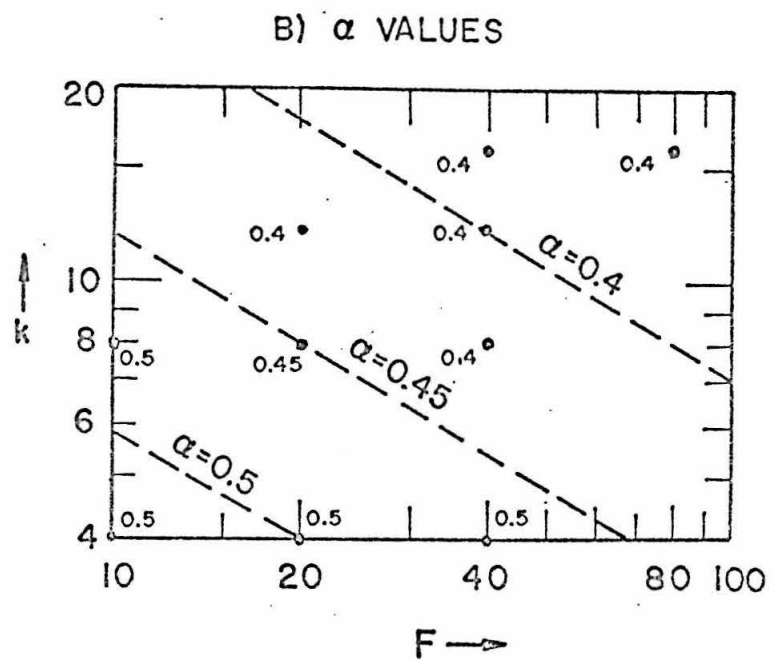
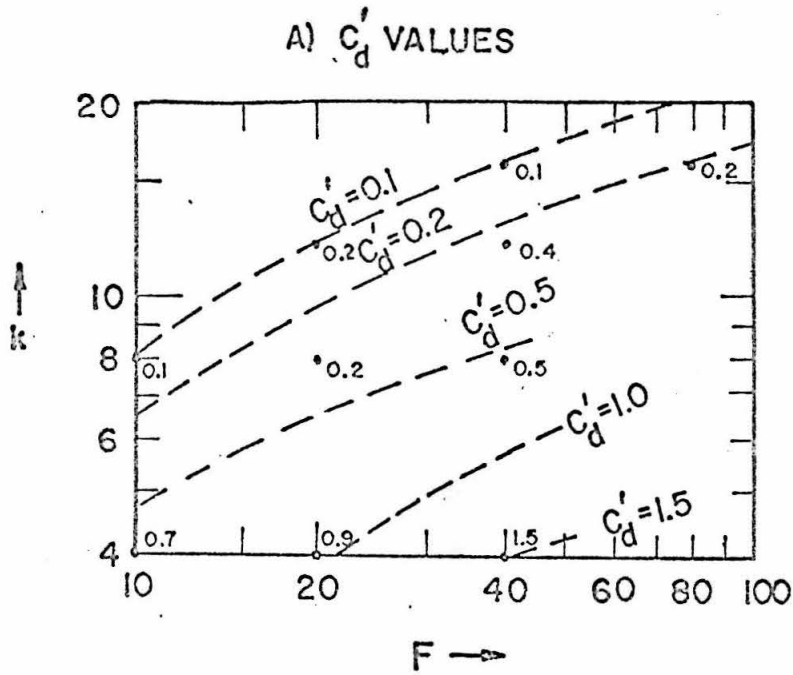


Fig. 61. Variations of the entrainment coefficient  $\alpha$  and the reduced drag coefficient  $C'_d$  for buoyant jets in uniform cross streams

The coefficient of entrainment  $\alpha$  varied from 0.5 to 0.4 and the drag coefficients,  $C_d'$ , from 0.1 to 1.5, or  $C_d$ , ( $C_d = \frac{\alpha \pi}{\sqrt{2}} C_d'$ ), from 0.1 to 1.7. (The drag coefficient  $C_d'$  is more convenient for this analysis, although  $C_d$  is the drag coefficient as usually defined in fluid mechanics.) Both coefficients  $\alpha$  and  $C_d'$  increased as the velocity ratio decreased. The entrainment coefficient  $\alpha$  decreased with increasing Froude number but the drag coefficient increased with the Froude number for a given velocity ratio.

The values of the entrainment coefficient are considerably larger than the values used for jets in stagnant environments. The effect of the ambient current tends to increase the dilution. Since the entrainment coefficient value depends on the shape of the profile assumed, smaller numerical values of the coefficients may have resulted if a profile close to the shape of the real profile was assumed.

##### 5. Comparison of results for stationary and towed jet experiments

The results of the towed jet experiments showed little difference from other experiments. The concentration measurements from Runs 40-8T, 40-12T and 80-16T revealed the dilution ratios were slightly smaller than those obtained from stationary jet experiments as shown in Figs. 60(g), 60(h) and 60(j). The jet trajectories also checked well as shown in Figs. 60(g), 60(h), 60(i) and 60(j).

The comparison of the motion pictures taken for both cases further confirmed this conclusion. Therefore, the effect of ambient turbulence and flow non-uniformity can be neglected as a first approximation for practical purposes in the range of these experiments. At still larger distances from the source, the ambient turbulence will ultimately become dominant in the mixing processes.

## CHAPTER VIII

### DISCUSSION OF THE RESULTS

The discussion of the results is given in two parts. First the results on the problem of a buoyant jet in a stagnant, stratified environment are discussed, then the problem of a buoyant jet in a uniform cross stream.

#### VIII-A. A Round Buoyant Jet in a Stagnant Environment with Linear Density Stratification

##### 1. Limitations of the theoretical solutions

The theoretical solutions obtained in Chapter IV are based on the assumptions listed in Chapter III. The applicability of the solutions depends upon the validity of these assumptions.

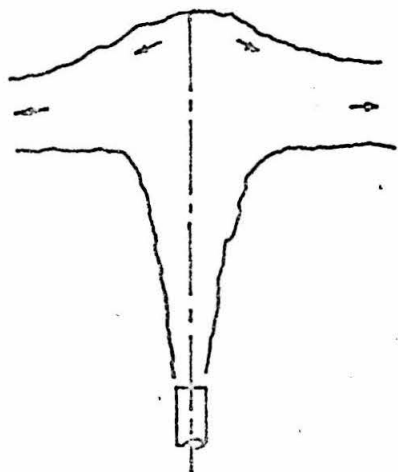
The assumptions on the similarity of both velocity and buoyancy profiles for jets in stratified environments have not been proved experimentally. However, based on the results for plumes in uniform environments obtained by Rouse, Yih and Humphreys (30), the assumptions are probably reasonable. But for jets in stratified environments the assumptions are not uniformly valid throughout the flow field. The assumptions are not expected to hold near the terminal points where the upward jet flows are interfered with by the sinking jet fluid from the top. The deviations are different for different types of the jet flows. The jet flows in density-stratified environments are classified into three types; namely, vertically rising, nearly vertically rising



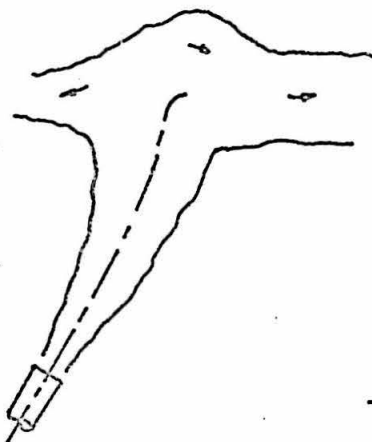
and jets with strong horizontal momentum fluxes as shown in Fig. 62. For a vertically rising or nearly vertically rising jet, the interference is expected to be great near the top region. But in the case of a jet with strong horizontal momentum flux the flow after reaching the terminal point will proceed predominantly in the direction of the horizontal momentum with little or no interference with the main jet flow. Thus the solutions can well be applied to the whole flow region for the jets with strong horizontal momentum flux. But the solutions for the other two types near the terminal points can be erroneous. The distinction between the last two types of flows can be established by examining the jet trajectories near the terminal points. If the local curvature is large then the flow belongs to the second type, i. e. a nearly vertically rising jet; otherwise it belongs to the third type.

The curvature effect of the jet trajectory is neglected in the analysis. The error involved is of the order of the ratio of the local characteristic length and the radius of curvature of the jet trajectory. Such error is small except near the terminal point for a nearly vertically rising jet. For inclined jets with low Froude number the initial sharp curving of the jet trajectory may also lead to some error. Such error can be roughly estimated by examining the solutions on the jet trajectories and jet half widths.

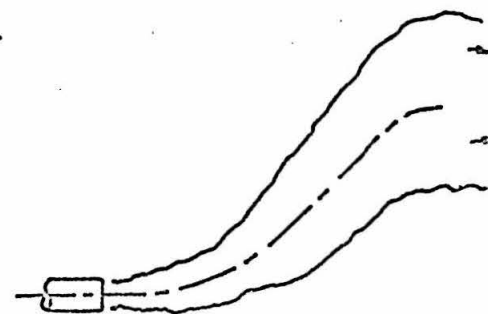
The Boussinesq assumption involves an error of the order of  $\Delta\rho/\rho_0$ . Therefore the solutions can be applied only when the density variation throughout the flow field is small. The approximation is good for the case of the sewage jets discharging into the ocean where



A VERTICALLY RISING JET



A NEARLY VERTICALLY  
RISING JET



A JET WITH STRONG  
HORIZONTAL MOMENTUM FLUX

Fig. 62. Types of buoyant jet flows in stagnant, density-stratified environments

the maximum difference in density is about 2.5%. But in experiments, sometimes the difference could reach 10% especially for modeling the low Froude number cases; the error will be correspondingly larger.

The density stratification of the ambient fluid can either be caused by temperature or salinity variations. The requirement that the density difference is small implies that the density gradient should also be weak. Such weak density stratification is not expected to significantly affect the detailed characteristics of a turbulent jet when the jet characteristic length is small. When the jet characteristic length is large, such as near the terminal point, the density stratification can actually suppress the jet into a flat layer of fluid as that observed after reaching the terminal point. Therefore the solutions can not be continued beyond the terminal points based upon the same formulation.

The density of the fluid may be related to the heat or salt content by the density deficiency equation (28) only if the density of the fluid varies linearly with the heat or salt content. The degree of approximation depends upon the properties of the fluid and its salt solutions. But for the small range of density variation as assumed here the approximation is reasonable and consistent with other assumptions. The density deficiency equation can also be applied if the density change involves both heat and salt provided  $\Delta\rho$  is a linear function of the temperature change and the salt concentration increment.

In applying the theoretical solutions the zone of flow establishment is taken to follow exactly the results by Albertson, Dai, Jensen and Rouse (4) on simple jets. For low Froude number cases the zone may be deflected by the buoyancy forces acting on the jets. But from what was observed in the experiments with the lowest Froude number  $F = 10$ , there seemed to be no substantial curving of the jet axis for distances  $s'/D$  less than 6.2.

## 2. Limitations of the experimental investigation

Experiments were carried out in a tank of finite size over time duration of about 5 minutes for each run. The transient effect on the jet flows was tested by taking time lapse photographs of the development of the dyed jet trajectories. Superpositions of the traces for both Jet Nos. 1 and 2 are shown in Fig. 24. There seemed to be little difference between the traces for the region of interest. Thus the transient effect on the jet trajectories can be neglected shortly after the jet reaches the terminal point. At this moment the effect of the walls of the tank would probably not be felt by the jet flow. The change of the ambient density stratification was also negligible considering the dimension of the tank and the volume of jet fluid discharged.

As stated by Ricou and Spalding (29) the entrainment rate of an axisymmetric jet could be considered independent of the jet Reynolds number,  $R = u_0 D / \nu$ , only if  $R$  is greater than 25,000. All the experiments in this study had  $R$  less than that number because of the necessity of modeling the gravity effect and the limitation of the

dimensions of the apparatus as shown in Table 1. Concentration measurements for ordinary jets with  $R = 6,000$  revealed deviations of less than 3% on center-line dilution values from the established results (see Fig. 31). Therefore the effect of low Reynolds number could affect the results probably within 5% for the range of  $R$  in the experiments.

In all the experiments for jets in density-stratified environments only photographs of the dyed jet trajectories were taken. Concentration or velocity measurements in the jet flow field have not been made because of the practical difficulty in performing such measurements in a stratified environment.

### 3. Comparison of the theoretical and experimental results

The comparison of the jet trajectories and the nominal jet boundaries is shown in Section V-C. Using  $\alpha = 0.082$ , the agreements are in general good except for the case of a vertical jet. For a vertical jet, the theory tends to underestimate the terminal height of rise; for this problem the best value of  $\alpha$  appears to be 0.057, although more experimental evidence is needed. The discrepancy may also be due to breakdown of many of the assumptions near the terminal region of the jet.

For a buoyant jet in a uniform environment, the theory by using  $\alpha = 0.082$  and  $\lambda = 1.16$  predicted trajectories and nominal jet boundaries that agreed well with the observed dyed jets. Without measured velocity and concentration distributions, it was not possible to determine whether other values might be slightly better.

4. Coefficient of entrainment  $\alpha$

The value of the entrainment coefficient  $\alpha$  used in comparison of theory and experiment was 0.082, the same value as obtained from the results of Rouse, Yih and Humphreys (30) on simple plumes.

Although the comparison covered only two quantities, i. e. the jet trajectory and the nominal jet width, it should provide the overall indication on the jet gross behavior. Both quantities are inter-related with the complete jet gross characteristics such as the volume flux and components of momentum flux parameters, and detailed profiles of velocity and density.

As long as the buoyancy force is in the same direction as the flow, similarity can be reasonably assumed. But as the jet overshoots its position of neutral buoyancy, the buoyant force becomes negative and decelerates the jet until it sinks back to a neutral level. During this flow reversal, similarity undoubtedly is a poor approximation. For vertical buoyant jets (three experiments), the maximum height of rise is predicted better by  $\alpha = 0.057$  than 0.082; present results do not permit a closer determination of  $\alpha$ .

5. Turbulent Schmidt number  $\lambda^2$  or spreading ratio  $\lambda$

The different rates of spreading of velocity and buoyancy profiles are considered by taking the turbulent spreading ratio  $\lambda$  to be 1.16 based upon Rouse et al.'s (30) data. The  $\lambda$  chosen gives a dilution ratio  $S_o$  about 15% greater than the case when the value of  $\lambda$  is taken to be unity as indicated by eq. (58) in Section IV-E.

Without detailed profiles it was not possible to determine  $\lambda$  directly from the present experiments.

VIII-B. A Round Buoyant Jet in a Uniform Cross Stream of Homogeneous Density

1. Limitations of the theoretical solutions

The theoretical solutions are obtained based upon the assumptions listed in Chapter III.

The velocity and buoyancy distributions were assumed to be in the following forms across a section normal to the jet axis:

$$u^*(s, r, \varphi) = U_a \cos \theta + u(s) e^{-r^2/b^2} \quad (18)$$

and

$$\rho_a - \rho^*(s, r, \varphi) = [\rho_a - \rho(s)] e^{-r^2/b^2} \quad (19)$$

The actual observed cross sections in the jets are in horse-shoe shapes, because the cross current develops two vortices within the jet flow and a wake behind it (see Fig. 57). Thus the assumed profiles are not entirely realistic. But the integral technique employed in the analysis will still give good results on gross behavior if reasonable similarity exists and the relative importance of the terms are preserved even though the exact shape of the profiles are replaced by some simpler profiles in the analysis. For example, in the analysis of buoyant jets in stagnant environments and in parallel ambient currents, "top-hat" distributions were used by Morton (21). The results are the same as for Gaussian profiles if an appropriate numerical value of the coefficient of entrainment is used.

In the integration over the jet cross section, the profiles were truncated at the distance  $\sqrt{2} b$  for the terms like  $U_a \cos \theta$  which do not contain factors of  $e^{-r^2/b^2}$ . This inconsistency of limits of integration involves a discrepancy of about 13% in the u terms in comparison with the case where the limit is taken to be  $\sqrt{2} b$  for all the terms.

The different rate of spreading between the velocity and buoyancy profiles was neglected for simplicity in the formulation - i. e.  $\lambda$  was assumed to be 1. This could lead to an underestimation of the dilution ratios. But due to lack of experimental information the exact spreading ratio  $\lambda$  is unknown. The error involved in determining the dilution ratios is believed to be of the same order of that for jets in stagnant environments, that is about 15%.

The rate of entrainment was assumed to be proportional to the vector difference of the local characteristic velocity and the ambient velocity as given by:

$$\frac{dQ}{ds} = 2\pi \alpha b |\bar{U}_a - \bar{U}_j| \quad (17)$$

The value of the entrainment coefficient  $\alpha$  was assumed to be constant. Because the entrainment mechanism here is affected greatly by the normal component of the ambient velocity the nature of the coefficient  $\alpha$  is expected to be different from the  $\alpha$  for jets in stagnant environments (see Section VIII-B-3 below).

The effect of the presence of the wake region produced by the jet flow was assumed to be represented by a gross drag term with a drag coefficient  $C_d'$ . This is a rough but necessary approximation. The



jet bends over toward the downstream direction not only due to the entrainment of the ambient horizontal momentum but also because of the drag force. (For lack of a better assumption, the drag is based on the velocity component normal to the jet.) The values obtained will be discussed in Section VIII-B-3 below.

The effect of the ambient turbulence was not considered in the analysis. Thus the results should only be applied in a uniform non-turbulent stream. The theoretical solutions are however expected to be applicable with reasonable accuracy to the cases where the ambient stream is weakly turbulent and to the region close to the nozzle. The effect could only be determined by experimental studies.

In summary the analysis based upon these assumptions should provide a reasonably good theoretical model of the gross jet behavior in cross streams. At the same time experimental studies were made to provide the necessary numerical coefficients and examine the comparison between the theoretical and observed results.

In application to practical problems, the zone of flow establishment is assumed to follow the relations shown in Section VI-E. For the cases of the velocity ratio  $k$  greater than 8 there was no available information on the length of the zone of flow establishment except  $k = \infty$  which gives  $s_e'/D = 6.2$ . Relations were obtained by simple interpolation from the cases of  $k = 4, 6, 8$  and  $\infty$ . The error involved is unknown, although probably small.

In evaluating the local maximum concentration  $c$ , an excess of 60 to 80% over the predicted value  $c$  should be added in view of the observed concentration profiles. The lateral widths  $r'_{0.5}$  are twice the widths  $r_{0.5}$  as shown in Figs. 57 and 58.

## 2. Limitations of the experimental investigation

Concentration measurements were made in all the experiments to determine the jet trajectories, half widths, and variation of dilution ratios (Chapter VII). No velocity measurements were made in the jet flows.

The experiments were carried out in a flume flow. The boundary layer of the flume flow was largely avoided by injecting the jets from the free surface. Two sizes of orifice plates were used in the experiments and the results reproduced well in the overlapped region of measurements. Thus the effect of the presence of the flume walls was considered to be negligible in the experiments.

The point concentration values were determined by a finite size probe as shown in Fig. 47. Since the measurements were carried out in the regions where the jet widths were large in comparison with the probe size, such sampling error was considered to be negligible. This was also confirmed by the reproducibility of the results from runs using two orifices of different size.

The minimum value of the jet Reynolds numbers for the runs of this study was 6,800. The effect was uncertain but believed to be unimportant in the range studied.

The maximum range of the measurements was up to  $s'/D = 250$  from the orifice. It was not feasible to carry out experiments at larger distances by the present technique. In the runs where only the larger size orifice plate was used the distance  $s'/D$  was around 140 or less.

3. Determination of the entrainment coefficient  $\alpha$  and the drag coefficient  $C_d'$

The coefficients of entrainment  $\alpha$  and the drag coefficients  $C_d'$  were determined by matching the theoretical and experimental results on jet trajectories and the dilution ratios  $S$  for jets of different initial conditions. The values of the coefficients are summarized in Table 5. The comparison of the results are shown in Figs. 60(a) to (j) in Section VII-C. Although the choice of  $\alpha$  and  $C_d'$  values for each case was based upon the best fitted results, certain deviation still existed. But such deviations are not out of proportion to the approximations made throughout the analysis.

The entrainment coefficient  $\alpha$  and the drag coefficient  $C_d'$  were found to vary for the different cases. This variation is probably caused mainly by the assumptions of constant shape of profiles for different velocity ratio cases since the shape of the profiles is expected to vary as the velocity ratio changes.

The value  $\alpha$  varied from 0.4 to 0.5 for the cases studied. The values are considerably larger than the value used for buoyant jets in stagnant environments, which is  $\alpha = 0.082$ . The basic entrainment mechanisms for these two cases are believed to be different. The component of the ambient velocity normal to the jet axis is a main

contributing factor to the entrainment for the jets in cross streams while in stagnant environments the jets entrain the ambient fluid by pure aspiration due to the jet flow. The value of  $\alpha$  for jets in cross streams could be smaller if a more realistic velocity distribution is assumed.

The value of  $\alpha$  tends to decrease as the velocity ratio  $k$  increases (see Fig. 61). This is reasonable because in the limiting case when  $k$  becomes infinite (or the ambient fluid is stagnant),  $\alpha$  should approach the value 0.082. The value of  $\alpha$  also decreases slightly as the  $F$  increases (i. e. as the buoyancy effect decreases). However, the overall change of the  $\alpha$  value is not large for the range studied.

The drag coefficient  $C_d'$  varies from 0.1 to 1.5, or  $C_d$  from 0.1 to 1.7, decreasing as the velocity ratio  $k$  increases. The effect of including the drag terms changes the location of the jet axis at large distance but makes relatively less change in other jet quantities such as the dilution ratio and the half width. Neglecting the drag terms will be permissible only when the velocity ratios are large and the Froude numbers small as indicated by the results obtained.

#### 4. Comparison of the theoretical and experimental results

The comparison of the theoretical and experimental results on jet trajectories, widths and dilution ratios are shown in Figs. 60(a) to (j). The overall agreements are considered to be good. Although the values of the coefficients were based on the comparison of the jet trajectories and dilution ratios from both experimental and theoretical results, the predicted jet half widths  $r_{0.5}$  agreed fairly well with the

measured values. Thus the theoretical solutions can be used for practical purposes in predicting the gross jet behavior.

The deviations are generally bigger for larger velocity ratio cases. The theory tends to underestimate the dilution ratios at  $s'/D$  over 100. From towed jet experiments it was confirmed that the discrepancy was not caused by ambient turbulence in the flume flow. This error may be caused by the error in the assumption on the zone of flow establishment. Before the profiles transform into the horse-shoe shapes there may exist a fairly long transition region between the assumed end of the zone of flow establishment and the fully developed region.

#### 5. Effect of the ambient turbulence

The effect of the turbulence in the flume flow was determined by conducting a set of towed jet experiments as described in Chapter VII.

For  $s'/D$  less than 250 with an ambient turbulence intensity under 5%, the effect was found to be unimportant on the jet gross behavior. Therefore under these conditions the jet mixing is dominated mainly by the interaction of the jet and the mean ambient stream. The self-generated turbulence is then the main factor in jet diffusion.

At larger distances or in the presence of more intense ambient turbulence intensity the jet will undoubtedly diffuse at a faster rate. This has not been investigated in this study.

CHAPTER IX

SUMMARY AND CONCLUSIONS

IX-A. Previous Knowledge about a Round Buoyant Jet in a Stagnant Environment.

The problem of a round jet in a stagnant environment is summarized in Table 6. The flow configurations, investigators, their approaches and results are all listed in the table.

Morton, Taylor and Turner (23) first applied the integral type analysis with an assumed entrainment relation:

$$\frac{dQ}{ds} = 2\pi \alpha u b \quad (12)$$

where  $Q$  is the volume flux at a normal cross section

$u$  is the local characteristic velocity

$b$  is the local characteristic length

$\alpha$  is the coefficient of entrainment.

They analyzed the problem of a plume in a linearly density-stratified environment by assuming a constant  $\alpha$ . Morton (22) subsequently investigated the problems of vertical buoyant jets in both uniform and stratified environments based upon the same approach.

Abraham (1, 3) pointed out that the  $\alpha$  values for simple jets and simple plumes were different (0.057 vs 0.082). Since the behavior of the buoyant jet initially was like a simple jet and later a plume, he argued that  $\alpha$  could not be assumed constant in solving buoyant jet problems. Instead, he proposed a semi-empirical method

Table 6. A brief summary of the studies on jets in stagnant environments

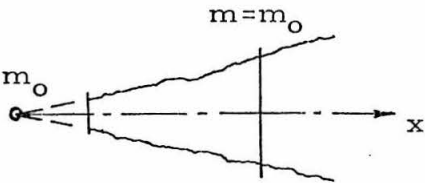
Type of Jet Flow	A SIMPLE JET (AN ORDINARY MOMENTUM JET)	
Flow Configuration	<p data-bbox="428 535 748 639">A continuous source of momentum only (axisymmetric)</p> 	
Contents Investigators	Methods of Approach	Results
Numerous	Various methods; an important branch of free turbulent flows.	<ol style="list-style-type: none"> <li>1. <math>u \sim x^{-1}</math>, <math>b \sim x</math></li> <li>2. Velocity profiles</li> </ol>
Albertson, Dai, Jensen & Rouse (5)	Experimental studies	<ol style="list-style-type: none"> <li>1. <math>u \sim x^{-1}</math>, <math>b \sim x</math></li> <li>2. Similarity of velocity profiles (Gaussian).</li> <li>3. Data give <math>\alpha = 0.057</math>.</li> </ol>
Ricou & Spalding (29)	Measurements of entrainment rates.	<ol style="list-style-type: none"> <li>1. Data agree with Albertson et al.</li> <li>2. Entrainment rate independent of R if <math>R &gt; 25,000</math></li> </ol>
Present Study (Section V-C)	Concentration measurements along jet axes.	$S_o = 0.185 \frac{x}{D}$ for $R \sim 6,000$ as shown in Fig. 31 (indicates $\lambda = 1.16$ ).

Table 6 (continued)

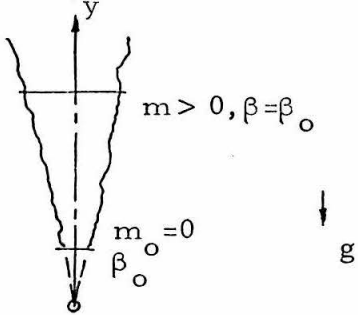
Type of Jet Flow	A SIMPLE PLUME	
Flow Configuration	<p data-bbox="419 529 745 624">A continuous source of buoyancy only. (axisymmetric)</p> 	
Contents Investigators	Methods of Approach	Results
Schmidt (32)	<ol style="list-style-type: none"> <li>1. Analysis based on mixing length hypothesis</li> <li>2. Measurements over heated grids.</li> </ol>	<ol style="list-style-type: none"> <li>1. <math>u \sim y^{-1/3}</math>, <math>b \sim y</math></li> <li>2. Velocity and temperature profiles.</li> </ol>
Rouse, Yih & Humphreys (30)	<ol style="list-style-type: none"> <li>1. Analysis based on similarity assumptions.</li> <li>2. Measurements over flames.</li> </ol>	<ol style="list-style-type: none"> <li>1. <math>u \sim y^{-1/3}</math>, <math>b \sim y</math></li> <li>2. Velocity and buoyancy profiles (Gaussian).</li> <li>3. Data give <math>\alpha = 0.082</math> <math>\lambda = 1.16</math></li> </ol>
Ricou & Spalding (29)	Measurements of entrainment rates.	Data agree with Rouse et al.



Table 6 (continued)

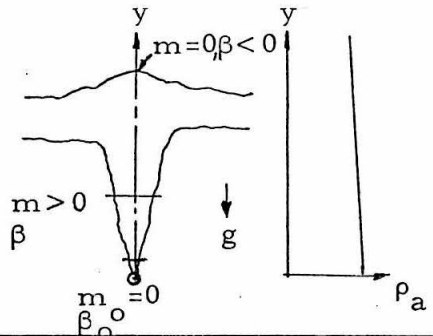
<p>Type of Jet Flow</p>	<p>A SIMPLE PLUME IN A LINEARLY DENSITY-STRATIFIED ENVIRONMENT</p>	
<p>Flow Configuration</p>	<p>A continuous source of buoyancy only (axisymmetric)</p> 	
<p>Contents Investigators</p>	<p>Methods of Approach</p>	<p>Results</p>
<p>Morton, Taylor &amp; Turner (23)</p>	<ol style="list-style-type: none"> <li>1. Integral type analysis based on:             <ol style="list-style-type: none"> <li>a. Similarity assumptions.</li> <li>b. Entrainment relation (4) with a constant coefficient of entrainment.</li> </ol> </li> <li>2. Photographic observations.</li> </ol>	<p>Gross flow behavior obtained by numerical integration. <math>\alpha = 0.093</math> suggested.</p>

Table 6 (continued)

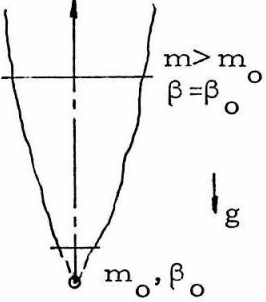
Type of Jet Flow	A VERTICAL BUOYANT JET (FORCED PLUME)	
<p>Flow Configuration</p>	<p>A continuous source of buoyancy and momentum (axisymmetric)</p> 	
<p>Contents Investigators</p>	<p>Methods of Approach</p>	<p>Results</p>
<p>Morton (22)</p>	<p>Integral type analysis based upon constant <math>\alpha</math> and <math>\lambda</math> values.</p>	<p>Gross flow behavior suggesting <math>\alpha = 0.082</math> and <math>\lambda = 1.16</math></p>
<p>Abraham (1)</p>	<p>Integral type analysis based upon specified jet width functions.</p>	<p>Gross jet behavior on <math>u</math>, <math>b</math> and concentration variations.</p>
<p>Frankel &amp; Cumming (14)</p>	<p>Concentration measurements.</p>	<ol style="list-style-type: none"> <li>1. Concentration variations along jet axes.</li> <li>2. Fluctuations of the concentrations.</li> </ol>
<p>Fan &amp; Brooks (in preparation, same technique as shown in (12))</p>	<p>Morton type analysis used for numerical integration of equations for a wide variety of cases.</p>	<ol style="list-style-type: none"> <li>1. Gross jet behavior</li> <li>2. Comparison of the results shown in Fig. 5.</li> </ol>

Table 6 (continued)

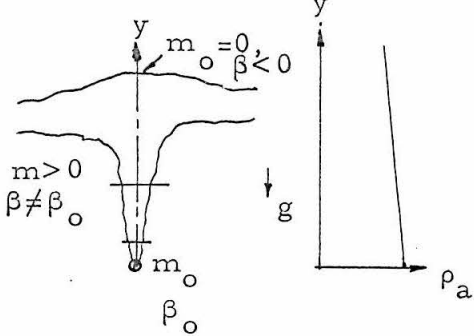
<p>Type of Jet Flow</p>	<p>A VERTICAL BUOYANT JET (FORCED PLUME) LINEARLY DENSITY-STRATIFIED ENVIRONMENT</p>	
<p>Flow Configuration</p>	<p>A continuous source of buoyancy and momentum (axisymmetric)</p> 	
<p>Contents Investi- gators</p>	<p>Methods of Approach</p>	<p>Results</p>
<p>Morton (22)</p>	<p>Integral type analysis assuming constant coefficients <math>\alpha</math> and <math>\lambda</math></p>	<ol style="list-style-type: none"> <li>1. Gross jet behavior</li> <li>2. Suggesting <math>\alpha = 0.082</math> and <math>\lambda = 1.16</math></li> </ol>
<p>Present Study (Chapter IV)</p>	<ol style="list-style-type: none"> <li>1. Morton type analysis. Numerical solution of differential equations for variety of cases at <math>\theta_o = 90^\circ</math></li> <li>2. Experiments compared with theory.</li> </ol>	<ol style="list-style-type: none"> <li>1. Gross jet behavior</li> <li>2. Comparison of the predicted and observed terminal heights by using <math>\lambda=1.16</math> and different <math>\alpha</math> values (see Table 2)</li> </ol>

Table 6 (continued)

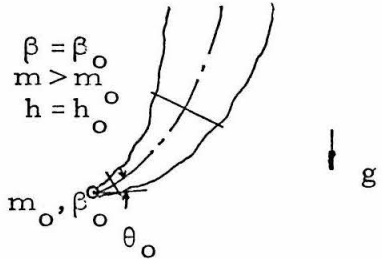
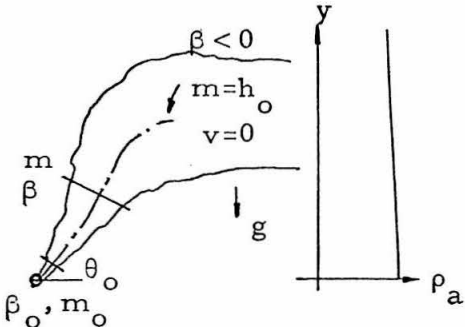
Type of Jet Flow	AN INCLINED BUOYANT JET (FORCED PLUME)	
<p>Flow Configuration</p>	<p>A continuous source of buoyancy and momentum at an angle <math>\theta_0</math> with the horizontal direction (three dimensional)</p> 	
<p>Contents Investigators</p>	<p>Methods of Approach</p>	<p>Results</p>
<p>Abraham (1, 2)</p>	<p>Integral type analysis by specifying jet width as a function of <math>\theta</math></p>	<p>Gross jet behavior for <math>\theta_0 = 0^\circ</math></p>
<p>Frankel &amp; Cumming (14)</p>	<p>Concentration measurements.</p>	<p>Variations of concentrations along jet axes for various <math>\theta_0</math> values.</p>
<p>Cederwell (10)</p>	<p>Integral type analysis</p>	<p>Concentration variations along jet axes.</p>
<p>Fan &amp; Brooks (12)</p>	<p>Morton type analysis for numerical integration of equations for many cases</p>	<ol style="list-style-type: none"> <li>1. Gross jet behavior for <math>\theta_0 = 0^\circ</math></li> <li>2. Comparison of the present results with Abraham's, Cederwell's and Frankel and Cumming's are shown in Fig. 6.</li> </ol>
<p>Present Study (Sec. V-C)</p>	<p>Experiments</p>	<p>Comparison of predicted and observed jet trajectories and nominal half widths (Figs. 29 and 30).</p>

Table 6 (continued)

Type of Jet Flow	AN INCLINED BUOYANT JET (FORCED PLUME) IN A LINEARLY DENSITY-STRATIFIED ENVIRONMENT	
<p>Flow Configuration</p>	<p>A continuous source of buoyancy and momentum at an angle <math>\theta_o</math> with the horizontal direction (three dimensional)</p> 	
<p>Contents</p> <p>Investi-gators</p>	<p>Methods of Approach</p>	<p>Results</p>
<p>Present Study (Chapters IV &amp; V)</p>	<ol style="list-style-type: none"> <li>1. Morton type analysis</li> <li>2. Experiments</li> </ol>	<ol style="list-style-type: none"> <li>1. Gross jet behavior</li> <li>2. Comparison of predicted and observed jet trajectories and nominal half widths using <math>\alpha = 0.082</math>, <math>\lambda = 1.16</math></li> </ol>

to account for this variable growth of the jet for horizontal and vertical discharges. Fan and Brooks (12) analyzed the same horizontal jet problem assuming a constant coefficient of entrainment as an approximation. Their results, using  $\alpha = 0.082$  agreed well with the experimental results (Chapter II), previous experiments, and Abraham's analysis.

All the analyses were based upon integral approaches covering the gross behavior of the jets. The details of the jet flows were forsaken for simplicity in the analysis.

#### IX-B. Contribution of the Present Study to the Problem of a Round Buoyant Jet in a Stagnant Stratified Environment.

##### 1. Theoretical Predictions.

By adopting the Morton-type integral approach, using similarity assumptions, the problem of an inclined round buoyant jet in a stagnant linearly density-stratified environment has been solved theoretically (see Chapter IV). The results, especially for horizontal discharge, are useful in prediction of the gross behavior of the inclined buoyant jets arising in pollution control problems. (More detailed results covering a wider range of initial conditions together with two-dimensional jet cases will be presented in a future report.)

The problem was formulated based upon the assumptions listed in Chapter III. The equations with seven unknowns were solved numerically. There were three relevant dimensionless parameters to the problem, namely the initial angle of discharge,  $\theta_0$ , the initial volume flux parameter,  $\mu_0$ , and the initial momentum flux parameter

$m_o$  (see Fig. 11 ). The density gradient and strength of the buoyancy source are included in the dimensionless parameters. For finite nozzles (diameter  $D$ ), the  $m_o$  and  $\mu_o$  were related with the jet Froude number  $F$  and a stratification parameter  $T$  defined as:

$$F = \frac{U_o}{\sqrt{g \frac{(\rho_o - \rho_1)}{\rho_o} D}} \quad (51)$$

and

$$T = \frac{\rho_o - \rho_1}{\left(-\frac{d\rho_a}{dy}\right)D} \quad (52)$$

Either set of parameters ( $\theta_o$ ,  $m_o$ ,  $\mu_o$  or  $\theta_o$ ,  $F$ ,  $T$ ) can be used to define the problem, but the second set is more convenient to use in practical problems.

## 2. Experimental Investigation.

Thirty-three jet experiments were carried out in a laboratory tank. Trajectories of dyed jets were determined photographically. (See Chapter V.)

Theoretical results on the jet trajectories and nominal half widths were compared with the observed dyed jet forms by using a constant coefficient of entrainment  $\alpha = 0.082$ . In general, the agreement was good. But, for vertical jets in stratified environments the prediction of terminal heights of rise by using  $\alpha = 0.057$  seemed

to give better results. For round buoyant jets in uniform environments the solutions for jet trajectories by using  $\alpha = 0.082$  agreed better with observed jet flows than Abraham's (1) solutions by specifying a rate of growth function.

Therefore, based upon the findings of the present study, a constant coefficient of entrainment  $\alpha = 0.082$  and a turbulent spreading ratio  $\lambda = 1.16$  are recommended for the analysis of the round buoyant jet in a stagnant environment, either uniform in density or linearly-stratified. The theoretical solutions obtained in this study based upon various assumptions are considered to be sufficiently accurate and satisfactory for practical purposes. The error of predictions may still be of the order of  $\pm 10$  to  $20\%$ ; however, this is reasonably good for turbulent stratified flow.

#### IX-C. Previous Knowledge About a Round Jet in a Uniform Cross Stream.

The previous studies on round jets in uniform cross streams are summarized in Table 7. The investigations were mostly experimental and on the determination of the jet trajectories. For ordinary momentum jets, measurements were made by G6rdier (15), Jordinson (17), Keffer and Baines (18) on jet velocities. Because of the rapid rate of decay of velocity, such measurements were limited to the region close to the nozzle. An integral type analysis was attempted by Keffer and Baines by assuming an entrainment mechanism based upon scalar difference of the velocities. For buoyant jets, measurements were made on jet trajectories by



Table 7. A Brief Summary of Studies on Jets in Cross Streams

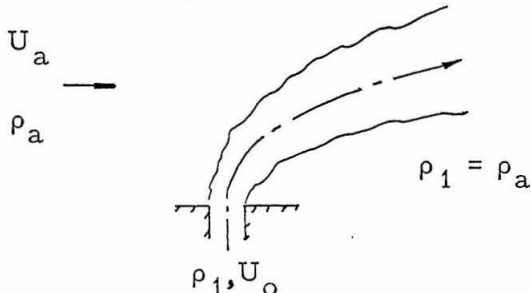
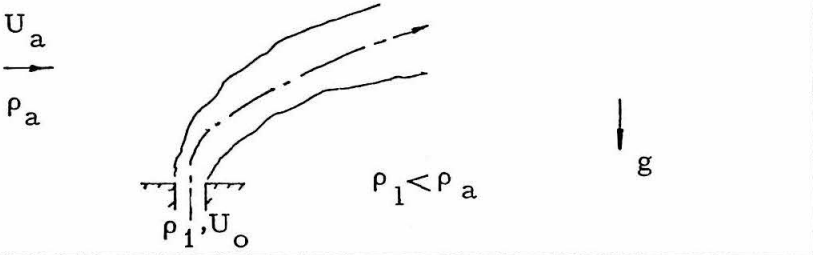
Type of Jet Flow	AN ORDINARY JET (A NON-BUOYANT JET) IN A UNIFORM CROSS STREAM	
Flow Configuration		
Contents Investi- gators	Methods of Approach	Results
Gördier (15)	Total head measurements near the nozzle	<ol style="list-style-type: none"> <li>1. Total head distribution (horse-shoe shape)</li> <li>2. Jet trajectories and velocity distribution along jet axes</li> </ol>
Jordinson (17)	Total head measurements near the nozzle	<ol style="list-style-type: none"> <li>1. Total head distribution (horse-shoe shape)</li> <li>2. Jet trajectories</li> </ol>
Keffer & Baines (18)	<ol style="list-style-type: none"> <li>1. Velocity measurements near the nozzle</li> <li>2. Integral type analysis assuming entrainment relation based on scalar difference of velocities</li> </ol>	<ol style="list-style-type: none"> <li>1. Similarity of velocity distribution along s-axis</li> <li>2. Jet trajectories and velocity distribution along jet axes determined from experiments</li> <li>3. Turbulence characteristics</li> </ol>

Table 7 (continued)

Type of Jet Flow	A BUOYANT JET (A FORCED PLUME) IN A UNIFORM CROSS STREAM	
Flow Configuration		
Contents	Methods of Approach	Results
Investi-gators		
Callaghan & Ruggeri (9)	Experimental determination of jet trajectories	Jet trajectories expressed in empirical forms.
Priestley (26)	Study of a smoke plume in a horizontal wind as a sheared-over vertical plume.	Jet trajectories
Csanady (11)	Analysis of smoke plume as a weak line thermal	<ol style="list-style-type: none"> <li>1. Jet trajectories at large distance.</li> <li>2. Excess of temperature over the center-line maximum: 28%</li> </ol>
Vizel & Mostinskii (35)	Analysis of jet trajectories based on the drag mechanism only	<ol style="list-style-type: none"> <li>1. Jet trajectories</li> <li>2. Drag coefficients by fitting experimental results.</li> </ol>
Present Study (Chapters VI & VII)	<ol style="list-style-type: none"> <li>1. Integral type analysis based on the entrainment relation (17) and a gross drag assumption.</li> <li>2. Concentration measurements</li> </ol>	<ol style="list-style-type: none"> <li>1. Jet gross behavior</li> <li>2. Numerical values of <math>\alpha</math> and <math>C_d</math> (Table 5)</li> <li>3. Concentration profiles (horse-shoe shape)</li> </ol>

Callaghan and Ruggeri (9), and Vizel and Mostinskii (35). The latter obtained an analytical expression based entirely on a drag model without considering the entrainment. The drag coefficients were found to be much greater than those for a solid body of corresponding size.

There was no previous investigation which could be used in predicting the gross behavior of a round buoyant jet in a uniform cross stream with results covering not only trajectories but also dilution ratios and jet half widths. (See Chapter II).

#### IX-D. Contribution of the Present Study to the Problem of a Round Buoyant Jet in a Uniform Cross Stream of Homogeneous Density.

##### 1. Theoretical analysis.

Integral type analysis was carried out (Chapter VI) by assuming an entrainment mechanism based upon the vector difference of the velocities:

$$\frac{dQ}{ds} = 2\pi \alpha b |\bar{U}_j - \bar{U}_a| \quad (17)$$

where  $\bar{U}_j$  and  $\bar{U}_a$  are respectively the jet center-line velocity and the ambient velocity. The effect of the pressure field was assumed to be lumped into a gross drag term with a constant drag coefficient  $C_d$ . Although the observed profiles were actually horse-shoe shaped due to vortices, the profiles were assumed to be circular in shape and similar.

The relevant parameters to the problem are the jet Froude number  $F$  and a velocity ratio  $k$  defined as:

$$F = \frac{U_o}{N \sqrt{\frac{\rho_a - \rho_1}{\rho_a} g D}} \quad (11)$$

$$k = \frac{U_o}{U_a} \quad (16)$$

The initial angle of discharge was limited to the right angle. The effect of ambient turbulence was not included in the analysis.

## 2. Experimental investigations.

Experiments were carried out in a laboratory flume by discharging heavy salt solutions into fresh water flowing in the flume. Ten cases with  $F$  varied from 10 to 80 and  $k$  from 4 to 16 were studied. Concentration measurements were conducted to determine the jet trajectories, half widths and dilution ratios. By matching both the trajectories and variation of dilution ratios between analytical and experimental results the values of  $C_d$  and  $\alpha$  were determined for each case. As presented in Chapter VII, the theoretical jet half widths agreed well with the observed values. Thus the analysis based upon the gross assumptions made describes the jet flow adequately and is applicable in practical problems.

## 3. Values of the coefficients $\alpha$ and $C_d$ .

The values of the entrainment coefficient  $\alpha$  were found to vary from 0.4 to 0.5 as shown in Table 5, Chapter VII. Also listed were values of the drag coefficients  $C_d$  which varied from 0.1 to 1.7. Approximate values can be chosen from the table for practical

applications. The large variation in  $C_d$  has not been explained, and must indicate some difficulty with the mathematical model.

Here the value of  $\alpha$  is much larger than that for a jet in a stagnant environment. It is probably caused by the difference in the entrainment mechanism. For a jet in a stagnant environment, the entrainment is mainly due to an aspirator action of the jet, whereas in a cross stream, the component of  $U_a$  normal to the jet is of considerable importance in the entrainment of the ambient fluid. The value of  $\alpha$  is also related to the shape of assumed profiles. The value of  $\alpha$  drops from 0.5 to 0.4 as  $k$  varies from 4 to 16 indicating a correct trend, since as  $k$  becomes infinite the value of  $\alpha$  should be equal to the  $\alpha$ -value for a jet in a stagnant environment. The  $\alpha$ -value varies also with the jet Froude number. Over a range of  $F$  from 10 to 80,  $\alpha$  changed from 0.5 to 0.4.

The values of  $C_d$  are roughly equal to or less than the drag coefficient for a solid body. The values indicate the importance of the effect of the pressure field.

The theory gives better results for low velocity ratio cases. For high velocity ratio cases, a long transition region may exist between the assumed zone of flow establishment and the region where the distributions of velocity and concentration become similar (in a horse-shoe pattern). This may account for the discrepancy between theoretical and experimental results.

#### 4. Effect of ambient turbulence.

The effect of ambient turbulence was not included in the analysis. A special set of experiments was carried out by towing

the jet along the stagnant ambient fluid. Results on jet trajectories and dilution ratios agreed well with results obtained in flume flow experiments. Thus under the flume flow conditions where the turbulence intensity was estimated to be under 5% the jet gross behavior was dominated by its self-generated turbulence up to a distance of travel of about 250D. (Chapter VII.)

5. Concentration profiles.

Several complete cross-sectional concentration profiles were obtained. (Figs. 57, and 58, Chapter VII.) The profiles are horse-shoe shaped with maximum concentration at two sides of the plane of symmetry. The maximum concentrations have excesses ranging from 80 to 60% of the value  $c$  at the jet axis. For practical applications such excesses should be considered. The lateral half width  $r'_{0.5}$  was observed to be about twice of the half width  $r_{0.5}$  on the plane of symmetry.

LIST OF REFERENCES

1. Abraham, G., "Jet Diffusion in Stagnant Ambient Fluid,"  
Delft Hyd. Lab. Pub. No. 29 (1963).
2. Abraham, G., "Horizontal Jets in Stagnant Fluid of Other  
Density," Proc. ASCE, J. Hyd. Div., 91, HY4 (July 1965),  
pp. 138-54; closing discussion, 93, HY1 (January 1967),  
pp. 63-68.
3. Abraham, G., "Entrainment Principle and Its Restrictions  
to Solve Problems of Jets," J. of Hyd. Res., 3, No. 2  
(1965), pp. 1-23.
4. Abramovich, G. N., "The Theory of Turbulent Jets,"  
English edition translated by Scripta Technica, MIT Press,  
Cambridge, Mass. (1963).
5. Albertson, M. L., Dai, Y. B., Jensen, R. A. and Rouse, H.,  
"Diffusion of Submerged Jets," Trans. ASCE, 115 (1950),  
pp. 639-97.
6. Bosanquet, C. H., Horn, G. and Thring, M. W., "The Effect  
of Density Differences on the Path of Jets," Proc. Roy. Soc.  
London, A263(1961), pp. 340-52.
7. Brooks, N. H., "Controlling Ocean Pollution," Engineering  
and Science, Calif. Inst. of Tech. (March 1966), pp. 13-17.
8. Brooks, N. H. and Koh, R. C. Y., "Discharge of Sewage  
Effluent from a Line Source into a Stratified Ocean,"  
Intern. Assoc. for Hyd. Res., IXth Congress, Leningrad  
(1965).

LIST OF REFERENCES (Continued)

9. Callaghan, E. E. and Ruggeri, R. S., "Investigation of the Penetration of An Air Jet Directed Perpendicularly to An Air Stream," NACA TN1615 (June 1948).
10. Cederwall, K., "Jet Diffusion: Review of Model Testing and Comparison with Theory," Hyd. Div., Chalmers Institute of Technology, Goteborg, Sweden (February 1967).
11. Csanady, G. T., "The Buoyant Motion Within a Hot Gas Plume in a Horizontal Wind," J. of Fluid Mech., 22 (1965), pp. 225-39.
12. Fan, L.-N. and Brooks, N. H., Discussion of Ref. 2, Proc. ASCE, J. of Hyd. Div., HY2 (March 1966), pp. 423-29.
13. Fan, L.-N. and Brooks, N. H., Discussion of Ref. 14, Proc. ASCE, J. of San. Div., SA 1, (February 1966), pp. 296-300.
14. Frankel, R. J. and Cumming, J. D., "Turbulent Mixing Phenomena of Ocean Outfalls," Proc. ASCE, J. of San. Div., SA2 (April 1965), pp. 33-59.
15. G6rdier, R. L., "Studies on Fluid Jets Discharging Normally into Moving Liquid," St. Anthony Falls Hyd. Lab. Tech. Paper 28, Ser. B, Univ. of Minn. (1959).
16. Grigg, H. R. and Stewart, R. W., "Turbulent Diffusion in A Stratified Fluid," J. of Fluid Mech., 15 (1963), pp. 174-86.



LIST OF REFERENCES (Continued)

17. Jordinson, R., "Flow in a Jet Directed Normal to the Wind,"  
Aero. Res. Council Rep. and Memo No. 3074 (1956).
18. Keffer, J. F. and Baines, W. D., "The Round Turbulent  
Jet in A Cross-Wind," J. of Fluid Mech., 15 (1963),  
pp. 481-96.
19. Koh, R. C. Y., "Viscous Stratified Flow Toward a Line  
Sink," W. M. Keck Lab. of Hyd. and Water Resources,  
Tech. Rep. No. 6, Calif. Inst. of Tech., (1964).
20. Lee, S. L. and Emmons, H. W., "A Study of Natural  
Convection above A Line Fire," J. of Fluid Mech., 11  
(1961), pp. 353-68.
21. Morton, B. R., "On A Momentum-Mass Flux Diagram for  
Turbulent Jets, Plumes and Wakes," J. of Fluid Mech.,  
10 (1961), pp. 101-12.
22. Morton, B. R., "Forced Plumes," J. of Fluid Mech., 5  
(1959), pp. 151-63.
23. Morton, B. R., Taylor, G. I. and Turner, J. S.,  
"Turbulent Gravitational Convection from Maintained and  
Instantaneous Sources," Proc. Roy. Soc. London, A234  
(1956), pp. 1-23.
24. Murgai, M. P. and Emmons, H. W., "Natural Convection  
above Fires," J. of Fluid Mech., 8 (1960), pp. 611-24.

LIST OF REFERENCES (Continued)

25. Owens, W. W., "Density of Aqueous Sodium Chloride Solutions - Tables and Graphs," W. M. Keck Lab. of Hyd. and Water Resources, Tech. Memo 65-11, Calif. Inst. of Tech. (September 1965).
26. Priestley, C.H.B., "A Working Theory of the Bent-over Plume of Hot Gas," Quart. J. of Roy. Met. Soc., 82 (1956), pp. 165-76.
27. Rawn, A. M., Bowerman, F. R. and Brooks, N. H., "Diffusers for Disposal of Sewage in Sea Water," Proc. ASCE, J. of San. Div., SA2 (March 1960), pp. 65-106.
28. Raichlen, F., "Some Turbulence Measurements in Water," Proc. ASCE, J. of Engrg. Mech. Div., EM2, (April 1967), pp. 73-97.
29. Ricou, F. P. and Spalding, D. B., "Measurements of Entrainment by Axisymmetrical Turbulent Jets," J. of Fluid Mech., 11 (1961), pp. 21-32.
30. Rouse, H., Yih, C. S. and Humphreys, H. W., "Gravitational Convection from A Boundary Source," Tellus, 4 (1952), pp. 201-10.
31. Sami, S., Carmody, T. and Rouse, H., "Jet Diffusion in the Region of Flow Establishment," J. of Fluid Mech. 23 (1967), pp. 231-52.

LIST OF REFERENCES (Continued)

32. Schmidt, W., "Turbulente Ausbreitung eines Stromes Erhitzter Luft," ZAMM, 21 (1941), pp. 265-78 and 351-63.
33. Turner, J. S., "A Comparison Between Buoyant Vortex Rings and Vortex Pairs," J. of Fluid Mech., 7 (1960), pp. 419-32.
34. Vanoni, V. A., "Final Report on 130-Foot Precision Tilting Flume," W. M. Keck Lab. of Hyd. and Water Resources, Tech. Memo 64-7, Calif. Inst. of Tech. (June, 1964).
35. Vizel, Y. M. and Mostinskii, I. L., "Deflection of a Jet Injected into a Stream," J. of Engrg. Physics, Vol. 8, No. 2 (February 1965), the Faraday Press, pp. 160-3, translation of Inzhenerno-Fizicheski Zhurnal.

APPENDIX A

SUMMARY OF NOTATIONS

- a subscripts denoting quantities of the ambient fluid
- A jet cross section normal to the jet axis
- b local characteristic length or half width of the jet
- b<sub>o</sub> half width of the jet at the end of zone of flow establishment
- c<sub>o</sub> initial concentration at the end of the zone of flow establishment, i. e. at O
- c concentration at jet axis
- c\* local concentration value
- C<sub>d</sub> drag coefficient
- C<sub>d</sub>' reduced drag coefficient =  $\frac{C_d \sqrt{2}}{\alpha \pi}$
- D initial jet diameter
- D<sub>o</sub> diameter of a sharp-edged orifice
- e exponential function
- f dimensionless buoyancy parameter
- F densimetric jet Froude number defined as  $\frac{U_o}{\sqrt{g \frac{\rho_o - \rho_1}{\rho_o} D}}$
- F<sub>o</sub> initial jet buoyancy flux
- g gravitational acceleration, 981cm/sec<sup>2</sup>
- G  $-\frac{g}{\rho_o} \frac{d\rho_a}{dy}$
- h dimensionless horizontal or x-momentum flux parameter

SUMMARY OF NOTATIONS (continued)

- k velocity ratio =  $\frac{U_o}{U_a}$  (jet: current)
- k'  $k + \cos \theta_o$
- m dimensionless momentum flux parameter
- $m_o$  initial dimensionless momentum flux parameter
- o subscript denoting initial values
- O origin of the coordinate systems (x, y), beginning of the zone of established flow
- O' origin of the coordinate system (x', y'), point of the jet discharge
- r radial distance measured from the jet axis on A
- $r_{0.5}$  r at which  $c^* = 0.5c$  on the plane of symmetry for jets in cross streams
- $r'_{0.5}$  r at which  $c^* = 0.5c$  on the plane normal to the plane of symmetry and the jet axis
- R initial jet Reynolds number defined as  $\frac{U_o D}{\nu}$
- s parametric distance along jet axis
- S center-line dilution ratio =  $c_o/c$
- $S_o$  center-line dilution ratio with respect to jet discharge concentration =  $\frac{2\lambda^2}{1+\lambda^2} S$
- $S_t$  terminal dilution ratio, i. e. S at the terminal point
- t subscript denoting values at the terminal point
- T stratification parameter

SUMMARY OF NOTATIONS (continued)

- u jet velocity at the center-line of the jet (excess over the ambient velocity component  $U_a \cos \theta$ )
- u\* jet velocity at a local point
- $U_a$  ambient velocity
- $U_j$  velocity along the jet axis
- $U_o$  jet discharge velocity
- v dimensionless vertical or y-momentum flux parameter
- x coordinate axis in horizontal direction on the same plane as jet axis with origin at O
- x' coordinate axis in horizontal direction on the same plane as jet axis with origin at O'
- $x_t$  x-coordinate of the terminal point
- y coordinate axis in vertical direction, same direction as gravitation, with origin at O
- y' coordinate axis in vertical direction, same direction as gravitation, with origin at O'
- $y_t$  terminal height of rise; y-coordinate of the terminal point
- $\alpha$ : coefficient of entrainment
- $\beta$ : buoyancy flux parameter
- $\xi$ : dimensionless vertical distance (y)
- $\xi_t$ : dimensionless terminal height of rise ( $y_t$ )
- $\eta$ : dimensionless horizontal distance (x)
- $\eta_t$ : dimensionless horizontal distance ( $x_t$ )

SUMMARY OF NOTATIONS (continued)

- $\zeta$  : dimensionless distance along s-axis (s)
- $\zeta_t$  : dimensionless distance ( $s_t$ )
- $\theta$  : angle of inclination of the jet axis (with respect to x-axis)
- $\theta_0$  : initial angle of inclination (with respect to x-axis)
- $\lambda$  : spreading ratio between buoyancy and velocity profiles; or  $\lambda^2$   
is the turbulent Schmidt number
- $\mu$  : dimensionless volume flux parameter
- $\mu_0$  : dimensionless initial volume flux parameter
- $\mu_t$  : dimensionless terminal volume flux parameter
- $\nu$  : kinematic viscosity in  $\text{cm}^2/\text{sec}$
- $\rho$  : density along the jet axis in gr/ml or center-line density
- $\rho_a$  : density of the ambient fluid
- $\rho_0$  : reference density taken as  $\rho_a(0)$
- $\rho_1$  : initial jet density
- $\rho^*$  : local density within a jet
- $\rho_a^*$  : local ambient density
- $\varphi$  : angular coordinate on a cross section normal  
to the jet axis
- $\sigma$  : standard deviation

APPENDIX B

PUBLISHED DISCUSSIONS

1. Discussion by the author and Professor Norman H. Brooks of "Turbulent Mixing Phenomena of Ocean Outfalls", by Richard F. Frankel and James D. Cumming. Published in the Proceedings of American Society of Civil Engineers, Journal of Sanitary Engineering Division, 92, SA1, February, 1966, pp. 296-300.

TURBULENT MIXING PHENOMENA OF OCEAN OUTFALLS<sup>b</sup>

---

Discussion by Loh-Nien Fan and Norman H. Brooks

---

LOH-NIEN FAN<sup>22</sup> AND NORMAN H. BROOKS,<sup>23</sup> M. ASCE.-- The laboratory research by Frankel and Cumming has provided greater insight into the problem of mixing of a buoyant plume in a homogeneous environment. This type of flow pattern is generated by jet discharges of sewage effluent from ports in an ocean outfall diffuser, when the ocean is not density-stratified.

The authors' results indicate that better dilutions are obtained for horizontal jets than for any upward inclination of jet discharge. In recent years, it has been the usual practice to use horizontal ports in multiple-port diffusers. However, were it not for the problem of bottom scouring, downward jets would be even better.

The large observed fluctuations of the concentration with time at a fixed point in a plume emphasize the difficulty of sampling to determine a mean concentration, either in the laboratory or the ocean. The authors are correct

---

<sup>a</sup> April, 1965, by Charles M. Proctor (Proc. Paper 4288).

<sup>b</sup> April, 1965, by Richard J. Frankel and James D. Cumming (Proc. Paper 4297).  
22 Graduate Research Asst., W. M. Keck Lab. of Hydraulics and Water Resources, California Inst. of Tech., Pasadena, Calif.

<sup>23</sup> Prof. of Civ. Engrg., W. M. Keck Lab. of Hydraulics and Water Resources, California Inst. of Tech., Pasadena, Calif.



in stating that individual samples with concentrations as much as twice as high as the time-average should be expected. However, in the ocean these spots of high concentration (and high gradient) will quickly disappear as a result of the natural oceanic turbulence.

The observations of the effect of the free surface, as shown in Figs. 9 and 10, are helpful. As the authors indicate, it is necessary to distinguish between data or solutions that apply at the surface from those which apply at the same height of rise within a deep body of water. The authors' curves are for measurements made below the surface transition zone, and apparently no direct observations were made of the thickness of surface transition zone. Their empirical estimate of the thickness of the transition zone (one-quarter of the depth) is apparently based on comparison of their experimental data with that

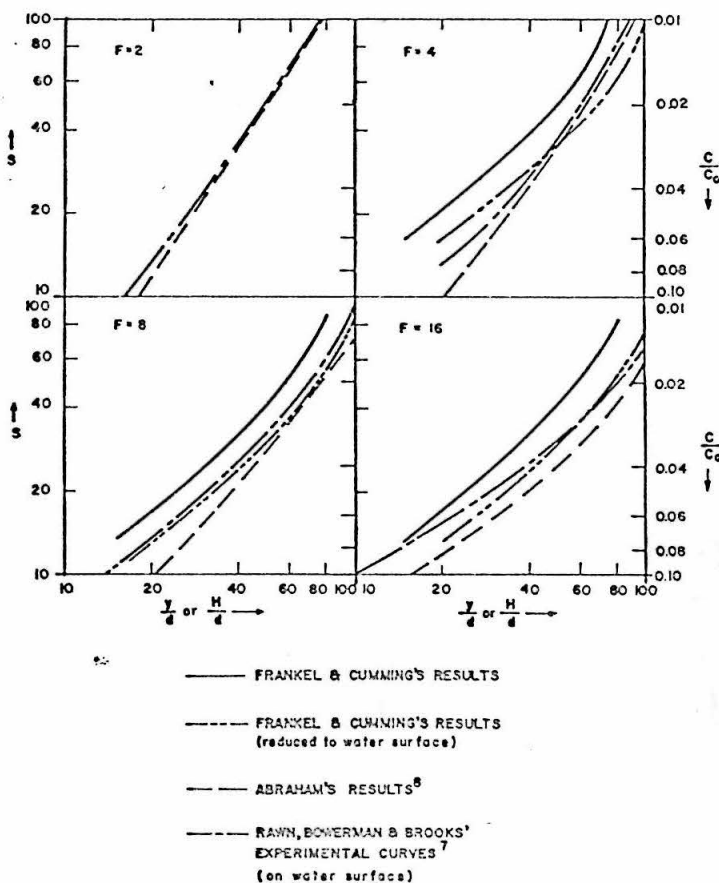


FIG. 18

of Rawn and Palmer (as analyzed by Rawn, Bowerman, and Brooks<sup>7</sup>) which apply to the surface.

Fig. 12 shows a comparison of various results for a horizontal jet at Froude number  $F = 10$ . A more complete comparison for horizontal jets is shown in Fig. 18, for  $F = 2, 4, 8,$  and  $16$ , in which  $S$  represents the commonly used dilution ratio, defined as  $S = C_0/C$ . Frankel and Cumming's results (solid lines) show higher dilution (lower concentration) in all cases; to make their results applicable to the surface they propose a shift of the curves to the right (as shown) corresponding to a one-third increase in depth-diameter ratio,  $y/d$ . The amount of this shift appears somewhat arbitrary and does not produce complete consistency for all Froude numbers and depths, but in general the agreement is good.

However, the question remains as to whether the difference in results is primarily the result of the surface zone rather than to a combination of experimental errors, various differences in experimental arrangement and procedure, and possibly Reynolds number (which is not specified in the paper). The thickness of the surface transition zone,  $H_s$ , should be considered not only as a simple proportion of the depth but also as a function of the parameters of the rising plume,  $y/d$ ,  $F$ , and the discharge angle. Furthermore,  $H_s$  should also be related to the character of the horizontal surface flow layer as well as the rising plume. The thickness of the horizontal flow layer depends on the dynamics of that current, including factors such as duration of experimental run, lateral constraints, and secondary circulation in the tank (or currents in the ocean). Considering these factors, the writers believe that, in most cases,  $H_s$  would be considerably less than  $1/4 d$ .

It is also interesting to note in Fig. 18 that Abraham's theory,<sup>8,24</sup> which neglects the surface transition zone, gives lower dilutions than the curves by Rawn, Bowerman, and Brooks, with best agreement at low Froude numbers. If a surface zone correction were applied in the same manner as for Frankel and Cumming, the difference between the curves for Abraham and Rawn, Bowerman, and Brooks would be greatly increased. Thus, the wide discrepancy between Frankel and Cumming's experiments and Abraham's theory is not explained by the effect of the surface zone. In a recent paper Abraham<sup>24</sup> has also commented on this discrepancy.

In performing experiments in the laboratory, the writers have found it more convenient to inject salt solutions into fresh water and observe the pattern of the falling plume. Because similarity is according to Froude's law, it makes no difference whether the apparent gravity acts up or down. Because friction and wave effects at the free surface are negligible, it can be simulated by the solid bottom of a laboratory tank.

The size of the probes used by the authors seems to be too large for small  $y/d$  where the jet width was small. By Fig. 3, the probes have a diameter of approximately 0.36 in, whereas the diameter of the nozzle used was only 0.365 in.<sup>13</sup> Thus, the dimension of the probe was of the same order as the jet width for a considerable range of  $y/d$ . In this range, the measured concentration,  $C$ , would necessarily give a smaller value than the actual  $C$  value on the jet axis, because the probe would read only the averaged  $C$  values over a

<sup>24</sup> Abraham, G., "Horizontal Jets in Stagnant Fluid of Other Density," *Journal of the Hydraulics Division*, ASCE, Vol. 91, No. HY4, Proc. Paper 4411, July, 1965, pp. 139-154.

region around the probe. The error would be less for larger  $y/d$  because the jet width would be proportionally bigger.

Fig. 19 presents a comparison of the results for vertical jets with Abraham's theoretical solution on log-log scale.<sup>8</sup> From  $y/d \geq 15$ , the measured values of  $S$  (or  $C_0/C$ ) are consistently lower than Abraham's solution but tending to the latter as  $y/d$  increases. This may be a result of the probe being too large. However, the reverse curvature of the curves between  $y/d$

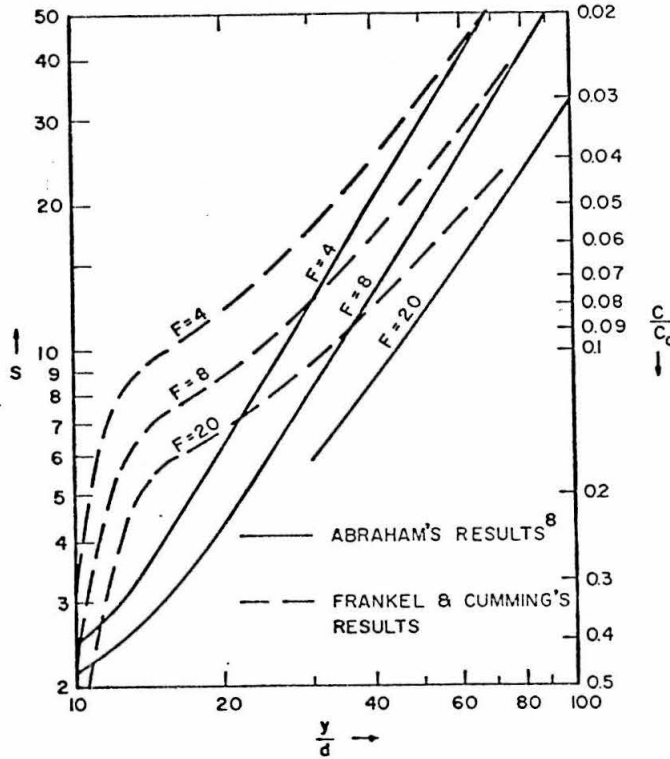


FIG. 19

= 10 and 15 remains to be explained. Also, in Fig. 17, the sharply curving parts of the curves for horizontal jets at low values of  $y/d$  do not seem plausible, and are not consistent with Fig. 15.

To simplify the discussion of the asymptotic rate of change of  $C$  with  $y$ , it is best to plot the curves on log-log graphs as in Figs. 18 and 19 rather than as semi-log graphs used by the authors (Figs. 12, 15, 16, and 17). On log-log graphs the slope  $n$  is simply the exponent in the equation  $S \sim y^n$  or  $C \sim y^{-n}$ , and it is not necessary to make derivative graphs as in Fig. 11. Theoretically, for vertical jets near the source,  $C \sim y^{-1}$ , and far away,  $C \sim y^{-5/3}$ ; except for

the anomaly around  $y/d = 10$ , the authors' curves do show an increasing slope in Fig. 19 as  $y/d$  increases. For  $F = 4$ ,  $y/d = 70$ , the slope or exponent is  $n = -1.4$ , which is not far from  $5/3$ . For the horizontal jets (Fig. 18) the asymptotic slope of the solid curves (authors' experiments) is approximately 1.8 (for  $F = 8$  and 16), again not far from  $5/3$ . It is difficult to determine the slopes accurately because the experiments were not conducted at constant  $F$  and variable  $y/d$ . Therefore, the curves shown for each Froude number have been interpolated.

These values of slope apparently contradict the authors' conclusion (page 58) that for large  $y/d$  the exponent approaches one. The writers do not agree with the authors' statement "... for ocean outfalls where density differences (and hence buoyancy) are small, relative changes in the concentration distribution for large values of  $y/d$  are similar for cases of both buoyancy and nonbuoyancy and can be approximated by  $(y/d)^{-1}$ ." Whether density differences are relatively large or small can only be expressed through the Froude number in this problem; therefore, Eq. 9 giving the  $5/3$  relationship is not subject to any lower limit on the values of density differences  $\Delta\rho/\rho_0$ . In fact the total buoyancy of a plume is preserved with distance, and a constant upward driving force is applied, causing a gradual increase in the over-all momentum flux above its initial value. The citation to Morton, Taylor, and Turner<sup>12</sup> on this point is not appropriate because their analysis pertains to a stratified ambient environment.

The writers disagree with the conclusion, page 57, that "Further increases in depth beyond  $y/d = 50$  give minimal advantages to mixing in the vicinity of the discharge point." This statement is not based on data, but is just an opinion; for example, at  $F = 16$ ,  $y/d = 50$ ,  $S = C_0/C = 40$  by Fig. 17, whereas at  $y/d = 80$ ,  $S = 90$ , which is surely better than 40. There is no phenomenon limiting growth of plumes for  $y/d > 50$ . A reasonable value of  $y/d$  can only be decided as part of a particular design problem. For example, the 120-in. outfall with 742 ports built in 1965 by the Sanitation Districts of Los Angeles County at Whites Point has minimum port diameters of 2.0 in. at depths of approximately 165 ft ( $y/d = 1,000$ ) and maximum of 3.6 in. at 195-ft depth ( $y/d = 650$ ). Port spacing is at 12 ft on both sides of a 4,440-ft-long diffuser pipe. The use of small ports was desirable to take full advantage of the natural density stratification in the ocean to produce a submerged sewage field. Design problems must also consider interference between adjacent rising plumes, which may sometimes be done by assuming a line source.<sup>25</sup>

---

<sup>25</sup> Brooks, N. H., and Koh, R. C. Y., "Discharge of Sewage Effluent from a Line Source into a Stratified Ocean," XIth Congress, Internatl. Assn. for Hydr. Research, Leningrad, USSR, September, 1965.

PUBLISHED DISCUSSIONS (continued)

2. Discussion by the author and Professor Norman H. Brooks of "Horizontal Jets in Stagnant Fluid of Other Density", by Gerrit Abraham. Published in the Proceedings of the American Society of Civil Engineers, Journal of Hydraulics Division, 92, HY2, (March, 1966), pp. 423-429.

(Note: The values of the dilution ratios from Fan and Brooks analysis in Fig. 8 on page 429 should all be multiplied by a factor of  $\frac{2\lambda^2}{1+\lambda^2}$ , about 1.15, and consequently the agreement with Abraham's curve is not quite as close as indicated.)

HORIZONTAL JETS IN STAGNANT FLUID OF OTHER DENSITY<sup>2</sup>

Discussion by Loh-Nien Fan and Norman H. Brooks

LOH-NIEN FAN<sup>19</sup> AND NORMAN H. BROOKS, M. ASCE.<sup>20</sup>—In this paper, Abraham has successfully analyzed the gross behavior of a turbulent buoyant jet (discharged horizontally), and compared the theory favorably with experiments. The analytical results are useful in the design of ocean outfall diffusers and may be used with reasonable confidence at a scale beyond the reach of laboratory experiments because of the physical basis of the analysis. It advances beyond the dimensional analysis approach presented previously for this problem by Rawn, Bowerman, and Brooks.<sup>14</sup>

Abraham's solution follows the integral approach by assuming that the velocity and buoyancy profiles are Gaussian across the jet, and integrating them over the jet or plume cross section. This procedure simplifies the relationships for the variation of gross properties along the path of the jet. One of the main difficulties in analysis of turbulent jets is to specify the rate at which fluid is entrained in the jet, or alternatively to specify the rate of growth of the plume or jet. From the present (1966) knowledge of free turbulent shear flows it is not clear how best to express this entrainment, especially in a sufficiently simple manner to permit a solution to the over-all problem of the curving buoyant jet.

The writers believe that the author's representation of the entrainment rate is not entirely logical. The author makes an assumption concerning the rate of growth of the jet by taking the velocity profile as in Eq. 6, namely

$$u = u_m e^{-k(r/s)^2}$$

in which  $k$  is not taken as constant but as an empirical function of  $\beta$ , the local angle of inclination of the plume (Eq. 16). Because the angle,  $\beta$ , varies with distance along the axis,  $s$ , then  $k$  is also variable with  $s$ . The profile may also be expressed as

$$u = u_m e^{-(r/b)^2} \dots \dots \dots (36)$$

in which  $b =$  the nominal radius of the jet ( $=\sqrt{2} \sigma$ ) and changes, of course, with distance  $s$  along the axis. Abraham, in effect, takes the nominal radius to be

<sup>a</sup> July, 1965, by Gerrit Abraham (Proc. Paper 4411).  
<sup>19</sup> Graduate Research Asst., W. M. Keck Lab. of Hydraulics and Water Resources, California Inst. of Tech., Pasadena, Calif.  
<sup>20</sup> Prof. of Civ. Engrg., W. M. Keck Lab. of Hydraulics and Water Resources, California Inst. of Tech., Pasadena, Calif.

$$b = \frac{s}{\sqrt{k(s)}} \dots\dots\dots (37)$$

in which  $k(s)$  indicates  $k$  is a function of  $s$ . Thus, the rate of spreading by his assumption is not linear with distance.

Abraham invented Eq. 16 to match two supposedly asymptotic cases—the horizontal momentum jet ( $\beta = 0$  and  $F = \infty$ ) and the vertical buoyant plume ( $\beta = \pi/2$  and  $F = 0$ ). The fact that  $k$  is different for these two cases does not prove that  $k$  should be a simple function of  $\beta$ ; rather, the writers believe that the variation of  $k$  results from the difference in the internal structure of the jet between the cases when buoyancy is insignificant and when it is a major driving force. This distinction is not a function of  $\beta$ . Furthermore, in the asymptotic cases cited,  $k$  was used as a constant, not varying with distance, and experimental values have considerable scatter.

The rate of entrainment by the author's analysis may be shown to be

$$\begin{aligned} \frac{dQ}{ds} &= \frac{d}{ds} \left( \pi u_m \frac{s^2}{k(s)} \right) \\ &= \frac{2 \pi u_m s}{k} - \frac{\pi u_m s^2}{k^2} \frac{dk}{ds} \dots\dots\dots (38) \end{aligned}$$

(Eq. 35 in the paper should also have included a second term with  $dk/ds$ .) This result is dubious because it implies that the entrainment rate is not uniquely determined by local conditions of the jet but rather by its distance from the origin and the geometry of its trajectory.

A better and more simple alternative is to assume that the rate of entrainment is proportional to the local characteristic (or maximum) velocity,  $u_m$ , and the local characteristic radius of the jet or plume, following the techniques used successfully by Morton, Taylor and Turner<sup>21</sup> and Morton.<sup>22</sup> Thus

$$\frac{dQ}{ds} = \frac{d}{ds} \left( \pi u_m b^2 \right) = 2 \pi \alpha b u_m \dots\dots\dots (39)$$

in which  $u_m$  and  $b$  are defined by Eq. 36, and  $\alpha$  = a dimensionless constant of proportionality. The effect of curvature is neglected, as the author has also done. By this means, full use is made of the continuity equation, which is actually bypassed by Abraham's assumption of  $k$  and  $\mu$  as functions of angle  $\beta$  (Eqs. 16 and 17).

The value of  $\alpha$  for buoyant plumes based on data of Rouse, Yih, and Humphreys<sup>6</sup> is 0.082, while for momentum jets the value is 0.057 based on data by Albertson, Dai, Jensen, and Rouse.<sup>2</sup> Therefore,  $\alpha$  cannot be a universal constant but should vary somewhat as the relative buoyancy or a local Froude number changes.

However, the coefficient  $\alpha$  will be assumed constant for simplicity, as others have done successfully. Morton *et al.*<sup>21</sup> found that in the case of buoyant

<sup>21</sup> Morton, B. R., Taylor, G. I., and Turner, J. S., "Turbulent Gravitational Convection from Maintained and Instantaneous Sources," *Proceedings, Royal Society, Series A*, London, England, Vol. 234, 1956, pp. 1-23.

<sup>22</sup> Morton, B. R., "Forced Plumes," *Journal of Fluid Mechanics*, Vol. 5, 1959, pp. 151-163.

plumes in a stratified environment the results based on a constant  $\alpha$  agreed with experimental observations. Later, Lee and Emmons<sup>23</sup> also reached the conclusion that  $\alpha$  can be considered as a constant in their study of line sources of buoyancy and momentum.

The analysis that follows will demonstrate how the problem solved by Abraham (depicted in Fig. 7) can also be readily solved using the continuity equation with constant entrainment coefficient  $\alpha$  as in Eq. 39. The writers believe that this assumption provides a fairly good approximate solution to the problem and it is consistent with the order of approximation implicit in various other assumptions made throughout the analysis. The results agree

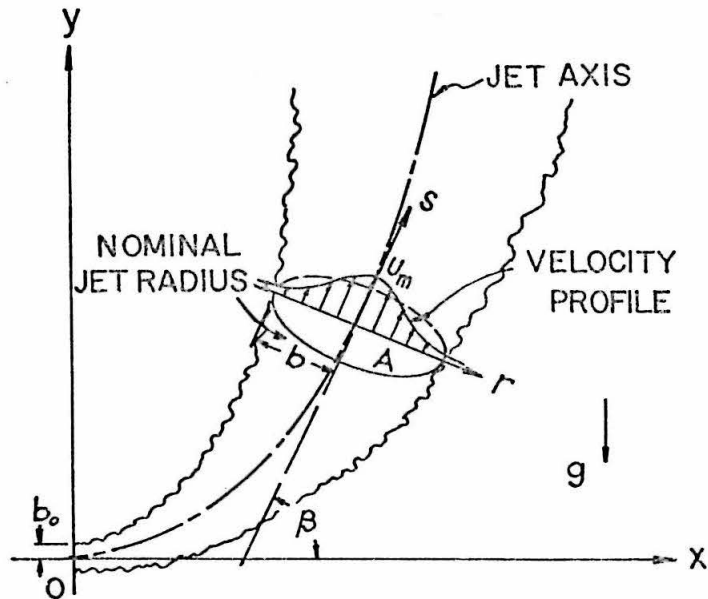


FIG. 7.—SCHEMATIC DIAGRAM OF A BUOYANT AXISYMMETRIC JET, DISCHARGED HORIZONTALLY

well with Abraham's and thus suggest that the simple entrainment formula is as valid as the author's approach using Eqs. 16 and 17.

First, the similarity assumption is made on both velocity and buoyancy profiles for the jet cross-section (Fig. 7), as in Eqs. 6 and 7 but written in slightly different forms

$$u = u_m e^{-(r/b)^2} \dots \dots \dots (36)$$

<sup>23</sup> Lee, S. L., and Emmons, H. W., "A Study of Natural Convection above a Line Fire," *Journal of Fluid Mechanics*, London, England, Vol. 1, 1962, pp. 353-368.



in which  $b =$  a local characteristic length; and

$$\rho_a - \rho = (\rho_a - \rho_m) e^{-(r/\lambda b)^2} \dots\dots\dots (40)$$

in which  $\lambda = 1/\sqrt{\mu} =$  a dimensionless spread ratio between velocity and buoyancy profiles, or the ratio of the turbulent diffusion coefficient for mass to that for momentum. The rate of increase of volume flux  $dQ/ds$ , based on the definition of  $\alpha$ , has been given by Eq. 39. Eqs. 11, 14, 13, 12, 9, and 10 then become respectively (see Fig. 7 for coordinate system):

Continuity  $\frac{d}{ds} (u_m b^2) = 2 \alpha u_m b \dots\dots\dots (41)$

Horizontal momentum  $\frac{u_m^2 b^2}{2} \cos \beta = \text{constant} \dots\dots\dots (42)$

Vertical momentum

$$\frac{d}{ds} \left( \frac{u_m^2 b^2}{2} \sin \beta \right) = g \lambda^2 b^2 \frac{\rho_a - \rho_m}{\rho_a} \dots\dots\dots (43)$$

Buoyancy flux  $u_m b^2 (\rho_a - \rho_m) = \text{constant} \dots\dots\dots (44)$

Geometry  $\frac{dy}{ds} = \sin \beta \dots\dots\dots (45)$

$$\frac{dx}{ds} = \cos \beta \dots\dots\dots (46)$$

The usual Boussinesq assumption of small density difference has been made.

For convenience of normalizing the equations, define dimensionless quantities as follows:

Volume flux parameter:

$$\gamma = \frac{u_m b^2}{u_o b_o^2} \dots\dots\dots (47)$$

Momentum flux parameters:

$$m = \frac{u_m^2 b^2}{2} \left\{ \frac{g \lambda^2 u_o^3 b_o^6 (\rho_a - \rho_o)}{4 \sqrt{2} \alpha \rho_a} \right\}^{-2/5} \dots\dots\dots (48)$$

$$h = m \cos \beta \dots\dots\dots (49)$$

$$v = m \sin \beta \dots\dots\dots (50)$$

Distance: 
$$\zeta = s \left\{ \frac{\rho_a u_o^2 b_o^4}{32 \alpha^4 \lambda^2 g(\rho_a - \rho_o)} \right\}^{-1/5} \dots \dots \dots (51)$$

$$\xi = y \left\{ \frac{\rho_a u_o^2 b_o^4}{32 \alpha^4 \lambda^2 g(\rho_a - \rho_o)} \right\}^{-1/5} \dots \dots \dots (52)$$

$$\eta = x \left\{ \frac{\rho_a u_o^2 b_o^4}{32 \alpha^4 \lambda^2 g(\rho_a - \rho_o)} \right\}^{-1/5} \dots \dots \dots (53)$$

Then Eqs. 41 to 46 can be written in the following dimensionless form:

$$\frac{d\gamma}{d\zeta} = \sqrt{m} \dots \dots \dots (54)$$

$$h = \text{constant} = h_o \dots \dots \dots (55)$$

$$\frac{dv}{d\zeta} = \frac{\gamma}{m} \dots \dots \dots (56)$$

$$\frac{d\xi}{d\zeta} = \frac{v}{m} \dots \dots \dots (57)$$

$$\frac{d\eta}{d\zeta} = \frac{h}{m} \dots \dots \dots (58)$$

in which

$$m = \sqrt{h_o^2 + v^2} \dots \dots \dots (59)$$

Thus normalized, the initial conditions for a horizontal jet at  $\zeta = 0$  are

$$\gamma = 1, h = h_o = m_o, v = 0, \eta = 0, \text{ and } \xi = 0 \dots \dots (60)$$

The zone of flow establishment is neglected because of its small extent in most applications; nevertheless, the initial values are based on Gaussian distributions of velocity and density defect, such as would occur at the end of the zone of flow establishment.

Solutions to this system of four ordinary differential equations (Eqs. 54, 56, 57, and 58) were obtained for values of the parameter  $m_o$  ranging from 0.3 to 20.0. The numerical integrations were performed by an IBM 7094 computer, adopting the Runge-Kutta method with automatic control on truncation errors. The results yield the four variables  $\gamma$ ,  $v$ ,  $\xi$ , and  $\eta$  as functions of  $\zeta$ . One of the advantages of this method of solution in normalized form is that the entrainment coefficient,  $\alpha$ , and the mixing ratio,  $\lambda$ , have not yet been specified, and may be chosen as desired.

The dilution of any contaminant may now be determined as follows. Let  $c$  be the concentration, which follows the same profile equation as for  $(\rho_a - \rho)$ , Eq. 40,

$$c = c_m e^{-(r/\lambda b)^2} \dots \dots \dots (61)$$

Because the flux of the contaminant is conserved,

$$\int c u dA = c_m u_m \int_0^\infty e^{-(r^2/b^2)(1+1/\lambda^2)} 2\pi r dr$$

$$= \frac{c_m u_m \pi b^2}{1+1/\lambda^2} = \text{constant} \dots\dots\dots (62)$$

Therefore, related to initial values  $c_o, u_o, b_o$ , the product  $c_m u_m b^2$  evaluated at any point along the plume is simply

$$c_m u_m b^2 = c_o u_o b_o^2 \dots\dots\dots (63)$$

Defining  $S_m$  as the dilution on the centerline, and using Eqs. 47 and 60

$$S_m = \frac{c_o}{c_m} = \frac{u_m b^2}{u_o b_o^2} = \gamma \dots\dots\dots (64)$$

For the convenience of comparison with existing results, the Froude number  $F$  (Eq. 3) is found to be related to the dimensionless initial momentum flux parameter  $m_o$  by

$$F^{1/2} = \frac{u_o}{\sqrt{\frac{\rho_a - \rho_o}{\rho_o} g D}} = \frac{\lambda}{2^{1/4} \sqrt{\alpha}} m_o^{5/4} \dots\dots\dots (65)$$

In deriving Eq. 65, the initial jet diameter  $D$  has been assumed to be  $\sqrt{2} b_o$  based on results of Albertson et al.<sup>2</sup> for zone of flow establishment. It should be noted that the quantity  $F^{1/2}$  used by Abraham is the same as  $F$  used by Rawn, Bowerman, and Brooks.<sup>14</sup>

Also found is the following relationship between  $y/D$  and  $\xi\sqrt{m_o}$

$$\frac{y}{D} = \frac{1}{2\sqrt{2}\alpha} \xi\sqrt{m_o} \dots\dots\dots (66)$$

With suitable numerical values of the dimensionless coefficients,  $\alpha$  and  $\lambda$ , the results of the numerical solutions to the differential equations can now be given in the form  $S_m = f(y/D, F^{1/2})$ , as shown in Fig. 8. Assuming that the over-all mixing is more similar to that of a buoyant plume than that of a momentum jet in the range of Fig. 8, the values  $\alpha = 0.082$  and  $\lambda = 1.16$  have been selected as being most reasonable, based on the literature.<sup>6,22</sup> The agreement in dilution values obtained by Abraham and by the writers is remarkably good in the range covered in Fig. 8. Although not shown here, the computed trajectories also check reasonably well: For example, the writers' trajectory for  $F^{1/2} = 24$  matches the author's for  $F^{1/2} = 20$  (not a large discrepancy).

One of the principal advantages of the entrainment equation (Eq. 39) over the author's approach is that it is more flexible and can be used on a wider variety of problems, such as those involving buoyant jets and plumes in a stratified environment. The variation of plume width  $b$  with distance need not

be specified in advance, as by the author, but can actually be derived from the equations of motion and continuity.<sup>21,24</sup> This is a necessity in problems where the density stratification actually stops the rising buoyant plume at an intermediate level, with the solutions<sup>21,24</sup> yielding in the limit  $u_m \rightarrow 0$ , and  $b \rightarrow \infty$ . Further research, including the cases of buoyant jets discharged into stratified environments at various angles, is in progress by the writers at the California Institute of Technology.

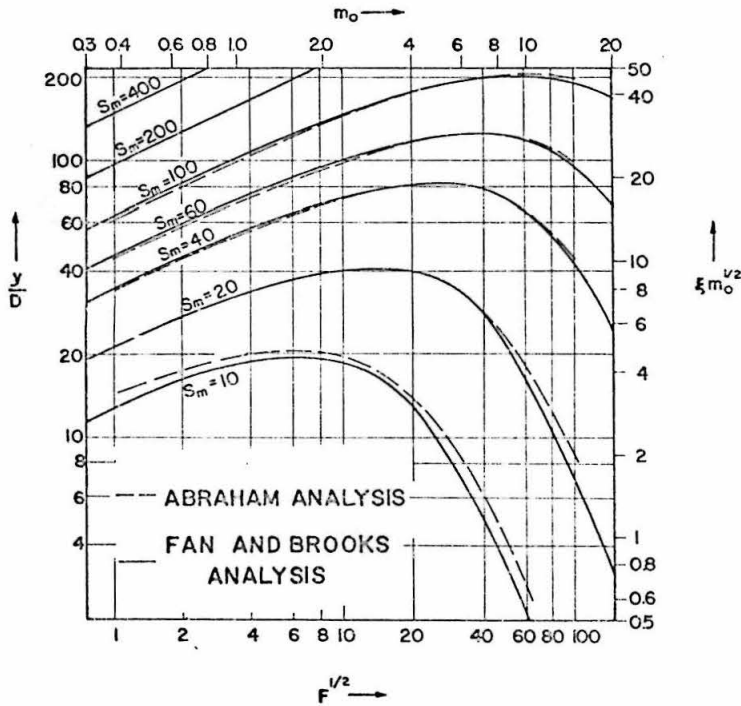


FIG. 8.—COMPARISON OF ABRAHAM'S AND WRITERS' ANALYSIS FOR CENTER LINE DILUTION,  $S_m$ , AS FUNCTION OF  $y/D$  AND  $F^{1/2}$

*Acknowledgments.*—The writers gratefully acknowledge the helpful suggestions of Robert C. Y. Koh, and the financial support of the United States Public Health Service Grant No. WP-00428.

<sup>24</sup> Brooks, N. H., and Koh, R. C. Y., "Discharge of Sewage Effluent from a Line Source into a Stratified Ocean," 11th Congress, Internatl. Assn. for Hydr. Research, Leningrad, USSR, September, 1965.